

A Systematic Design and Analysis Method of Elastic 3D Printed Knee Supportive Orthotic Devices to Meet Individual Needs

著者	Nikolaev Dachkinov Pancho
year	2022
その他のタイトル	個別ニーズを満たす弾性3Dプリント膝支持装具の体系的な設計と分析方法に関する研究
学位授与年度	令和4年度
学位授与番号	17104甲生工第450号
URL	http://doi.org/10.18997/00009024

Kyushu Institute of Technology

**Graduate School of Life Science and System
Engineering**

Department of Human Intelligence Systems

Doctoral Thesis

**Topic: “A Systematic Design and Analysis Method of Elastic 3D
Printed Knee Supportive Orthotic Devices to Meet Individual
Needs”**

**個別ニーズを満たす弾性 3D プリント膝支持装具の体系的な設
計と分析方法に関する研究**

by

Pancho Nikolaev Dachkinov

Supervisor: **Hiroaki Wagatsuma**

Kitakyushu, Japan 2022

Table of Contents

List of Acronyms	7
Acknowledgement	8
Abstract.....	9
Objective and Tasks	11
1 Introduction.....	12
2 Literature Review.....	16
2.1. Determining and Overview of the Properties of 3D Printed Models.....	16
2.2. Compliant Mechanisms Definition and Varieties	17
2.3. Application of the 3D Printing and Compliant Mechanisms in the Fabrication of Orthotic and Prosthetic Devices.....	18
2.4. Examples for Applications of the 3D Printed Compliant Mechanisms in Orthopedics21	
3 Methodology	24
3.1 Requirements of the Assistive Device:	24
3.2 Application and Implementation of the Compliant Hinges	24
3.3 Biomechanical Model of the Knee	25
3.4 ACL Rehabilitation Protocol	29
3.5 Analyzing the Grid Structure as a Cellular Solid.....	34
3.5.1 Structural Analysis of Modeling Cellular Solids IN-Plane Properties	36
3.5.2 Honeycombs: Out of Plane Properties:.....	45
3.5.3 Sandwich Panels	46
4 Results.....	48
4.1 Research Background and Past Work.....	48
4.1.1 Development of a Compliant Multi-material Universal Joint	48
4.1.2 A Computational Model for 3D Printing of Orthoses Based on a Systematic Structural Analysis for Reverse Engineering Oriented Production	51
4.2 Flexible Bar Geometric Designs for Personalized Knee Orthoses Inspired by Compliant Mechanisms	52
4.2.1 Introduction.....	52
4.2.2 Methodology	52
4.2.3 Results.....	54
4.2.4 Discussion	57
4.2.5 Physical Tests and Comparison of the Models	58
4.2.6 Implementation of the Compliant Mechanisms in the Rehabilitation Protocol of Athletes with ACL Complications	62
4.2.7 Summary of the study	64
5 Discussion.....	66
5.1 Determining the Elastic Properties of Flexible 3D Printed Beams with Variable Infill Densities and Patterns	66
5.1.1 Introduction and Background	66

5.1.2 Methodology	67
5.1.3 Results and Discussion	72
5.1.4 Summary	75
5.3 Out of Plane Motion.....	76
5.4 Development of a Regular Polygon Mesh Applied as an Orthotic Wearable for the Knee Joint	77
6 Conclusion	79
References.....	82
Publications.....	88

List of Figures

Fig. 1 Implementation of the Compliant Mechanisms in the Fabrication of Orthotic devices 10

Figure 1. 1 Ligaments of the Knee Joint.....	12
Figure 1. 2 Implementation of the 3D Printing for Orthotic Fabrication for the Knee Joint..	14
Figure 3. 1 Compliant Cross-spring Joints Variations.....	24
Figure 3. 2 Compliant Cross-spring Joints Pretotypes.....	25
Figure 3. 3 Developing a Supportive Device as a Combination of Compliant Mechanism	25
Figure 3. 4 Vector Model of the Knee	26
Figure 3. 5 Honeycomb Structure	35
Figure 3. 6 Unit Cells of Cellular Solids with Different Geometry	35
Figure 3. 7 Variables, affecting the honeycomb mechanical properties	37
Figure 3. 8 Parameters of the Cell when Compression Loads Applied	38
Figure 3. 9 Parameters of the Hexagonal Cell when Compression Loads Applied.....	38
Figure 3. 10 Cantilever Deflection.....	39
Figure 3. 11 Elastic Buckling.....	41
Figure 3. 12 Loaded Cross-section of an Elastic-perfectly Plastic Material.....	42
Figure 3. 13 Applied moment on the Incline Member.....	42
Figure 3. 14 Fracture Toughness	44
Figure 3. 15 Triangular Cell Honeycombs	44
Figure 3. 16 Square Cell Honeycombs	45
Figure 3. 17 Out of Plane Schematics.....	45
Figure 3. 18 Loading of a Sandwich Beam.....	46
Figure 4. 1 Design of the Compliant Joint.....	48
Figure 4. 2 A Model and s 3D Printed Prototype	49
Figure 4. 3 Loading Conditions of the Joint and the Individual Beams	49
Figure 4. 4 Strains Induced due to Axial and Transverse Loading.....	50
Figure 4. 5 Displacement vs Load plot for axial loading.....	50
Figure 4. 6 Compliant Mechanism as a Knee Orthosis	51
Figure 4. 7 Experimental Setup	51
Figure 4. 8 Results Comparison of the Physical Test	52
Figure 4. 9 Beam Groups	53
Figure 4. 10 Relationship between the 3D printing Infill Density and the Printing Duration .	54
Figure 4. 11 Loads on the Beams.....	54
Figure 4. 12 Non-linear Static Stress Analysis of the Bars with the Largest Deformations....	56
Figure 4. 13 Mechanical Behaviors of the Bars Based on the Geometry	56
Figure 4. 14 Non-linear Deformation of the Bars – FEA Results	56
Figure 4. 15 3D Printing Time of the Samples Mass of the Samples	57
Figure 4. 16 Physical Prototype Used in Orthotic Support.....	58
Figure 4. 17 Artificial Leg for Simulating Knee Flexion	58
Figure 4. 18 Artificial Leg Experimental Setup.....	58
Figure 4. 19 Model of the Experimental Setup.....	59
Figure 4. 20 Sample Models	61
Figure 4. 21 Comparison of the Tested Samples	61
Figure 4. 22 Moment vs Walking Gait Phase	62
Figure 4. 23 Grading the Models Based on their Peak Moments	63
Figure 4. 24 Rehabilitation Implementation of the Supportive Devices	63

Figure 5. 1 3D Printing Samples with Variable Infill Density	68
Figure 5. 2 Infill Geometries in the Slicing Software	69
Figure 5. 3 Modeling the Infill Patterns as Cellular Solids.....	69
Figure 5. 4 Parameters of the Cells	70
Figure 5. 5 Impact of infill-density on 3D Printing Parameters and Modulus of Elasticity (analytical).	73
Figure 5. 6 Impact of infill-density on 3D Printing Parameters and Modulus of Elasticity (analytical)	73
Figure 5. 7 Stresses and Displacements of the beam from COMSOL FEA analysis.	73
Figure 5. 8 Experimental Setup	74
Figure 5. 9 Variation of the Infill Density	75
Figure 5. 10 Topology Optimization for Orthotic Device Fabrication.....	76
Figure 5. 11 3D Representation of the Beam.....	76
Figure 5. 12 Material Combination.....	77
Figure 5. 13 Grid structures Variations.....	77
Figure 5. 14 Planar Mesh Structure	78

List of Tables

Table 2. 1 Literature Overview Summary	23
Table 3. 1 Tibial Peak Loading	26
Table 3. 2 Kinematics and Kinetics of the Knee During Common Activities.....	28
Table 3. 3 Task Progression After ACL Reconstruction with Specific Requirements.....	34
Table 4. 1 3D Printing Processes	53
Table 4. 2 Evaluation of the Samples	57
Table 4. 3 Description of the Tested Models	60
Table 4. 4 Maximum Offloading of the Supports	62
Table 4. 5 Task Based Protocol for Rehabilitation with Prescribed Devices	64
Table 5. 1 Research Background on the 3D Printing Materials	67
Table 5. 2 Combinations of infill density and infill patterns	68
Table 5. 3 3D Printing Parameters for the Samples	68
Table 5. 4 Properties of the 3D Printing Flexible Filament	69

List of Acronyms

ACL - Anterior Cruciate Ligament
PCL - Posterior Cruciate Ligament
AM - Additive Manufacturing
FDM - Fused Deposition Modeling
FFF - Fused Filament Fabrication
PLA - Polylactic Acid
ABS - Acrylonitrile Butadiene Styrene
TPU - Thermoplastic Polyurethane
CSP – Cross-Spring Pivot
CAD – Computer Aided Design
CAM – Computer Aided Manufacturing
STL - Standard Tessellation Language
RE - Reverse Engineering
AFO - Ankle Foot Orthoses
ESAR - Energy Storage and Return
FEA - Finite Element Analysis
FEM - Finite Element Method
MDB - Multibody Dynamics
ASA - Acrylonitrile Styrene Acrylate
PETG - Polyethylene Terephthalate Glycol
PPGW - Polypropylene Glass Wool
GCSFP - Generalized Cross-spring Flexure Pivot
PRB - Pseudo-rigid Body
DOF – Degrees of Freedom
SLS - Selective Laser Sintering
SLM - Selective Laser Melting
LDV - Laser Doppler Vibrometer
PDCA – Plan Do Check Act
DXF - Drawing Exchange Format
CNC – Computer Numerical Control
BW – Body Weight
ROM – Range of Motion

Acknowledgement

I would like to recognize the efforts of everyone who has supported me throughout the doctoral course and has contributed to improve the quality of my work.

I want to thank my family for their constant tireless support and believe in the outcome of this research.

I would like to acknowledge and give my gratitude to my supervisor for all the opportunities he has presented at me, for making this work a reality for the countless valuable lessons and experience through the years. His guidance and wise advice were always highly appreciated.

I want to express my special thanks to the members of the committee for their valuable feedback and allowing my defense process to be enjoyable and memorable moment.

I would like to thank all our laboratory members for being great supportive friends and making my experience not only easier but very enjoyable. I will always remember their stories now, being part of my story.

It is my true pleasure and honor express my gratitude toward my great international friends in the area. They have been with me through the good and bad times and have never doubted me.

Thank you for your positive attitude, wonderful moments, and many memories I will bring back home with me.

Special thanks to our laboratory staff members for making our life easier by helping us with all the administrative work at the background. Your support is greatly appreciated.

I want to thank to the Foreign Student Association of our campus for being an integral part of my life and playing a major role in my personal development and well-being. Thank you for all the fun we had together during these tears and all cultural interactions with remarkable individuals from across the world.

In addition, many thanks to the student section office and all the administrative staff members of Kyushu Institute of Technology for providing a great environment for conducting our research work.

Also, many thanks to all professors and teachers for their wonderful lectures and learning materials during our courses.

Special thanks to the partnering companies providing projects, funding, and equipment for smoothly carrying our work.

I would like to recognize the contribution of the Institute of Robotics – Bulgarian Academy of Sciences in my professional development and helping me pave my career path. All amazing researchers and staff members working there. Here is the time to express my deep gratitude to the Horizon2020 “CybSpeed” Project for letting me explore new “horizons” and travel to great foreign research institutions in Japan, France, and Morocco.

My deepest appreciation to my university – Technical University of Sofia, Bulgaria for helping me build my foundation in the field of Engineering. Thank you for the lessons and hard efforts that shaped my future vision.

At last, but certainly not least, I would like to give my many thanks to all my Bulgarian friends who have been with me for all these tears and have remained supportive and honest and kind.

The success of this study would have not been possible without all of you, your undoubted belief, friendship, and kindness. Your contribution is appreciated and will always be remembered.

I am looking forward to our next venture together!

Thank you!

A Systematic Design and Analysis Method of Elastic 3D Printed Knee Supportive Orthotic Devices to Meet Individual Needs

Abstract

The focus of this research is on the development of an Orthotic device for the human knee joint by implementing the compliant properties of flexible 3D Printed mechanisms. The main purpose of this study is to address the aspects of customization and especially in the low-budget solutions where currently there is a lack of wearable options due to the cost limitations. Additionally, there is an existing gap for devices with not only personalized flexibility but with adjustable one, controllable during the rehabilitation process of the patients. After the knee injury occurs, a surgical intervention might be needed to replace the damaged ligaments. After that, the patient's lower limb is fixed, and they are required to move by using crutches. The next phase of the recovery is using orthotic devices. Currently there are solid supportive devices on the market for the initial stage of the healing. Later, when the condition improves, and these supportive devices are being replaced by soft fabric type wearables and supplemented with low impact rehabilitation exercises. The problem with that solution is the lack of a middle supportive devices that makes the transition during the recovery smoother. The missing transitioning pieces can be serious issue amongst athletes who wish to accelerate their recovery process and start practicing on the field as soon as possible. The knee joint is especially vulnerable during those periods of transition between the hard hinge type devices and the soft sleeves, and usually this is the time when many people get injured again. Therefore, it can be assumed that there is a gap on the current market for an Orthotic device with an adjustable elasticity based on the stage of the rehabilitation process, individual requirements of the patients and their lifestyle. This necessity is even more present among the budget solutions for supportive device realization. In addition, this work is focused on ACL (Anterior Cruciate Ligament) injuries since, as explored in the literature below, they occur 10 times more often than the PCL complications, and in general, from all ligament injuries, half are at the ACL. The ACL usually tears during sports.

Some of the main questions this research tries to answer can be formulated as: Is there an actual need for such solution? What are the current solutions and how this problem has been addressed? Who are the targeted groups experiencing this problem? What are the main advantages and disadvantages of the proposed concepts? Lastly, is the implementation on its own a possible task?

In this work a more “unconventional” techniques, suitable for the purposes of Orthotic device design and fabrication is introduced and analyzed. The problem has been approached from a different perspective. Instead of looking for ways to improve the existing solutions, the findings of another field – 3D Printing and in particular, soft 3D Printing of compliant mechanisms were implanted and adapted according to the requirements of the above stated problem.

At first, a definition of a compliant mechanism is “a flexible mechanism that transmits force and motion through elastic body deformation”. Simply put, a mechanism that relays on the deformation caused by an external loading to perform the motion. From this notion is clear that compliant mechanisms have possible applications for Orthotic purposes. This, combined with the fact that these mechanisms are a good fit for 3D Printing, makes them strong candidate for the development and fabrication of supportive devices designed regarding the individual specificities.

In this thesis, several models of compliant flexible 3D Printed mechanisms implemented in Orthotic devices for the knee joint have been presented and investigated.

The models of the Orthotic device were verified by non-linear Finite Element Analysis due to the anisotropic nature of the 3D Printing materials and the occurring large deformations. Additionally, some of the proposed models were confirmed in an experimental environment by using a robotic arm and an artificial leg to measure the relationship between the force and the displacements of the samples.

A rehabilitation protocol for athletes with ACL complications was developed and proposed. To take full advantage of the capabilities of the additive manufacturing processes and to better optimize the samples, the cellular solid model was implemented to describe the 3D Printing structure from inside and explore the parameters important for controlling the stiffness/flexibility of the mechanisms. Three different infill types and seven infill densities were explored.

It was established that flexible 3D Printing can fulfil the criteria of fabricating compliant supportive devices with adjustable resistance and deformation depending on the required parameters.

Also was found the relation between the relative density and the moduli of elasticity, and relative density and stress of 3D Printed parts with different infill density and infill geometry. This can be valuable tool throughout the design phase in order to optimize the compliant supportive device, its stiffness and strength to weight ratio.

Finally, it can be concluded, 3D Printing by using flexible filaments is suitable manufacturing process for custom-made supportive wearables, especially for low-cost options. It gives extra levels of personalization unavailable to the traditional technologies with removing material. Implementation of compliant mechanisms allows for deeper control on the parameters related with the flexibility, ergonomics, and reliability of the Orthotic device.

In the context of the Forth Industrial Revolution, Additive Manufacturing technologies emerge as better and better alternatives as toolless methods with minimal material waste drastically decreasing the prototyping costs and time and only limited by the imagination of the designers and makers, to shape our new perspectives of what is possible.

Keywords: 3D Printing, Flexible 3D Printing, Computer Aided Design, Compliant Mechanisms, Additive Manufacturing, Orthotic Devices, Knee Supportive Devices, Orthotic Wearables, Rehabilitation Protocol, Reverse Engineering, Infill Optimization, Cellular Solid Model.

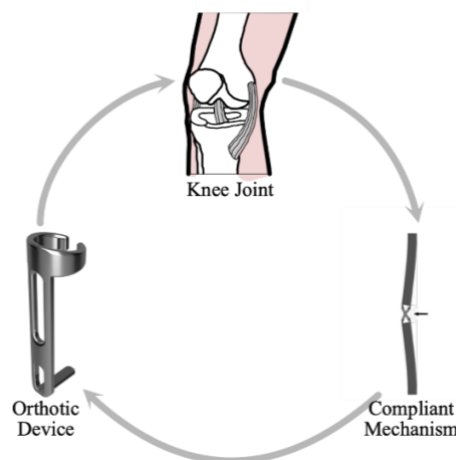


Fig. 1 Implementation of the Compliant Mechanisms in the Fabrication of Orthotic devices

Objective and Tasks

This work aims to develop a methodology for the design process of a customizable Orthotic device for the knee joint for athletes with ALC complications targeted toward low-income group patients by using the advancements in Additive Manufacturing for prototyping and fabricating flexible compliant models. The support must be easy to adjust and attach without the help of a medical professional. Some of the main requirements for the wearable device include: providing movement assistance, restricting out of plane motion, allowing sufficient range of motion, cost efficiency and usage of harmless materials.

To achieve the main purpose, there are several tasks that shape its direction such as designing the models in a 3D modeling environment, verifying the concepts by non-linear FEA simulations, creating prototypes by using 3D Printing technology and conducting some empirical measurements to determine the optimal solutions. Implementing an analytical method of improving the flexibility qualities of the models. Developing a working prototype for confirming the initial hypothesis.

1 Introduction

The proper function of the knee joint is essential for the daily life activities such as walking, climbing stairs, running, and jumping. However, it is a vulnerable joint and knee injuries can occur and harm seriously the normal living activities [1]. Therefore, a better understanding of the physiology, anatomy and biomechanics of the knee joint is crucial for providing an accurate treatment and helps in designing and optimizing assistive devices such as orthosis to fit into successful rehabilitation programs.

The knee joint has a complex structure and can get easily injured. It is one of the most stressed joints that carries almost the entire body weight. Stability and mobility are allowed by an inner and an outer ligaments together with a front and rear cruciate ligaments.

A commonly occurring condition at the knee joint is known as a Cruciate Ligament Rupture. Ligaments are tuff bands of tissue that attach the bones to other bones. The ligaments prevent different parts of the knee to move too far from one another and control the stability of the joint. A schematic representation of the knee ligaments is shown on Figure 1.1.

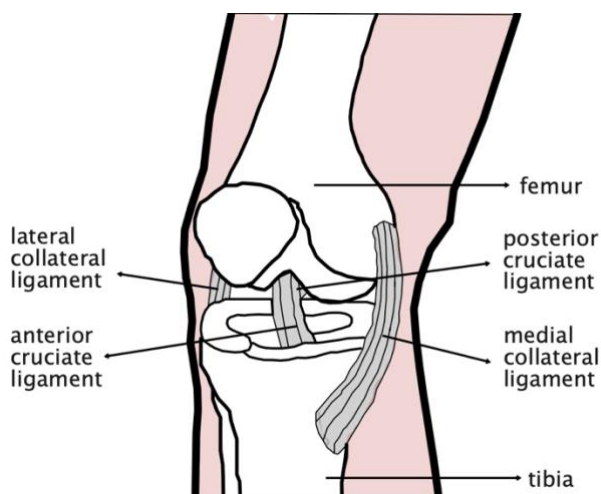


Figure 1. 1 Ligaments of the Knee Joint

The anterior cruciate ligament (ACL) and the posterior cruciate ligament (PCL) with the collateral ligaments keep the knee joint together. They limit extension of the lower limb, guide the joint during the motion and provide the necessary stability [2]. The anterior cruciate ligament ruptures ten times more often than the posterior cruciate ligament, and the number of these injuries has grown significantly in the last few decades. Sports usually cause tears in the anterior cruciate ligament when the knee is overstretched or twisted too far with a fixed lower leg. A rupture of the posterior cruciate ligament is often caused by a direct impact from the front against the lower leg or accidental overextension of the knee joint.

When the cruciate ligament is ruptured, the injured knee joint is severely swollen, painful and the range of motion is limited. Once the acute complaints have decreased, the instability may remain. This results in "buckling" of the knee joint during some activities such as climbing stairs or playing sports. Over time, instability in the knee joint can lead to damage to the menisci and cartilage, and even premature joint wear.

Cruciate ligament ruptures are typically fixed with cruciate ligament replacement surgery. The damaged cruciate ligament is replaced with a piece of a tendon. Stabilising orthoses are recommended after the surgery since the replacement material takes 10 to 12 weeks to grow.

Surgical innervation is not always required. Every case is specific and depends on age, activity, the ability to participate in sports, motivation, and the lifestyle of the patient. In addition, it must be considered that when the cruciate ligament is torn, cartilage damage can occur early

on without treatment, especially important for recreational and professional athletes, for whom further complications can cause additional injuries to the cartilage and meniscus.

To mitigate that impact after an injury and accelerate the healing process of the knee, there are various wearables and orthoses available on the market. These devices help support the knee, limit the range of motion at the initial stage of the recovery and give the necessary stability of the joint. There are two commonly spread types of orthoses and wearables. First one is hard, solid device that limits the motion and is used right after the injury for several weeks. The second type is an elastic flexible wearable that provides tightness to the joint and is suitable for the later stages of the recovery process. However, there are no commercially available options that allow for smooth transition between the rigid and the soft supports. During that time, the joint is especially vulnerable, and the existing solutions don't account for that period of the healing process. At the same time, the patients also start the rehabilitation process and gradually increase the range of motion and the intensity of the exercises; athletes begin their training programs and prepare for getting back to the field of their sport. This can be dangerous and lead to new injury of the knee joint that hasn't healed properly yet.

Therefore, there is a void for a supportive device that will provide the necessary smooth transition from the hard to the soft orthoses customised to the unique conditions of the patients. A device that can easily provide variable flexibility by replacing the elastic supportive components several times depending on the stage of the recovery and steadily increase the range of motion.

A possible candidate to address these requirements before the new type of supportive device are mechanisms called compliant.

Compliant mechanisms are mechanisms that rely on deformation caused by an external loading to execute a motion. In the recent years there is an increased interest in the implementation of compliant mechanisms due to their advantages and increased capabilities of 3D Printing as an appropriate technology for fabricating complex geometry [3].

The advancements in 3D Printing and Additive Manufacturing (AM) and the increased interest from a research perspective in the last years have enabled their applications outside of the prototyping stage and directly into functional parts. Additive Manufacturing has been widely adopted in industries such as Space Engineering, Automotive, Medicine and Stomatology, Jewelry and Fashion, and more.

3D Printing in all its variations as an additive process has become accessible and affordable technology in the present time. That can be explained by the constant improvements of the process and filaments.

The increased interest is mainly due to the capabilities of 3D Printing as an appropriate technology for fabricating complex geometry. Some of the unique characteristics of the process are:

- Ability to create hollow parts from inside.
- Fabricating parts with variable structure from the inner volume – infill pattern and density.
- Cost-efficient benefits – there are no tools required; the price of the components depends less on their complexity and more from the printing time and material usage.
- Environmentally friendly process – there are no wasted materials some of the materials from failed parts could be recycled.

3D Printing is used for creating not only prototypes but functional parts as well due to its unique abilities of fabricating the models by adding layers of material unlike the conventional technologies - by removing material. To achieve such implementation, investigating the mechanical properties of the materials is crucial.

The variety of materials is growing fast, and researchers have focused their attention to explore the quality of these filaments. In addition to the materials, the process of 3D Printing being

additive in its nature, allows for exclusive specific techniques to be applied such as control of the infill density and infill geometry from inside of the model – a property unavailable to the traditional manufacturing processes. To better optimize the design of a model, all the above parameters need to be considered. Although, some of the 3D Printing capabilities have already been investigated due to its growing popularity, it is important to note that the results of these studies may vary depending on the printer type and materials which significantly influence the mechanical properties and quality of the parts.

As already mentioned, amongst its advantages in comparison with the conventional technologies are the ability to control the geometry from inside and therefore the density of the structure and optimizing the mass to strength ratio of the part, realizing complicated shapes, and avoiding entirely the assembly process, suitable for fabricating the above-mentioned compliant mechanisms.

These compliant mechanisms permit for controllable elasticity (depending on the geometry and the infill density, and pattern) and repetitive cycle motion. The monolithic structure leads to a motion that is adaptive and wear-free. There are no clearances, and no heat is generated due to the friction between the components. Those unique properties make them strong candidate for orthotic devices applications. In addition, the 3D Printing compatibility of the compliant mechanisms allows deeper customization regarding the individual patient's requirements.

The above highlights will unlock the great potential of the Additive Manufacturing for customizable solutions depending on the specific patients' conditions.

Furthermore, another feature, due to the additive character of the process is the control of the infill density variability which contributes to a local control of the stiffness of the model. A combination of those factors will open a further potential of the Additive Manufacturing for customizable solutions that fit the individual requirements in the context of the reverse engineering for orthotic devices.

An illustration of the implementation of flexible 3D Printing for orthotic devices is shown on Figure 1.2.

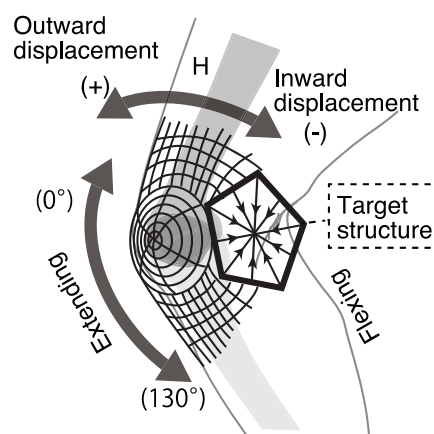


Figure 1. 2 Implementation of the 3D Printing for Orthotic Fabrication for the Knee Joint

That model consists of separate portions. Those parts are designed independently from each other based on the specific requirements to provide lateral stability of the knee joint, sufficient range of motion and flexibility. The parts are 3D Printed from a flexible filament and can be easily replaced with models with different elasticity increasing or decreasing the resistance depending on the circumstances.

As discussed in the [34] review of 22 studies, the properties of 3D printed orthoses have been compared with the conventional supportive devices. The 3D printed orthoses showed similar or superior effects on the biomechanical and kinematic parameters compared to the traditional solutions.

The remaining of this thesis is structured as follows: Section 2 explores the literature review on the topic, Section 3 provides the methodology used in this work, Section 4 summarizes the results, Section 5 gives the discussion of this work and Section 6 concludes the thesis.

2 Literature Review

2.1. Determining and Overview of the Properties of 3D Printed Models

The advancements in the Additive Manufacturing have led not only to realization of complex geometry but also to the development to variety of new filaments with different behavior and properties.

One of the most spread materials is Polylactic Acid (PLA). This a relatively low cost and environmentally friendly filament used by the Fused Deposition Modeling (FDM) (a process also known as Fused Filament Fabrication (FFF)) 3D Printers. The mechanical properties of this material are explored at a tensile and flexural tests by (Aveen et al., 2018) and (Catana et al., 2021) in [4] and [5] respectively. PLA has been compared with other popular 3D Printing filaments such as Acrylonitrile Butadiene Styrene (ABS) by (Ahmed et al., 2016) [6], Brčić et al., 2021 [7]. In [6] the authors investigate the flexural (bending) stiffness of 3D printed samples by conducting a 3-point bending test. The force-displacement relationship is obtained for all beam samples printed from four different filaments. In that study the highest values of the stress were recorded for PLA and the lowest - ABS. The other two materials tested were carbon reinforced ABS and PLA and it was concluded that adding carbon fibers to the material increased their stiffness. Other works investigate the relative density of flexible cellular structures fabricated from Thermoplastic Polyurethane (TPU) filament (Płatek et al., 2020) [8]. Effects of the infill density within a monolith part on the mechanical behavior of tensile tests for several different filament types have also been covered in [(Johnson & French, 2018) [9]. Amongst the tested materials are ABS, PLA, ASA (acrylonitrile styrene acrylate) and PETG (Polyethylene terephthalate glycol). The specimens were printed with varied infill percentage (density) from 15% to a 100%. As expected, the results for PETG show that the highest stiffness was for the sample printed with 100% infill density. In addition to the tensile stress analysis, some studies such as (Alvarez C. et al., 2016) [10] also investigate the printing time and the impact resistance of the models. Researchers have also conducted experiments where the infill geometry of the samples is varied (Fernandez-Vicente et al., 2016) [11], (Galeta et al., 2016) [12]. In some cases, the infill orientation and its influence on the parts' performance is explored by fatigue bending and tensile stress tests (Letcher & Waytashek, 2014)[13]. From the study can be observed that the strongest specimens from ultimate strength tensile test are the one printed with 45-degree orientation of the infill in comparison with 0 - (throughout the length of the sample) and 90-degrees (perpendicular to the sample) (which has the lowest values). The results for the bending test show that 0-degree orientation of the infill produced the parts with the highest stress values and 90-degree being the weakest option. All testing samples were printed from PLA. An intriguing discovery of the study is that the raw PLA filament exhibited similar mechanical properties to that of the printed specimens. The infill geometry has been investigated in terms of relationship between loading conditions and printing costs in (Baich et al., 2015) [14]. Some studies examine both the infill percentage (density) and infill geometry (pattern) (Farbman & McCoy, 2016) [15]. In this article the researchers perform a tensile stress test on ABS and PLA 3D printed models. The strength to weight ratio for the samples was compared. It was found that the specific tensile strength decreases as the infill percentage decreases and that the hexagonal infill pattern was stiffer than the rectangular infill geometry. A simulation study for the same loading conditions was also carried out. Lastly, there are works that have developed a new types and variations of 3D Printing materials especially TPU (Xiao & Gao, 2017) [16].

2.2. Compliant Mechanisms Definition and Varieties

Determining the properties and the performance of the 3D Printing filaments is necessary to optimize the parts. Due to its nature, 3D Printing as an Additive Manufacturing processes is suitable for fabricating compliant mechanisms. Compliant mechanisms are single printed mechanisms where the entire process of assembling is avoided. That leads to frictionless parts where no clearances and heat are generated due to the friction between the components. These types of mechanisms rely solely on the deformation they execute the motion. They can be precisely controlled if the characteristics of the materials are known and therefore, better understanding of the filament's properties will allow more reliable design of compliant mechanisms and will expand their applications in the future.

The properties of the compliant mechanisms (compliant joints) are analyzed by (Trease et al., 2005) [14], (Liu et al., 2014) [18]. In [17] several new types of compliant joints were developed. Rotational and translational joints are presented capable of larger range of motion and minimal axial drift. Analytic stiffness equations of the models are derived, and a parametric simulation is used to verify the performance. In [18] the authors propose a modified version of a Generalized Cross-spring Flexure Pivot (GCSFP). To enhance its poisoning capabilities the pivot that traditionally consists of two symmetric crossing leaves, has an additional third one to minimize the axial drift of the joint especially at large angles. The methodology of designing such mechanisms is provided by (Megaro et al., 2017) [19] and (Ion et al., 2019) [20 17].

Although, combining the above factors with the unique capability to control the geometry of the model from inside – its orientation and density unlike any traditional technology, make 3D Printing fitting for application in the compliant mechanisms fabrications by allowing for greater range of motion due to the larger deformations, there are certain challenges that must be considered while developing compliant mechanisms [3]:

- when large displacements occur, there are nonlinearities in the geometry and the material.
- depending on the orientation of the load, the stiffness of the part can vary in orders of magnitude.
- finding the balance between stiffness and flexibility is a complex design problem.
- to prevent the mechanism from fatigue failure of the material, high stress concentrations should be avoided.
- determining the desired motion parameters is a difficult task.

In rigidly articulated joints the clearances between the components causes backlash in the assemblies. Further, there is friction due to relative motion leading to wear of the parts and increasing the clearances and generating heat in the joint. All the above disadvantages result in poor accuracy and performance.

On the other hand, to address these issues researchers in the last years have focused on the compliance of the joints rather than restricting such deformations. Compliant joints provide smooth controllable motion, avoiding entirely the assembly process.

Flexural hinges have been widely studied in the literature and several applications in machine design which harness the advantages of flexure-based design elements have been realized. Being monolithic in structure and with the advent in Additive Manufacturing techniques, it is even simpler nowadays to design, prototype, test and verify the performance of these hinges in various applications, especially in the field of Precision Engineering. The most popular type of flexural hinge is the Cross-spring pivot, commercially known as Free-flex joints.

Primitive flexural joints primarily consist of leaf-type or notch-type configurations, but they have their own inherent limitations. Notch-type hinges have high stiffness in transverse directions and the rotation capability is limited by stress concentrations. However, the leaf-type flexures provide large rotations but at expense of drifting rotation centers. In-order to mitigate these issues, several complex flexural hinges have been proposed like the cartwheel hinges

[21], butterfly hinges [21]. While these hinges provide greater benefits over conventional leaf or notch type, cross-spring pivots are relatively simpler to design and versatile in applications. The diversity of these flexures stems from the fact that they were extensively explored in the literature for decades. They were first studied analytically in [22] and more recently in [23]. Goncalves provides a thorough theoretical formulation and laser based optical experiments to characterize the performance of Cross-spring pivots.

Relaying on material deformation, flexure joints have become major component in development of precise instruments with high resolution of positioning.

A different research point of view on the compliant mechanisms is due to their potential and applications in the field of biomechanics is also gaining popularity in the literature as well. The topology is investigated in [24] and [25] gives the design of parallel-guiding mechanisms. In [26] a design based on compliant building block for micro/nano positioning is described. In [27] and [28] the design and applications of more commonly spread type of compliant joint – a cross-spring pivot are analyzed.

2.3. Application of the 3D Printing and Compliant Mechanisms in the Fabrication of Orthotic and Prosthetic Devices

In addition to the improvements in the compliant joints research, the compatibility of the 3D Printing materials and their properties is crucial to the proper function of the mechanisms.

Other works show the application of the 3D Printing the Orthopedics for creating orthoses such as [29], [30] and [31]. The methodology of designing such orthotic devices for the human arm is provided in [32]. A customized orthoses for the knee joint by using 3D Printing is designed and developed in [33]. The applications and implementation of the Additive Manufacturing for orthotic devices is summarized in [34], [35] and [36].

As previously mentioned in [34], 3D printed orthoses had similar or better performance in comparison to the conventional ones with superior performance of their biomechanical and kinematic parameters. The orthoses as devices that assist the function of the human body have the following requirements: limit the range of motion, weight bearing properties, limit the movements in other planes and assisted joint movement. The conventionally applied methods for fabricating orthotic devices are time-consuming and require a manual correction of the shape of the orthosis to properly fit the patient. Furthermore, manufacturing multiple customized orthoses with the same dimensions and fit is a challenging task on its own. However, by implementing the 3D printing technology, orthoses can be designed with exact dimensions in a CAD Engineering software, and the above mentioned disadvantages of the traditional method can be sufficiently addressed due to the high accuracy of the 3D printers. In addition, manually produced orthosis requires approximately a week to be fabricated, but in contrast, a 3D printer can perform this task within a day. Therefore, due to all of these benefits, a significant attention is being paid to the 3D printing processes and their implementation in the field of orthoses.

The researchers in this review, found that 3D printed orthoses can improve biomechanical and kinematic parameters, and their effectiveness is similar to that of conventional orthoses. Furthermore, participants in the study defined that wearing the 3D printed orthoses is comfortable. Additionally, in some instances, the effectiveness of 3D printed orthoses and their comfort were reported to be better than those of the traditional solutions. In 10 of the studies included in this review, the 3D printed orthotic devices were compared with conventionally produced orthoses. In all those studies, 3D printed orthoses showed superior or similar results in the evaluation parameters (satisfaction, wrist spasticity, wrist-hand function, gait parameter, arch height index, and plantar foot pressure and joint range of motion, and patient satisfaction with 3D printed orthoses was also comparable with that of conventional orthoses.

Some of the reasons for the higher level of satisfaction amongst the patients are:

- The surface of the orthotic device in contact with the body part of the patient is optimized for the 3D printed orthoses. The majority of the conventional orthoses are made manually. Even if the orthosis is produced based on the patient's body casting, human error should not be overlooked.
- Lighter weight than the traditional solutions. The weight of the orthosis is not limited to the selection of main material. By using 3D printing technology, the weight can be further reduced with great precision by the inclusion of small holes on the narrow surface which leads to weight reduction and provides better ventilation. In addition, designing to omit bolts, nuts, metal rings, etc., or outputting parts to a 3D printer can help reduce the weight of the orthosis and improve the ergonomic design.

The reported results for stability, pain, pressure, function of the affected area, and satisfaction were generally excellent - the pain was reduced, and the joint's ROM was improved. Considering the advantages of 3D printed orthoses, the Additive Manufacturing technologies are expected to be more widely adopted in the clinical practice in the near future.

However, 3D printed orthosis is not flawless in all aspects. There are limitations of the 3D printers as well such as the printing volume. It is difficult to manufacture an orthosis with an exceptionally large circumference or height. In addition, for 3D printing technology to be actively implemented in the fabrication of orthoses, practitioners in related fields, such as clinicians, prosthetists, orthotists, and occupational therapists, will need to acquire CAD utilization skills and increase their understanding of 3D printing technology.

As limitations of this review the authors point out that previous studies had a small percentage of randomized trials and fewer results comparing conventional and 3D printed orthoses. Such comparison is necessary to provide the effectiveness of the traditional and the 3D printed orthosis, and evaluate objective indicators such as joint ROM, pressure distribution, and kinematic data.

3D Printing has a large influence on manufacturing and soft robotics [37]. Originally, CAD/CAM software models have a long history in engineering fields, providing enormous benefits in mass production. Amongst the highlights is the availability of 3D Printing for small-lot series and prototypes [38, 39].

In prosthetics and orthotics fabrication, the experts called "prosthetists" normally take responsibility for the design and realization of the supportive devices after a prescriptions of a medical doctor. The process includes steps of body-part measurement, molding for fabrication, assembling the parts and adjustment to the targeted body part [40]. Since expert knowledge and technique have supported the manufacturing process in such a comprehensive way, the reverse engineering (RE) production cannot be fully reconstructed as a partial replacement of the steps of the mechanical approach.

Empirical approaches have been explored to establish the reverse engineering principles in prosthetics and orthotics [41, 42, 43, 44, 45, 46, 47, 48, 49, 50, 51, 52]. In the early stage, the concept design of the reverse engineering orthosis was presented by Teng et al.(2013) [41], while the presented device was too simple to reconstruct realistic orthoses.

As explained in [43] by Baronio et al. (2016), the reverse engineering is an essential process to digitalize and compute the 3D anatomical models obtained from the patients in order to create the virtual 3D model of the orthosis ready to be printed. In the context of the reverse engineering, 3D Printing as an integral part of the process is the final steps of the supportive device fabrication. This research work focuses on the production of a customized hand orthosis based on the accurate geometry of the forearm and the actual printability of the model. Although its custom design meant to fit the specific hand geometry and provide certain level of comfort to the subject wearing it, this device is static and aims to limit the range of motion during the healing process and is not suitable for active rehabilitation program. A review of 3D

Printing upper limb prostheses is presented in [44]. It analyses the benefits and drawbacks of the existing solutions of 3D printed upper limb prosthetic devices. The overview includes quantitative analysis of 58 devices, their mechanical and kinematic specifications and the 3D Printing technology used for their fabrication. While a relatively large sample of devices are analyzed, the study concludes that there is a lack of evidence for the user acceptance level, functionality and durability of the 3D printed prosthetic devices. In addition, contrary to the common claim, 3D Printing was not necessarily the cheapest option in all cases for instance compared to injection molding. However, 3D Printing provides much greater level of customization than other technologies. The vast majority of the devices presented in this study were manufactured by using the FDM method.

The focus of [45] is on 3D printed Ankle Foot Orthoses (AFO). The 3D printing technique and automated design software, and clinical results after the application of this AFO to a patient with a condition known as “foot drop” are presented. Drop foot is a condition when the patient experiences difficulty lifting the front part of the foot. A 3D model file of a patient’s lower leg is created by a 3D scanner, and after that, the file is transferred to the automated orthosis software and the “STL” (Standard Tessellation Language) file is created. The model was printed using a FDM type 3D printer, and a mechanical stress test was performed. A subject of the study alternated between the 3D-printed and conventional AFOs for 2 months. During that time, it was observed that there is no damage on the 3D printed device. An important progress tracking parameter investigated in this research was the gait speed of the patient. The gait speed increased after wearing the conventional AFO and 3D-printed AFO compared to the speed without an AFO. In terms of the weight and ease of use the 3D printed model was better accepted by the patient.

The workflow of CAD/CAM orthoses design was discussed by Weiss et al. (2013) [46] and Santos et al. (2017) [47], while it was still a simple and partial replacement of the fabrication process to reduce the burden of prosthetists without an automated adjustment and structural analysis.

Recently, those pioneering works were evolved to parametric formulations to describe target models [49, 52]. Finally, a remaining problem is an integrated framework of systematic verifications of a structural analyses [53, 54] and strength evaluation [55, 56].

In parallel to past works discussed above, a challenging and remarkable approach is to introduce the essence of compliant mechanisms [57] for the orthoses design [58, 59, 60, 61, 62, 63, 64, 65, 66]. Compliant mechanisms can provide a smooth flexible motion with a specific force and deformation requirements. Since they can be formed in a monolithic and jointless way, compliant mechanisms are a good match for the 3D Printing method. In consideration to the possible integration of the reverse engineering orthosis with compliant mechanisms, it may open a new door of possibilities to provide 3D Printing orthosis designs by using flexible fibers and as well as controlled distribution of the strength depending on body-part segments specificity.

In [61] researchers describe the design of a compliant mechanism used for a dynamic hand orthosis. However, the results show that mechanism did not reach its design constraints mainly due to a poor stiffness to compliance relationship. Therefore, it has to be noted that some designs and materials may not be suited for various applications but instead, for lower forces and/or less displacements. The paper concludes that the physiological stiffness models are an important part during the modelling of the orthotic devices.

In [63] the authors aim to develop a low cost a prosthetic foot compliant mechanism. As discussed in this paper, many of the existing solutions are unaffordable for the amputees below the low-income bar. The approach used in this study is based on topology optimization followed by a 3D CAD model to match the dimension requirements. Additionally, the typical pressure line of an average human foot was incorporated into the model to endorse flexibility

and efficient energy storage and return (ESAR) when compared to the behavior of the conventional rigid prosthetic foot products. The methodology is verified by a Finite Element Analysis (FEA) of the model accounting for three major phases the human foot undergoes throughout the gait cycle.

In addition, a risk-free mechanism is required for human assist devices to prevent unnecessary overload in the joint motion, which may occur in embedded motor systems. Racu et al.(2018) [64, 65] proposed the use a compliant mechanism for the ankle rehabilitation device as a safety technique, which does not provide damage the patient's foot during the joint motion. Those facts imply that a compliant mechanism is beneficial for human assist devices not only for assistive mechanisms but also for safety techniques. However, compliant mechanisms have a large variety of designs, and then expert knowledge and decision-making are required to avoid a combinatorial explosion of parameters. It seriously undermines the interests of the challenging approach. In this study, for taking the first step toward the solution of this complex problem, a consistent framework coupling with an automated generation of the compliant mechanism design is proposed, which converts from the skeleton model with a few parameters to a detailed three dimensional one according to the upstream design concept [67].

Traditionally, exoskeleton-type assistive devices have been provided for the patients with motor disorders especially after neurological injuries and those devices have made rapid strides in recent years by integrating motorized parts and spring-damper mechanisms [68]. For example, assistive strategies were modeled with a rotational actuator, a simple pendulum model, and a damped pendulum model, which enhance abilities for normal and fast gaits [68 , 69]. Indeed, those require a dynamic adaptation to motion kinetics depending on the walking environment and model-based analyses highly important for evaluating of the joint torque and knee stiffness [69, 70], which extend capabilities of exoskeleton-type assistive devices [71, 72, 73].

A systematic mathematical analysis based on the multibody dynamics [74, 75,] for motion kinetics occurring the knee joint support can be introduced and applied. In the realization of the systematic analysis, necessary joint torque and knee stiffness can be estimated clearly and it helps to design supportive mechanisms to provide a load reduction of the joint in the rehabilitation stage.

2.4. Examples for Applications of the 3D Printed Compliant Mechanisms in Orthopedics

Some market available as well as in development solutions of orthotic devices fabricated by 3D Printing are illustrated in [76, 77]. In [78] a 3D printed safe landing Garment is presented. This device aims to decrease the landing loading on the knee joint especially for athletes. As mentioned in the article, the human weight during a landing can go up to 7 times more than the normal, this can cause serious injuries. The approach here uses a 3D printer to create a hexagonal compression patterns that are printed flat on a fabric and after that wrapped around the knee. This model can be custom made and applied without additional assistance. Similar approach of printing flat mesh from a soft flexible material is taken in [79]. Here the mesh wearable is used during the healing process of ankle and knee joints. This work is carried by MIT research team who developed an adjustable mesh material according to the patients' specific condition and that helps the healing of muscles and tendons. Although the material can maintain a sufficient strength, it is very thin and can be worn as an elastic fabric. Another benefit of this particular design – it doesn't get in the way while exercising. The material used for this model is TPU. Experiments with volunteers were conducted as well. The reports from the participants state and confirm that the mesh wearable allows freedom in all directions while at the same time prevents the ankle from bending inwards. This 3D printed mesh material is expected to be applied to various medical tools as a surgical mesh that can be applied not only to braces but also to stents such as blood vessels and trachea.

3D Printing Capabilities Overview			
Authors	Method	Subject	Results
Ahmed et al., 2016	Bending stiffness of 3D printed samples by conducting a 3-point bending test	Comparison between PLA and ABS	Higher values of the stress were recorded for PLA and lower for ABS. Adding carbon fibers to the material increased their stiffness.
Johnson et al., 2018	Tensile Tests PLA, ABS, ASA, PETG Samples	Effects of the infill density within a monolith part on the mechanical behavior of tensile tests for different filament types.	PETG showed that the highest stiffness was for the sample printed with 100% infill density.
Letcher et al., 2014	Tensile Test Bending Test PLA Samples	Infill orientation and its influence on the parts' performance.	Tensile test: 45-degree orientation of the infill is the strongest; 90-degrees the lowest values. Bending test: 0-degree the highest stress values and 90-degree - the weakest.
Farbman et al., 2016	Tensile Test PLA and ABS Samples FEA Study	Influence of the infill percentage density and pattern on the strength of the parts.	The specific tensile strength decreases as the infill percentage decreases. The hexagonal infill pattern is stiffer than the rectangular.
Compliant Mechanisms Variations and Application			
Authors	Method	Subject	Results
Trease et al., 2005	Analytic Stiffness Equations FEA Study	Rotational and translational compliant joints are developed.	Larger range of motion and minimal axial drift.
Liu et al., 2014	Adding an additional third leaf to the Cross-spring Pivot Analytic Stiffness Equations FEA Study	A modified version of a Generalized Cross-spring Flexure Pivot.	Enhanced the poisoning capabilities. Minimized axial drift of the joint especially at large angles.
Application of the 3D Printing and Compliant Mechanisms in the Fabrication of Orthotic and Prosthetic Devices			
Authors	Method	Subject	Results
Baronio et al., 2016	3D Scanning 3D Modeling 3D Printing	Production of a customized hand orthosis.	Custom design to fit the specific hand geometry provide comfort to the patient. It is a static device and limits the range of motion during the healing process. Not for active rehabilitation.
Kate et al., 2017	Quantitative analysis of 58 devices The mechanical and kinematic specifications and the 3D Printing technology used for their fabrication	A review of 3D Printing upper limb prostheses.	A lack of evidence for the user acceptance level, functionality and durability of the 3D printed prosthetic devices. 3D Printing was not always the cheapest option. 3D Printing provides greater level of customization. Most of the devices presented in this study were manufactured by using the FDM method.

Cha et al., 2017	3D Scanning 3D Printing Mechanical Stress Test Subject Test – Gait Speed	3D Printed Ankle Foot Orthoses (AFO)	The gait speed increased after wearing the AFO compared to the speed without an AFO. In terms of the weight and ease of use the 3D printed model was better accepted by the patient. Durable design.
Bos et al., 2017	Design Topology Optimization Analytic Equations	Design of a Compliant Mechanism Used for a Dynamic Hand Orthosis	The mechanism did not reach its design constraints due to a poor stiffness to compliance relationship
Srikanth et al., 2017	Topology Optimization 3D Modeling FEA Study	Low-Cost Prosthetic Foot Compliant Mechanism	Minimized material storage while preserving the stiffness characteristics
Examples for Applications of the 3D Printed Compliant Mechanisms in Orthopedics			
Authors	Method	Subject	Results
MIT, (https://3dprintingindustry.com/news/the-mit-scientists-making-3d-printed-fabrics-as-soft-as-skin-157609/)	3D Modeling 3D Printing Experiments	3D Printed Flexible Mesh for Knee and Ankle Support	The material can maintain a sufficient strength Very thin Light weighted Adjustable Allows freedom in all directions; prevents the ankle from bending inwards

Table 2. 1 Literature Overview Summary

3 Methodology

3.1 Requirements of the Assistive Device:

As already discussed in the previous chapters, this study focuses on the development of an assistive compliant orthotic device for the human knee joint by using flexible 3D Printing. The device will rely on the deformation of the elastic filament to perform the motion. By applying some of the advantages of the compliant mechanisms and Additive Manufacturing processes, the requirements of such orthosis are:

- Customizable – stiffness/flexibility ratio regarding the specific patient’s condition.
- Easily adjustable – replacing the elastic modules with stiffer or more flexible once depending on the recovery stage of the patient.
- Assist the range of motion (ROM).
- Limit out of plane ROM.
- Low cost – due to the affordability of the 3D Printing materials the device has to be suitable for all patients.
- Durability – the device should keep its reliably in time.
- Light weighted – it will be used by the patient for the entire day and therefore the mass of the device is a crucial parameter.
- Ergonomic – the comfort of the wearable support is very important for the recovery process.
- Easy to use - the patient should be able to apply and remove the device on their own.
- Compact – the patient should be able to wear the support with other clothes.
- Aesthetics – the device should not be visually disturbing the patient.

To achieve all these requirements, the supportive device has been divided into several segments which were individually analyzed.

3.2 Application and Implementation of the Compliant Hinges

At first, more simple versions of compliant joints were explored. As shown in Figure 3.1, several models taken from the literature [16, 18] were designed and investigated. As it can be observed from the figure, the compliant cross-spring pivots are characterized with the following main parameters: w - width of the rib, l - length of the cross-spring, t - thickness of the cross-spring, d - diameter of the inner circle, D - diameter of the outer circle, b – width in direction perpendicular to the drawing, α - the angle between the cross-springs and n – the number of the cross-springs.

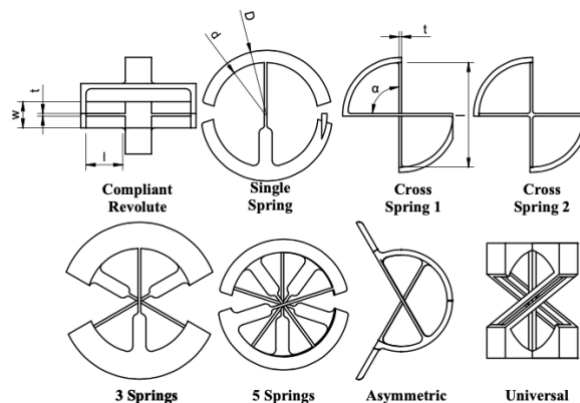


Figure 3. 1 Compliant Cross-spring Joints Variations

Next, to verify their behavior and performance, some of the models were 3D Printed from PLA material as illustrated on Figure 3.2.

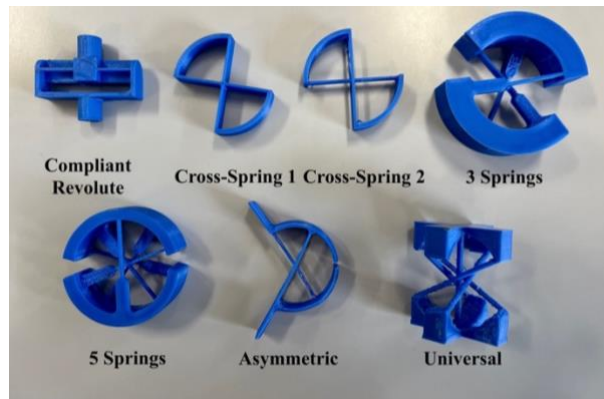


Figure 3. 2 Compliant Cross-spring Joints Pretotypes

The goal is after analyzing these cross-springs individually, to combine them in order to create a flexible mesh 3D Printed from TPU filament that will wrap around the knee joint. The step-by-step process is described on Figure 3.3.

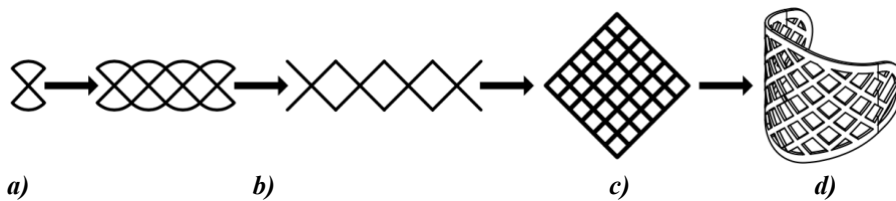


Figure 3. 3 Developing a Supportive Device as a Combination of Compliant Mechanism

On Figure 3.3 a) is shown a single cross-spring joint. On b), the compliant joints are attached to each other forming a chain. After that, on c) more compliant mechanisms are combined in a mesh. In d) the compliant flexible mesh is illustrated as a wearable support that can be wrapped around the knee.

3.3 Biomechanical Model of the Knee

A biomechanical model of the knee joint is provided in [80]. According to this model, the knee experiences forces and moments at the joints of the knee and the ankle. The variety of activities will determine the range and magnitude of these forces at the connecting points of the joints. As long as forces acting at the knee are reduced enough by the supportive device, the healing of the connective tissue can progress. Figure 3.4 gives a vector model of the knee.

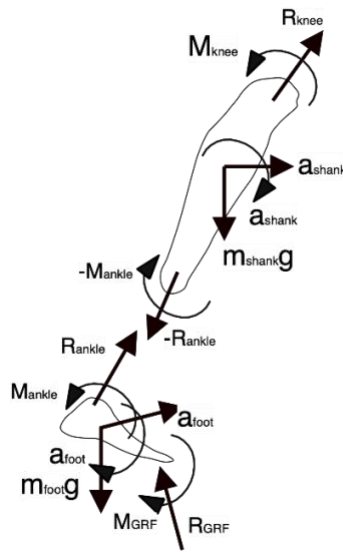


Figure 3. 4 Vector Model of the Knee

These forces and moments can be obtained by the following equations:

$$R_{knee} + m_{shank} \cdot g - R_{ankle} = m_{ankle} \cdot a_{shank} \quad (3.1)$$

$$R_{knee} = m_{ankle} \cdot a_{shank} - m_{shank} \cdot g + R_{ankle} \quad (3.2)$$

$$M_{knee} - M_{ankle} = I_{shank} \cdot a_{shank} \quad (3.3)$$

$$M_{knee} = I_{shank} \cdot a_{shank} + M_{ankle} \quad (3.4)$$

$$\sigma_{x \text{ or } y} = k \cdot \frac{F}{A} \rightarrow \tau_{xy} = E\sigma. \quad (3.5)$$

The values for some of the loading on the femur obtained empirically are provided in Table 3.1 by [81].

Activity	Peak Tibial Forces (xBW)	Notes
Walking	2.5-2.8	Laboratory Floor
Treadmill Walking	2.1±0.2	1 to 3 miles per hour
Power Walking	2.8±0.4	4 miles per hour on a treadmill
Jogging	4.2±0.2	5 miles per hour on a treadmill
Stationary Cycling	1-1.5	Level 1-5, 60-90 rpm
Stair Master	2.4±0.1	Level 1
Stair Master	3.3±0.3	Level 3
Elliptical Machine	2.3±0.2	Level 1
Elliptical Machine	2.2±0.3	Level 11
Leg Press	2.8±0.1	Resistance=1xBW
Leg (Knee) Extension	1.5	Resistance=0.2xBW

Table 3. 1 Tibial Peak Loading

Biomechanics of the Knee Joint

A systematic review of the knee joint biomechanics and physiological conditions is given in [1]. As the authors have stated, understanding the biomechanics of the knee joint is an urgent need for the design and of knee orthotic devices and optimization of the rehabilitation programs. This review consists of 138 papers published between 2000 and 2019 divided into 2 categories: biomechanics of normal and of a diseased knee joint. For the former, the movement and biomechanics of a normal knee during four common daily activities which include walking, running, stair ascent and descent and sit-to-stand were discussed. For the latter, an overview of common knee disorders such as musculoskeletal and neurological on the biomechanics were analyzed. The review concludes that there is no clear current assessment of the biomechanics of a normal and diseased knee.

In this article the authors also discuss the function of the knee during common daily motions. The main functions of the knee include supporting the body weight (BW), absorbing the shock of heel strikes when landing, and assisting the lower limb swing. The passive knee flexion can reach 160 degrees in sagittal plane. The peak load during walking is 2-3 times BW, 2-5 BW during sit-stand-sit, 4-6 BW during stair climbing and 7-12 BW during running.

The walking gait can be divided into two main phases:

- Stance phase – between 0-65% of the gait:
 - Initial – heel strike to foot flat.
 - Middle – foot flat to another heel strike.
 - Terminal – opposite heel strike to toe off.

The knee joint at stance phase is regarded as a shock damping system to accept the BW.

- Swing phase – about 65-100% of the gait:
 - Initial – toe off to knee maximum flexion.
 - Terminal – knee maximum flexion to heel strike.

The main function of the knee during the swing phase is assisting flexion and extension for toe clearance foot placement and shifting over the load to the next step.

This paper reports that the knee biomechanics is affected mainly by the walking speed. With the increase of the speed the range of motion (ROM), the maximum extension moment and maximum absorption power will also increase. In general, the ROM for normal walking is between 53 and 75 degrees. The range of moments during walking is – 0.458 to 1.265 Nm/kg. For the knee there is only absorption power for the swing phase. For the entire gait cycle the knee absorption powers are much greater than the generation powers. The range of power is about 1.035-3.214 W/kg during walking.

The stair climbing (ascent and descent) can be divided into two phases:

- Stance – 0-62% of the cycle.
 - Initial - foot contact to opposite toe off.
 - Middle - opposite toe off to opposite foot contact.
 - Terminal - opposite foot contact to toe off.
- Swing – 62-100% of the cycle.

The knee biomechanics during stair climbing is mainly affected by the ration of the leg length and the stair height.

The peak flexion during stair ascent occurs in the swing phase and the peak extension in the terminal stance phase. For stair descent, the peak flexion is in the terminal stance phase, and the peak extension – in the swing phase. The range for the peak flexion is between 83 and 102 degrees and for the peak extension – 0-11 degrees for stair ascent and 83-705, and 1-19 degrees for stair descent, respectively. In general, the ROM of the knee during stair climbing is 89 to 94 degrees for stair ascent and 76 to 90 degrees for stair descent.

For stair ascent, the peak extension moment and the peak flexion moment occur in the stance phase and for the flexion moments – in the swing phase. For the descent, the maximum

extension moments occur in the stance phase and the peak flexion – in the swing phase. The range of the moments is from 1.01 to 1.815 Nm/kg for stair ascent and from 0.435 to 1.815 Nm/kg for stair descent. The range of power for stair ascent is from 1.309 to 3.481 W/kg and for descent – 2.114- 6.056 W/kg. Almost all power during ascent is generation power and for the descent, almost all is absorption power.

The sit-to-stand begins in a sitting posture and ends in a standing position. During the whole standing movement, for the knee joint there are only extension angles, extension moments and generation power. The maximum values of the angle, moment and power occur nearly at the same moment when the subject leaves the chair. The biomechanics of the knee joint is mainly affected by the rate of leg length and chair height. The range of the peak angle is between 82 and 96 degrees. The range of motion of the knee is between 60 to 87 degrees from sit-to-stand in general. The peak moment is 0.619-2.187 Nm/kg and the range of the moment in general for the entire motion of sit-to-stand is from 0.619 to 1.578 Nm/kg. The research about the knee power generation is rare and the values differ significantly.

The peak values discussed above for the knee joint’s kinetics and kinematics are summarized in Table 3.2.

Activity	Max Angle, (°)	Max Moment, (Nm/kg)	Max Power, (W/kg)
Walking	53-78	0.129-0.945	0.286-0.834
Stair Ascent/Descent	83-102	0.027-0.144	-1.44-2.887
Sit-to-stand	82-96	0.619-2.187	0.56-1.973

Table 3. 2 Kinematics and Kinetics of the Knee During Common Activities

Actual Motion of the Knee Joint

Due to the nonuniform shape of the articulating surfaces of the knee and the complex shapes of the femur and the tibia, the knee cannot be modeled as a perfect hinge joint. The real motion of the joint is polycentric where the center of rotation shift continually during the articulation. The femur and the tibia can be approximated as bielliptical surfaces where the tibia rolls on the femur which leads to an anterior-posterior transition throughout the flexion and extension. When the flexion angle is less than 20 degrees, there will be a small anterior-posterior translation. Therefore, the knee joint can be approximated as a gradual transition from pure rolling, the combined motion of rolling and sliding to pure sliding.

Additionally, to the sagittal plane flexion and extension, in horizontal (transverse) plane there is an external and internal rotation. At the last 10-15 degrees before full knee extension the medial femoral condyle (the ball-shaped located at the medial (internal) part of the femur where the articulation occurs) is internally rotated and the tibia is externally rotated. At the same time, the lateral meniscus is anteriorly translated, and the medial meniscus is posteriorly translated. Due to the large contact surface of the medial tibiofemoral joint, the length of the medial femoral condyle is longer than that of the lateral one and therefore, and because of the limitations of the cruciate collateral ligaments quadriceps femoris on the knee motion, the knee joint is self-locking as an eccentric wheel to maintain the stability of the joint during extension.

In frontal (coronal) plane, the knee adduction moment and the loads on the medial and lateral compartments are the main biomechanical parameters. For the former, the maximum adduction moment ranges between 0.26 to 0.36 Nm/(kg.m) during walking, 0.34 to 0.44 Nm/(kg.m) for stair climbing and 0.45 Nm/(kg.m) for sit-to-stand. For the latter, the knee joint always has a little varus – the medial compartment always carries more weight (about 60-80% of the entire weight) than the lateral. In addition, the weight bearing line is different during each phase of the gait.

Biomechanics of the Injured Knee

According to the pathogeny, the knee disorders can be mainly musculoskeletal and neurological. For the former, the pathogeny is inside the knee joint, but the neural control system is normally functioning. Common musculoskeletal disorders are knee osteoarthritis, knee ligament injuries, and meniscus injuries. The ligament injuries will be discussed in greater details later in this chapter. For the latter, the knee actuation is properly working but the neural system is affected. Although not considered knee injuries, the neurological disorders can influence the knee motion biomechanics. Amongst the neurological disorders are spinal cord injuries, stroke, and cerebral palsy.

Knee osteoarthritis patients presented a longer gait time, a smaller stride length and ROM, a greater knee flexion angle at heel strike, and an unobvious fluctuation of knee flexion angle in the stand phase of walking.

Knee ligament injuries are common and serious injuries in sports and can significantly change the biomechanics. Depending on the location, the injuries can be divided into ACL, PCL, TCL, FCL and PL. As many researchers have pointed out, if these injuries are not treated properly, other secondary injuries can occur at the same time such as osteoarthritis, cartilage injury and meniscus injury. The ligament reconstruction is recognized effective treatment that can recover the joint biomechanics drastically. For the above-mentioned ligament injuries, nearly half of them are injuries of the ACL. For patients with ACL injuries, several studies have found the following conditions: lower ROM in stair climbing, greater peak adduction angle and smaller flexion angle during walking, slower speed, and stride length during walking. In the kinetics aspect, it was observed 430 % and 475% increase in the patella-femur contact force during up slope and down slope, respectively. The peak adduction moment in weight-bearing activities in patients with ACL was greater after the injury than before. Additionally, it was found that patients with ACL injuries have greater energy absorption during landing.

ACL injuries are sometimes coupled with meniscus injuries which leads to increased stress and reduced stability of the joint during extension and flexion of the knee.

Understanding how pathologies affect the knee joint biomechanics is important for designing knee assistive devices and optimizing rehabilitation exercise program.

It is important to state that in this review the different values between the various studies are significant. Also, it is hard to find research that has systematically studied all aspects of the knee biomechanics.

3.4 ACL Rehabilitation Protocol

The rehabilitation protocol and how the devices can be implemented during different stages of the recovery is very important for the safe healing of the patients. A methodology for athletes after ACL reconstruction therapy is developed by Juntendo University [82].

Early stage: ~4 weeks

Missions:

- 1) Protect the tendons and the ligaments treated during the surgery.
- 2) Pain control.
- 3) Swell control.
- 4) Recovery of the walking ability.
- 5) Enhance muscle strength in the quadriceps.
- 6) Increase in range of motion (especially in extension).

Mid stage: ~ 12 weeks

- 1) Extend the normal range of motion (especially in extension).

Later stage: ~ 20 weeks

Assure the normal range of motion (extension and flexion).

- 1) Largely enhance muscle strength and force production.

2) Running (check carefully necessary conditions).

Preparation to return to sports ~ 32 weeks

- 1) Quantity and quality of the body movement and activity before the injury.
- 2) Enough muscle abilities.
- 3) Recovery of the staying ability.

A task-based progression approach for ACL reconstruction rehabilitation is developed in [83]. In its basic form, movement retraining after ACL reconstruction is about progressively increasing the difficulty and intensity of the exercises from the ability of the patients to walk to highly demanding sport specific activities. However, there is a lack of specificity of when to transition from one task to another. The ability to perform a certain activity is not related to healing time, but more specifically to functional return to training. Therefore, this article provides a task-based progression with specific criteria and monitoring suggestions as a guideline during ACL reconstruction rehabilitation.

Loading Management During Rehabilitation

For task-based progression, the level of loading that a task can place on the body should be initially established. The loading can be defined as:

- Peak loading (e. g., peak ground reaction force);
- Volume loading (load times repetition);
- Rate loading (duration of the loading).

All types of loads and load tolerance should be included in the rehabilitation process.

Deficits in strength will mean insufficient neuromuscular capacity which will lead to greater loading on the joints and connective tissue.

Additionally, the range of motion has to be considered in order to minimize the patellofemoral joint stress. In close kinetic chain exercises such as squats, lunges and leg press, the quadriceps force and the patellofemoral joint stress are the highest near full extension and, therefore, it is recommended to initially restrict high load functional training to flexion angles between 0 and 80 degrees.

Monitoring Parameters During the Rehabilitation Process

The athletes have to be monitored during exercise to ensure their form, response to the activity and progression. Monitoring parameters suggested in this research are:

- The response to the exercise.
- Movement quality during the task.
- Strength.
- Muscle soreness.

To monitor the response to exercise, every task-based activity must consider the healing ability of the joint to withstand the loading demands. At that stage important parameters that must be carefully observed are pain and swelling of the knee. The exercises should be pain-free. Progression through tasks is only allowed if there is no pain or swelling.

The quality of the motion means if the current task is too difficult for the patient to perform. To reduce the risk of reinjury, the athlete should aim for symmetry of the motion. The inability to maintain alignment may mean the task is too challenging for the current stage of the recovery.

In addition, to perform functional tasks, is dependent on the neuromuscular system and its ability to generate force. If the musculoskeletal strength is not restored for the particular task, that may result in movement compensations and/or acceptance of passive loading from the joint and the connective tissue which could lead to potential overload of the joint. Furthermore, muscle imbalances may cause altered movement quality which can lead to greater motion compensations and reinforce improper form.

Knee extensor strength is a major barrier to functional progressions.³⁰ It is advised to assess knee extensor strength (respecting the time after surgery and possible ACL graft loading) and use this information to plan when to implement certain tasks or transition into different phases of rehabilitation. In addition, functional tasks require large force production for absorption from the whole kinetic chain. For instance, some tasks such as bilateral landing, running or single limb plyometrics may involve ground reaction force several times (2-6) body weight. A better understanding of the ability of the lower limb to generate and accept force will result in more precise transition between the tasks.

Assessing knee extensor strength using concentric or isometric assessment via the isokinetic dynamometer or using the leg press 8 or 10 repetition maximum (RM) can provide an indication of strength and be used to regularly monitor the patients to support task-based progressions.

Final monitoring component is the muscle soreness i. e., delayed onset of muscle soreness (DOMS). The degree of the soreness depends on several factors including the type and novelty of the exercise, duration, intensity and more. Higher level of muscle soreness can impact the future performance and increase the time of progression for the muscles to recover.

Task-Based Progression for ACL Recovery

Normal Walking Gait

The initial milestone and task target is typically to restore the normal walking gait after surgery without additional support from crutches or crutches. Following ACL reconstruction, a patient cannot fully withstand their own body weight or walk without crutches for a about two to four weeks. The abnormal gait patterns often become further exacerbated when the patient returns to running. Thus, re-establishing proper walking gait early and safely after surgery is a key priority.

Normal gait biomechanics cannot occur without optimal joint motion and so the restoration of joint range of motion is essential to improve the walking gait. After ACL reconstruction, patients should achieve full controlled extension while still using the crutches. To be able to reach full terminal extension, the ability to recruit the quadriceps and maintain active extension is crucial at that stage of the recovery. Quadriceps inhibition can prevent recovery of quadriceps muscle strength and the safe and expedient progression of rehabilitation. Persistent quadriceps lag on single leg raise has been shown to indicate an inability to actively fully extend the knee. If this is not achieved by week five post surgery, it would be considered a predisposing factor for significant quadriceps weakness at 6-months post-operation. Prior to leaving the crutches, it is suggested to achieve full active knee extension, control of effusion and no 'joint overload' (e.g., clinical increase of swelling, or pain and no quadriceps lag on active straight leg raise).

Bilateral Squat

Some patients after ACL reconstruction failed to symmetrically load their legs during squatting up to 12 months post-operation and this was related to poor functional outcomes. A bilateral squat is a foundation exercise, involving triple flexion and extension of the lower limbs, while maintaining trunk control. Bilateral squat progressions can begin with squat, wall squat, goblet squat, back squat, front squat and overhead squat. Initially, all squat variations should be performed without additional load and then with gradually increasing the external loading to to improve strength. At the beginning targeting lower knee flexion angles (< 90 degrees) are recommended. Optimal squat form is a great precursor to single leg progressions (e.g., split squat).

Unilateral Exercises (Single Leg Squat)

This is a functional movement that represents a single leg triple flexion and extension while maintaining control over the entire body with minimal support. It is a foundation movement

progression for other exercises requiring acceleration and single leg landing. Since the task requires almost the entire body weight bearing, it is recommended that the patient is able to leg press 100% body weight before performing a single leg squat in order to have the required strength. It is estimated, the split squat will have about 60% of the body weight on the front leg and 40% on the back leg. The authors of this paper suggest that a progression for a single leg squat includes split squat, reverse lunge, walking lunge, step up and single leg squat.

Bilateral Landing

During bilateral landing, the neuromuscular system of the patient is a subject to the ground reactions forces around 1.5-2 times body weight depending upon the height of the jump. Prior to practicing landing tasks on the ground, it is recommended that the athlete has attained at least one times body mass for a single limb and two-times body mass for double limb for set of eight repetitions on the leg press. Bilateral landing allows for the training of controlled eccentric acceptance of the body weight at the required speed, an important accomplishment that prepares the athlete for single limb acceptance drills such as running. Variations and progressions include landing from a box, landing from running on the spot, landing from a jump. These can also be vertical, horizontal or even rotational. Use of different landing surfaces can support the reduction in peak reaction forces at the beginning, such as use of a pool, sand or a mat.

Running

Running represents a functional activity and is often considered a milestone mark for the ACL reconstruction patients. It is a high load task and requires substantial strength and neuromuscular control. Each step taken during running represents weight acceptance of around 2-3 times body weight depending on the speed. Assessing running gait training on a treadmill may allow the clinician to provide feedback cues to support the improvement of the athletes running technique. Key aspects include normalization the range of motion of the involved joints which can be examined via video recording. Further analysis of stride length, contact times and force absorption by force plate embedded treadmills can facilitate more in-depth analysis and support optimal progression. Pain free symmetrical gait at near maximal sprint speeds should be the main goal of gait retraining. Optimal gait at slower running speed (8 km/h) is required for advancement to unilateral deceleration and landing training. It is essential that treadmill running mechanics are restored prior to progression to outdoor running or agility drills. It is important to note that many measurable parameters do not normalize during the first year following an ACL reconstruction.

Bilateral Plyometrics

Plyometrics are commonly used by athletes for developing explosive speed, strength, and power. These kinds of exercises consist of eccentric muscle contraction followed by a concentric contraction in a short amount of time by the same muscle or muscle groups. In addition, plyometric training can improve the limb strength, power, and increase joint awareness of the patients. High intensity plyometrics training can lead to muscle damage due to its eccentric component and excessive joint loading that could lead to reinjury. Typical impact from plyometric tasks performed on land is between 2-6 times body weight.

Unilateral Landing

ACL injuries often occur during deceleration and landing and these progressions can put the patients at higher risk of reinjuring the joint. However, the ability to absorb force during

eccentric loading is essential for the functional training process. Tasks requiring single leg landing and deceleration typically cause loading of the joint of 2-3 times body weight. Therefore, prior to performing these tasks, the athlete needs to have good single leg strength. It is recommended that the patient is able to push 1.5 times body weight or for eccentric loading 2 times body weight in a single leg press before progressing to single leg deceleration. Initially, single leg landing routines should be practiced on a surface that absorbs forces such as a mat or sand while progressively increasing the landing height.

Unilateral Plyometrics

The progression at that stage should be from a single plane to multi-planar plyometric motions to serve as a foundation for sport-specific drills. Unilateral plyometrics have usually 2-6 times body weight landing forces. The eccentric portion of this activity may lead to muscle soreness in addition to the risk of reinjury for the joint that the task itself presents.

Drills with Change of the Direction

Multidirectional movements and speed increases place higher stress on the joints and therefore gradual speed progress and complexity of the motion are important in order to prevent the risk of reinjury. Good control in 90-degree cut is recommended before transitioning to more complicated sport-specific tasks.

Sport-specific Movement

Sport-specific skill-based movements help the athlete to better prepare for sage participation in their sport. A program including gradually more challenging tasks such as multidirectional drills, sport-specific exercises and speed increase during motion has to be developed for that stage of the recovery.

Additionally, it is critical to evaluate the role and importance of perception/ cognition in movement and ensure this process is trained in the movement specific drills.

Lastly, contact training is an essential part of the sport-specific program to prepare the athlete for team sports participation. The progression of the task-based protocol is given in Table 3.3.

Task №	Task Category	Description	Strength Level	ROM
1	Walking	Walking without crutches	Good quad recruitment	Full extension
2	Bilateral Squat	Squat to 90° with less than 20% asymmetry	50% BW single leg leg press	Full extension, flexion >90°
3	Single Leg Squat	Single leg squat to 90°	80% BW single leg leg press	120° flexion
4	Bilateral Landing	Bilateral landing control from submaximal jump	100% BW single leg leg press or 150% BW double leg leg press/ squat	>130° flexion
5	Running	Treadmill running with 8 km/h	125% BW single leg leg press/ squat	>130° flexion

			and/or Isometric extension > 70% Limb Symmetry Index (LSI)	
6	Bilateral Plyometrics	30 cm bilateral drop jump	>80% LSI extension and 125% BW single leg leg press/ squat or 200% BW single leg leg press/ squat	Full
7	Unilateral Jump/ Landing	Single leg deceleration from forward and lateral running	> 80% LSI Isometric extension and/or 150% BW single leg leg press/ squat	Full
8	Unilateral Plyometrics	Single leg drop jump	> 80% LSI Isometric extension and/or 150% BW single leg leg press/ squat	Full
9	Change in Direction	90°cut manuver	> 80% LSI Isometric extension and/or 150% BW single leg leg press/ squat	Full
10	Sport-specific Movements	45° re-active change in direction	> 90% LSI Isometric extension and/or 200% BW single leg leg press/ squat	Full

Table 3. 3 Task Progression After ACL Reconstruction with Specific Requirements

3.5 Analyzing the Grid Structure as a Cellular Solid

When combing multiple flexible beams, a grid structure is created. The approach of analyzing this type of compliant flexures called cellular solids is given is [84]. An example of such structure is shown in Figure 3.5.

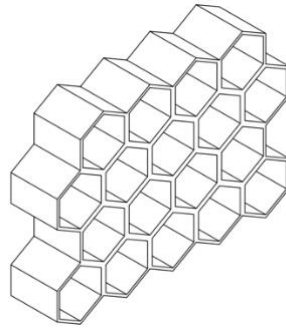


Figure 3. 5 Honeycomb Structure

2D Honeycombs: Polygonal cells in the plane; prismatic in the third direction.

The properties of these materials depend on:

- The material they are made of and its density ρ_s , elasticity E_s and strength σ_s properties.
- Relative density: the density of the cellular structure divided by the density of the solid: $\frac{\rho^*}{\rho_s}$.
- Cell geometry

Relative density

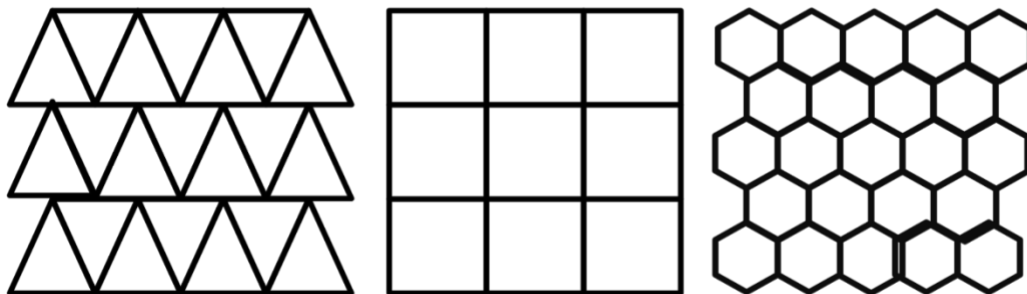
- Density of the cellular material, ρ^* ;
- Density of the solid material, ρ_s .

$$\frac{\rho^*}{\rho_s} = \frac{M_s}{V_t} \cdot \frac{V_s}{M_s} = \frac{V_s}{V_t} \quad (3.6)$$

Volume fraction of the solid (1 - the porosity).

where: M_s is the mass of the solid, V_t and V_s are the total volume and the volume of the solid respectively.

Unit Cells



a) Triangles b) Squares c) Hexagons

Figure 3. 6 Unit Cells of Cellular Solids with Different Geometry

There are several popular types of cellular solids with different number of the sides of the regular polygon as illustrated on Figure 3.6: triangles, squares, hexagons. Cells can be stacked in more than one way and therefore have different number of edges per vertex.

The three-dimensional variations of the cellular solids are known as foams.

3.5.1 Structural Analysis of Modeling Cellular Solids IN-Plane Properties

There are three main approaches for modeling cellular solids:

1. Unit cell: e. g. Honeycomb – hexagonal cell; for a foam – tetrakaidekahedron cell (idealization).
2. Dimensional analysis – for foams - complex geometry, difficult to model; instead modelling the deformational and failure mechanisms.
3. Finite Element Analysis (FEA):
 - can be applied to random structures.
 - local effects/defects can be observed.

Honeycombs – in-plane behavior

They have prismatic cells and are widely available in polymers, metals, and ceramics. Their application is for sandwich panels for energy absorption. Some natural materials such as woods and corks have a honeycomb structure.

Stress-strain behavior in-plane

For compression:

There are three regimes that can occur:

- linear elastic – cell wall bending.
- Stress plateau – buckling (for elastomeric materials), yielding (for metals), brittle crushing (for ceramics).
- Densification – cell walls touching.

By increasing the $\frac{t}{l}$ ratio (annotation from Figure 3.11 below), the E^* and σ^* will increase and ϵ_D (the densification strain) will decrease.

For tension:

- linear elastic – bending of the cell walls.
- Stress plateau – only if the material yields (no buckling in tension; brittle materials will fracture).

Variables, affecting the honeycomb mechanical properties:

Relative density:

$$\frac{\rho^*}{\rho_s} = \frac{\left(\frac{t}{l}\right)\left(\frac{h}{l}+2\right)}{2\cos\theta\left(\frac{h}{l}t\sin\theta\right)} \quad (3.7)$$

For regular hexagonal honeycombs $\frac{h}{l} = 1, \theta = 30^\circ$:

$$\frac{\rho^*}{\rho_s} = \frac{2}{\sqrt{3}} \frac{t}{l} \quad (3.8)$$

- Solid cell wall properties: $E_s, \sigma_{ys}, \sigma_{fs}$ (Yong's Modulus of the solid, yield strength of the material, fracture strength of the material respectively).
- Cell geometry: $\frac{h}{l}, \theta$.

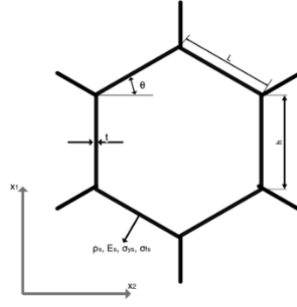


Figure 3. 7 Variables, affecting the honeycomb mechanical properties

For in-plane deformations the following assumptions can be made:

- t/l is small neglect axial and shear deformations.
- deformations are small – neglect any changes in the geometry of the cell during deformation.
- cell wall is linear elastic and isotropic.
- Symmetry: regular honeycombs have orthotropic – the structure remains the same after rotated 180° about 3 mutually perpendicular axes.

For linear elastic deformations the Hooke's Law can be applied:

$$\begin{bmatrix} \epsilon_1 \\ \epsilon_2 \\ \epsilon_3 \\ \epsilon_4 \\ \epsilon_5 \\ \epsilon_6 \end{bmatrix} = \begin{bmatrix} 1/E_1 & -\nu_{21}/\epsilon_2 & -\nu_{31}/\epsilon_3 & 0 & 0 & 0 \\ -\nu_{12}/\epsilon_1 & 1/E_2 & -\nu_{32}/\epsilon_3 & 0 & 0 & 0 \\ -\nu_{13}/\epsilon_1 & -\nu_{23}/\epsilon_2 & 1/E_3 & 0 & 0 & 0 \\ 0 & 0 & 0 & 1/\sigma_{23} & 0 & 0 \\ 0 & 0 & 0 & -\nu_{45}/\epsilon_4 & 1/\sigma_{13} & 0 \\ 0 & 0 & 0 & -\nu_{46}/\epsilon_4 & -\nu_{56}/\epsilon_5 & 1/\sigma_{12} \end{bmatrix} \begin{bmatrix} \delta_1 \\ \delta_2 \\ \delta_3 \\ \delta_4 \\ \delta_5 \\ \delta_6 \end{bmatrix} \quad (3.9)$$

Matrix notation:

$$\begin{array}{ll} \epsilon_1 = \epsilon_{11} & \sigma_1 = \sigma_{11} \\ \epsilon_2 = \epsilon_{22} & \sigma_2 = \sigma_{221} \\ \epsilon_3 = \epsilon_{33} & \sigma_3 = \sigma_{33} \\ \epsilon_4 = \gamma_{23} & \sigma_4 = \sigma_{23} \\ \epsilon_5 = \gamma_{13} & \sigma_5 = \sigma_{13} \\ \epsilon_6 = \gamma_{12} & \sigma_6 = \sigma_{12} \end{array}$$

In-plane (x_1, x_2) – 4 independent elastic constants: $E_1^*, E_2^*, \nu_{12}^*, G_{12}^*$,

The compliance matrix is symmetrical (reciprocal relation):

$$\frac{-\nu_{12}}{E_1} = \frac{-\nu_{21}}{E_2} \quad (3.10)$$

Notation for the Poisson's Ratio:

$$\nu_{ij} = \frac{\epsilon_j}{\epsilon_i} \quad (3.11)$$

On Figure 3.8 are shown the loading conditions and deformations for the three most common types of regular polygons used for cells – triangles, squares and hexagons respectively.

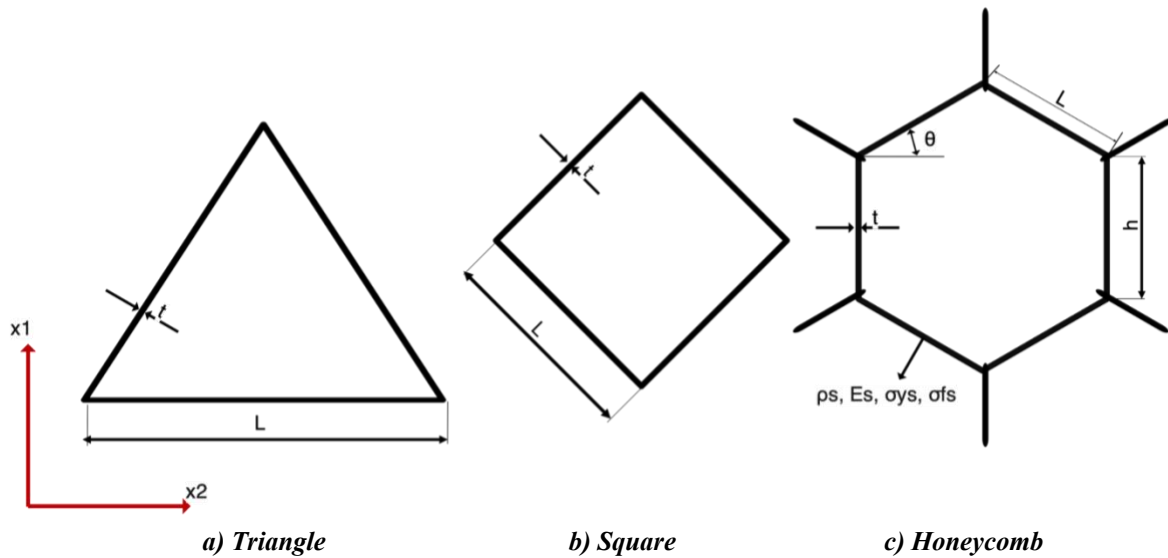


Figure 3. 8 Parameters of the Cell when Compression Loads Applied

Figure 3.8 gives more detailed view of the parameters of the hexagonal cells as well as the displacements.

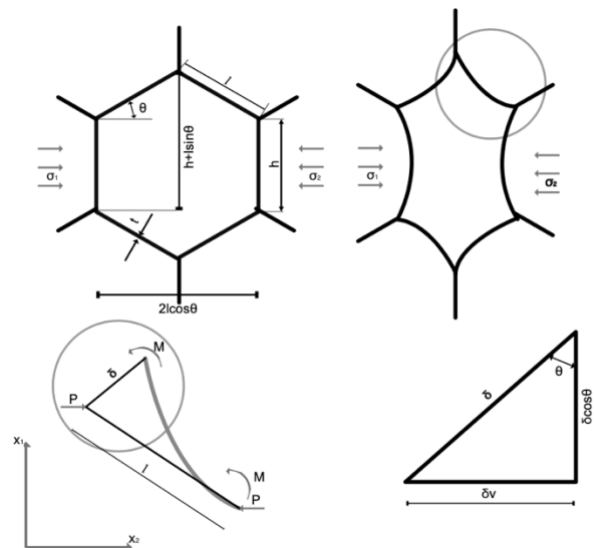


Figure 3. 9 Parameters of the Hexagonal Cell when Compression Loads Applied

The parameters shown in Figure 3.9 are:

- Depth b .
- σ_1 and σ_2 – global stress.
- In x_1 direction, the length of the unit cell is: $2l \cos \theta$.

- In x_2 direction, the length of the unit cell is: $h + l\sin\theta$.

From here, the global stress σ_1 can be derived:

$$\sigma_1 = \frac{P}{A} = \frac{P}{(h + l\sin\theta)b} \quad (3.12)$$

where: P is the applied loading; A is the cross-sectional area; h is the length of the beam; l is the length of the incline member (for regular honeycombs, $h=l$).

The strain ε_1 is equal to:

$$\varepsilon_1 = \frac{\delta\sin\theta}{l\cos\theta} \quad (3.13)$$

where: θ is the angle between the incline member and the horizontal axis and δ is the deflection of a member.

For a single cantilever as illustrated on Figure 3.9, the moment and the deflections are given in (3.14) and (3.15) respectively:

$$M_B - M_A = \int_A^B V dx \quad (3.14)$$

$$\Delta = \frac{FL^3}{3EI} \quad (3.15)$$

The honeycomb structure can be represented as two cantilevers of length $\frac{l}{2}$ as shown on Figure 3.10.

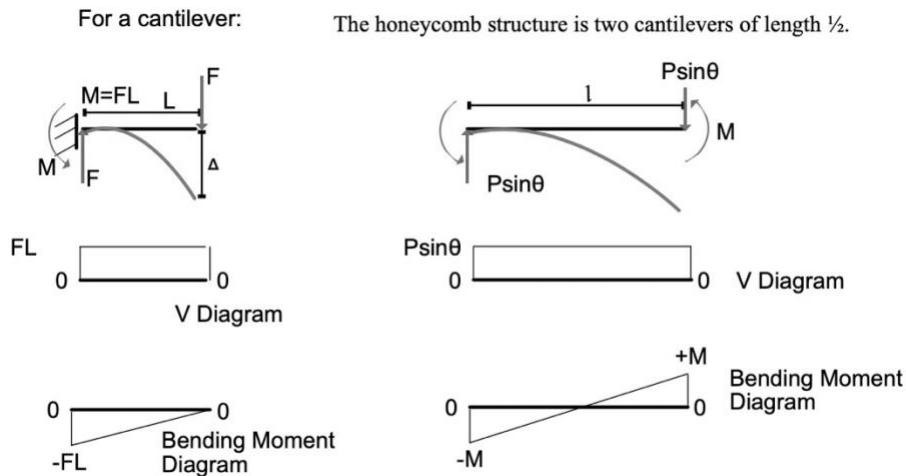


Figure 3.10 Cantilever Deflection

$$\delta = \frac{(2)P\sin\theta(l/2)^3}{3E_s I} = \frac{P\sin\theta l^3}{12E_s I} \quad (3.16)$$

$$I = \frac{bt^3}{12} \quad (3.17)$$

where: E_s is the modulus of elasticity of the solid material; I is the moment of inertia.

Combining (3.12) and (3.13) for the Young's modulus of the cellular structure can be calculated:

$$E_1^* = \frac{\sigma_1}{\varepsilon_1} = \frac{P}{(h + l \sin \theta) b} \cdot \frac{l \cos \theta}{\delta \sin \theta} = \frac{P}{(h + l \sin \theta) b} \cdot \frac{l \cos \theta}{P \sin \theta} \cdot \frac{12 E_s b t^3}{12} \quad (3.18)$$

$$E_1^* = E_s \left(\frac{t}{l} \right)^3 \cdot \frac{\cos \theta}{\left(\frac{h}{l} + \sin \theta \right) \sin^2 \theta} \quad (3.19)$$

* Refers to the cellular solid properties.

Important parameters:

- Properties of the solid: Young's Modulus of the solid E_s ;
- $\left(\frac{t}{l} \right)^3$ related to the relative density (volume fraction of the solid).
- $\left(\frac{h}{l} + \sin \theta \right) \sin^2 \theta$: factor that depends on cells geometry.
- For regular hexagonal honeycomb: $\frac{h}{l} = 1$; $\theta = 30^\circ$:

$$E_1^* = \frac{4}{\sqrt{3}} E_s \left(\frac{t}{l} \right)^3 \quad (3.20)$$

Poisson's Ratio (Loading in x_1 direction):

$$\nu_{12}^* = -\frac{\varepsilon_2}{\varepsilon_1} \quad (3.21)$$

Shortens:

$$\varepsilon_1 = \frac{-\delta \sin \theta}{l \cos \theta} \quad (3.22)$$

Lengthens:

$$\varepsilon_2 = \frac{\delta \cos \theta}{h + l \sin \theta} \quad (3.23)$$

$$\nu_{12}^* = -\frac{\varepsilon_2}{\varepsilon_1} = \frac{\delta \cos \theta}{h + l \sin \theta} \cdot \frac{l \cos \theta}{\delta \sin \theta} = \frac{\cos^2 \theta}{\left(\frac{h}{l} + \sin \theta \right) \sin \theta} \quad (3.24)$$

Poisson's Ratio only depends on the cell's geometry.

- For regular hexagonal honeycomb: $\frac{h}{l} = 1$; $\theta = 30^\circ$: $\nu_{12}^* = 1$.
- ν_{12}^* can be negative.

Non-linear Elasticity:

Compressive strength (plateau stress):

Cell collapse by:

- elastic buckling.
- plastic yielding.
- brittle crushing.

Elastic Buckling $(\sigma_{el}^*)_2$

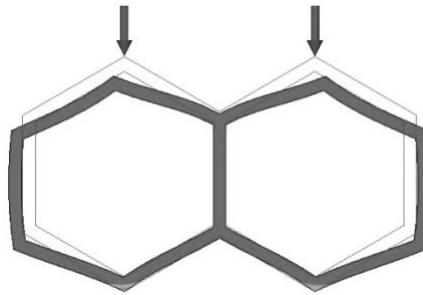


Figure 3. 11 Elastic Buckling

- Elastomeric honeycombs – cells collapse by buckling of the walls when loaded in x_2 direction.
- No buckling for σ_1 - bending of the incline cells leads to densification.

Euler Buckling Load:

$$P_{er} = \frac{n^2 \pi^2 E_s I}{h^2} \quad (3.25)$$

Where: n is end constraint factor; for pin-pin, $n=1$, for fixed-fixed, $n=2$; n depends on the stiffness of the adjacent incline members. Also, n depends on the ratio h/l .
For $h/l=1$, $n=0.686$; $h/l=1.5$, $n=0.76$, $h/l=2$, $n=0.806$.

$$(\sigma_{el}^*)_2 = \frac{P_{er}}{2l \cos \theta b} = \frac{n^2 \pi^2 E_s b t^3}{h^2 2l \cos \theta b 12} \quad (3.26)$$

$$(\sigma_{el}^*)_2 = \frac{n^2 \pi^2 E_s}{24} \frac{\left(\frac{t}{l}\right)^3}{\left(\frac{h}{l}\right)^2 \cos \theta} \quad (3.27)$$

For regular hexagonal cells:

$$(\sigma_{el}^*)_2 = 0.022 E_s \left(\frac{t}{l}\right)^3 \quad (3.28)$$

Since

$$E_2^* = \frac{4}{\sqrt{3}} E_s \left(\frac{t}{l}\right)^3 = 2.31 E_s \left(\frac{t}{l}\right)^3 \quad (3.29)$$

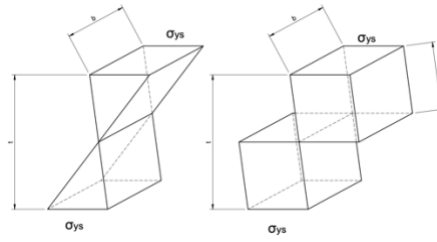
The strain at buckling $(\epsilon_{el}^*)_2 = 0.10$ for regular hexagonal honeycombs.

Plastic Stress: Plastic Yielding $(\sigma_{pl}^*)_1$:

Plastic Collapse:

- Failure by yielding in the cell walls.
- Yield strength at cell walls is σ_{ys} .
- The plastic hinge forms when the entire cross-section is fully yielded.

For elastic-perfectly plastic material when increasing the load, the entire cross-section yields and forms a plastic hinge as shown on Figure 3.12 b).



a) Elastic Deformation b) Plastic Hinge

Figure 3. 12 Loaded Cross-section of an Elastic-perfectly Plastic Material

The internal moment of the formation of a plastic hinge, M_p :

$$M_p = \frac{(\sigma_{ys}bt)}{2} \frac{t}{2} = \frac{\sigma_{ys}bt^2}{4} \quad (3.30)$$

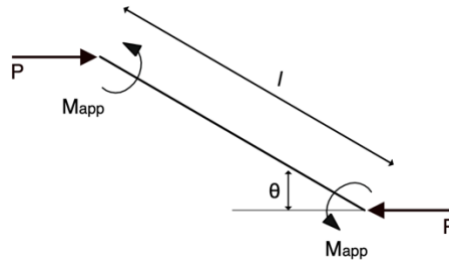


Figure 3. 13 Applied moment on the Incline Member

For the applied moments noted on Figure 3.13, the following equation can be obtained:

$$2M_{app} = -Pl\sin\theta = 0 \Rightarrow M_{app} = \frac{Pl\sin\theta}{2} \quad (3.31)$$

Equating the applied moment to the plastic moment and associating P to the applied stress σ_1 :

$$\sigma_1 = \frac{P}{(h + l\sin\theta)b} \quad (3.32)$$

Plastic collapse of the honeycomb at $(\sigma_{pl}^*)_1$ when $M_P = M_{app}$:

$$(\sigma_{pl}^*)_1 (h + l \sin \theta) b \frac{l \sin \theta}{2} = \sigma_{ys} \frac{bt^2}{4} \quad (3.33)$$

$$(\sigma_{pl}^*)_1 = \sigma_{ys} \left(\frac{t}{l}\right)^2 \frac{1}{2(h/l + \sin \theta) \sin \theta} \quad (3.34)$$

For regular hexagonal cells:

$$(\sigma_{pl}^*)_1 = \sigma_{ys} \frac{2}{3} \left(\frac{t}{l}\right)^2 \quad (3.35)$$

In the other direction:

$$(\sigma_{pl}^*)_2 = \sigma_{ys} \left(\frac{t}{l}\right)^2 \frac{1}{2 \cos^2 \theta} \quad (3.36)$$

For thin honeycombs elastic buckling may precede the plastic collapse. elastic buckling = plastic collapse stress at:

$$\frac{n^2 \pi^2 E_s}{24} \frac{\left(\frac{t}{l}\right)^3}{\left(\frac{h}{l}\right)^2 \cos \theta} = \left(\frac{t}{l}\right)^2 \frac{\sigma_{ys}}{2 \cos^2 \theta} \quad (3.37)$$

$$\left(\frac{t}{l}\right)_{critical} = \frac{12}{n^2 \pi^2} \frac{\left(\frac{h}{l}\right)^2}{\cos \theta} \frac{\sigma_{ys}}{E_s} \quad (3.38)$$

For regular hexagonal honeycombs:

$$\left(\frac{t}{l}\right)_{critical} = 3 \frac{\sigma_{ys}}{E_s} \quad (3.39)$$

e.g., Metals: $\frac{\sigma_{ys}}{E_s} \sim 0.002 \Rightarrow \left(\frac{t}{l}\right)_{critical} = 0.6\%$

Most metal honeycombs are denser and yield, don't buckle.

For polymers: $\frac{\sigma_{ys}}{E_s} \sim 3 - 5\% \Rightarrow \left(\frac{t}{l}\right)_{critical} = 10 - 15\%$

Low density polymers may buckle before yield.

Tension:

- Elastic moduli are the same as in compression.
- No elastic buckling in tension.
- Plastic plateau stress approximately the same as in compression (negligible geometrical difference).
- For brittle honeycombs, fast fracture.

Fracture Toughness K_{Ic} :

- Assume the crack length is large compared to the cell size as shown on Figure 3.17.
- Axial forces can be neglected.
- The modulus of rupture is constant for the cell wall.

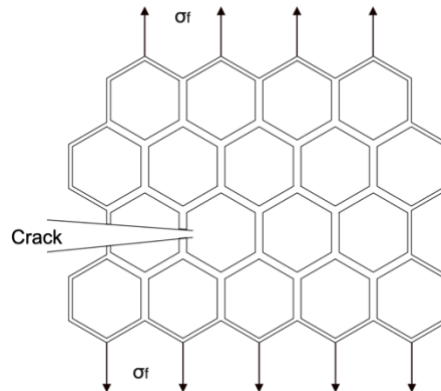


Figure 3.14 Fracture Toughness

In-Plane Triangular Cells:

Figure 3.18 contains the geometry and the parameters of a single triangular cell honeycomb. Those types of structures are characterized by the following:

- Depth b into the page (direction, perpendicular to the drawing).
- Behaves like a truss.
- Analyzed as pin joints (no moments at the nodes).
- Only axial loads along the members.
- Forces in each member are proportional to P .

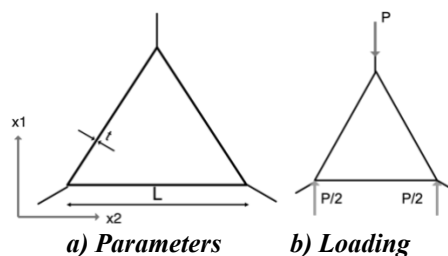


Figure 3.15 Triangular Cell Honeycombs

$$\epsilon \propto \frac{\delta}{l} \quad (3.40)$$

$$\delta \propto \frac{P}{E_s b t} \quad (3.41)$$

$$E^* \propto \frac{\sigma}{\epsilon} \propto \frac{P l}{l b \delta} \propto \frac{P E_s b t}{b P l} = C E_s \left(\frac{t}{l} \right) \quad (3.42)$$

where: C is a constant related with the cell geometry, for equilateral triangle, $C=1.15$.

Note: stiffer than hexagonal honeycombs - for hexagonal honeycombs, $E^* \propto \left(\frac{t}{l} \right)^3$.

In-Plane Square Cells:

The in-plane constants for triangular and square cells are fundamentally different from the hexagonal cells due to the bending moments on the cell walls are equal to zero for certain directions of the loading. In that case, elastic deformation is possible only by the axial extension or compression of the cell walls, and the resulting moduli are larger, by a factor, typically, of $\left(\frac{t}{l}\right)^2$ than for directions in which bending is possible. Square cells and their parameters are illustrated on Figure 3.16.

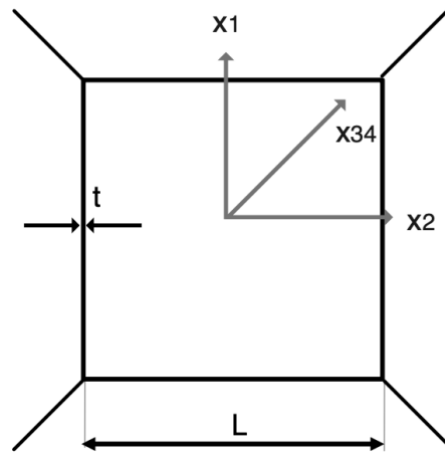


Figure 3.16 Square Cell Honeycombs

The Young's moduli E_1^* and E_2^* parallel to the cell walls are:

$$\frac{E_1^*}{E_s} = \frac{E_2^*}{E_s} = \frac{t}{l} \quad (3.43)$$

Those in the diagonal direction, called E_{34}^* , are given by:

$$\frac{E_{34}^*}{E_s} = 2 \left(\frac{t}{l}\right)^3 \quad (3.44)$$

This result can be obtained from the limit of the equations for hexagonal cells when $h=0$ and $\theta=45^\circ$.

3.5.2 Honeycombs: Out of Plane Properties:

The out of plane schematics of the honeycomb cellular structures is shown on Figure 3.17.

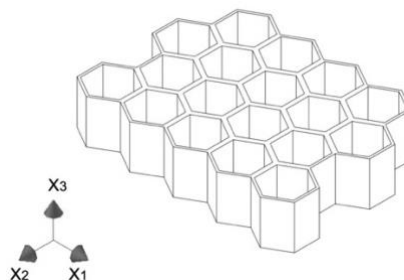


Figure 3.17 Out of Plane Schematics

In this orientation, the honeycomb structures have the following characteristics:

- Used as cores of sandwich panels.

- Used to absorb energy.
- The cell walls contract and expand instead of bending.
- Stiffer and stronger in x_3 direction.

Linear-elastic Deformations:

Young’s Modulus, E_3^* :

Cell walls contract or extend axially.

$$E_3^* = E_s \left(\frac{\rho^*}{\rho_s} \right) = E_s \left(\frac{t}{l} \right) \frac{(h/l + 2)}{2(h/l + \sin\theta) \cos\theta} \quad (3.45)$$

Note: $E_1^*, E_2^* \propto \left(\frac{t}{l} \right)^3$; huge anisotropy.

Poisson’s Ratio:

For loading in x_3 direction, cell walls strain by $\nu_s \epsilon_3$ in the other 2 directions.

$$\nu_{31}^* = \nu_{32}^* = \nu_s^* \quad (3.46)$$

3.5.3 Sandwich Panels

Honeycombs are lighter than the foams for a given stiffness or a strength. Foams provide thermal insulation. The mechanical properties of the sandwich panel depend on the face and core materials and panel geometry. Typically, the panels have requirements for stiffness/strength and the weight has to be minimized.

Sandwich beam stiffness:

Figure 3.18 is a schematic view of a sandwich beam with a bending loading applied at the middle.

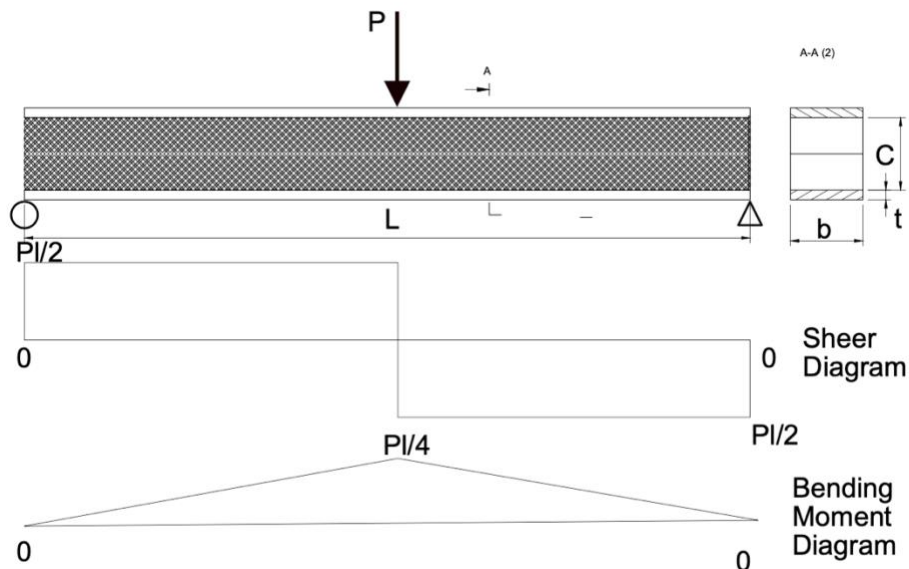


Figure 3. 18 Loading of a Sandwich Beam

Parameters of the sandwich panels:

Face: ρ_f, E_f, σ_f

Core $\rho_c^*, E_c^*, \sigma_c^*$

Solid of the core: ρ_s, E_s, σ_{ys}

$E_c^* \ll E_f$

$\delta = \delta_b + \delta_s$ – bending and shear deflection.

$$\delta_b = \frac{Pl^3}{B_1(EI)_{eq}} \quad (3.47)$$

where B_l is a constant depending on the loading configuration. For 3-point bending, $B_l=48$; for a cantilever: $B_l=3$.

Parallel axes theorem:

$$(EI)_{eq} = \frac{E_c^*bc^3}{12} + \left(E_f \frac{bt^3}{12}\right)^2 + E_fbt \left(\frac{c+t}{2}\right)^2 \quad (3.48)$$

$$(EI)_{eq} = \frac{E_c^*bc^3}{12} + \frac{E_fbt^3}{6} + E_fbt \left(\frac{c+t}{2}\right)^2 \quad (3.49)$$

4 Results

4.1 Research Background and Past Work

4.1.1 Development of a Compliant Multi-material Universal Joint

A 3D model of a cross-spring compliant joint was created [85]. It performs the motion by deformation in the elastic region and is suitable for precision engineering applications and instruments. The proposed concept is a modification of a traditional cross-spring pivot, which effectively provides frictionless and wear free in-plane motion. The joint's behavior is analyzed based on a non-linear FEA simulation and the properties were investigated with various loading conditions.

The main purpose of this model is to explore the spatial behavior of the beams that the joint consists of to verify the application of such a 3D printed structure for a knee supportive wearable where the model will function and have to undergo not only single plane stress but a combination of deformations due to the complex motion of the knee.

The motion of the proposed model occurs as two rotations in orthogonal planes. The design of the compliant multi-material joint consists of two three leaf cross-spring pivots rotated at a 90° angle according to the Z-axis of the origin coordinate system as shown on Figure 4.1.

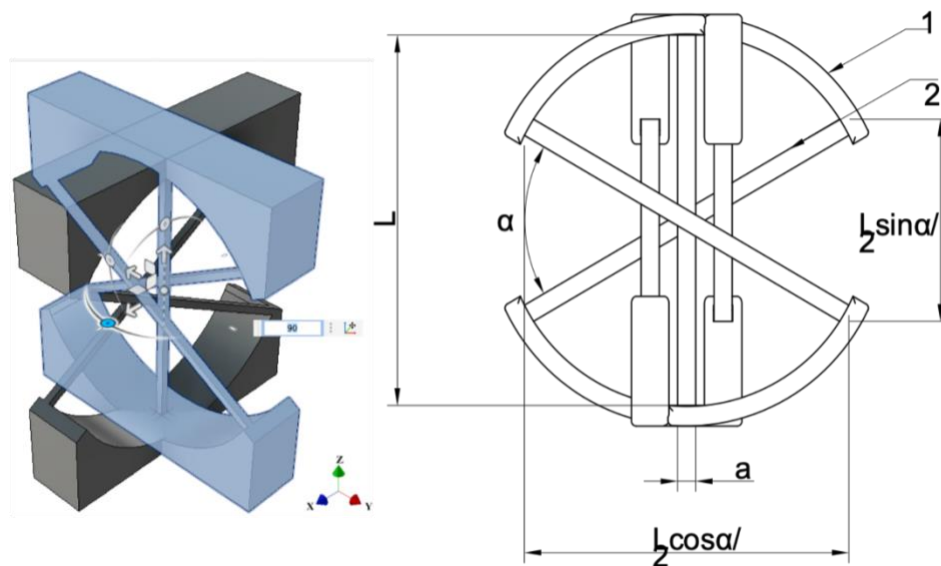
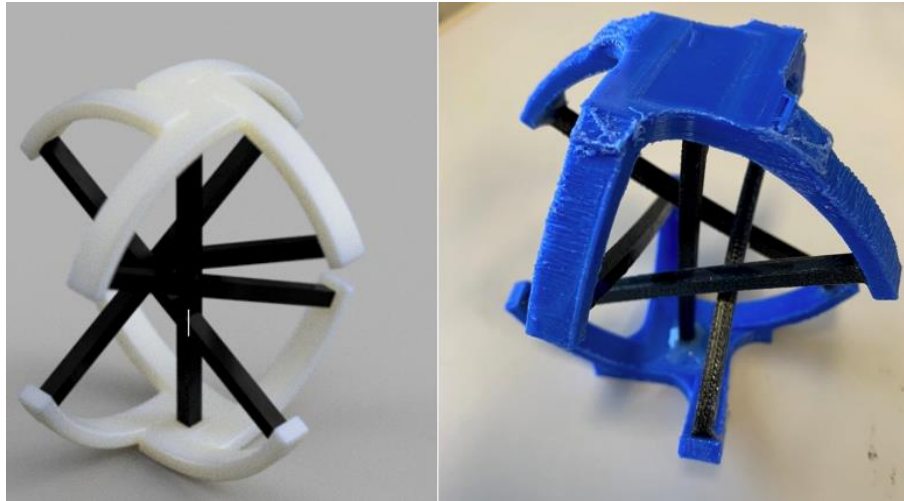


Figure 4. 1 Design of the Compliant Joint

On Figure 4.2 are shown a) a 3D rendered model and b) a physical 3D printed prototype of the compliant multi-material joint. The platforms are printed from a solid material PLA (polylactic acid) and the beams from a flexible filament – TPU (Thermoplastic Polyurethane). This multi-material combination provides unique capabilities. The platforms that attach to other components are rigid but the beams that execute the motion throughout deformation are flexible.



a) 3D Rendered Model b) 3D Printed Prototype
Figure 4.2 A Model and s 3D Printed Prototype

The performance of joint has been analyzed under various loading conditions illustrated alongside with the deformations on Figure 4.3 such as a) compression, b) tension, c) bending of the model. On the right side of the figure, the platforms are removed, and the direction of the forces is annotated for the different loading cases.

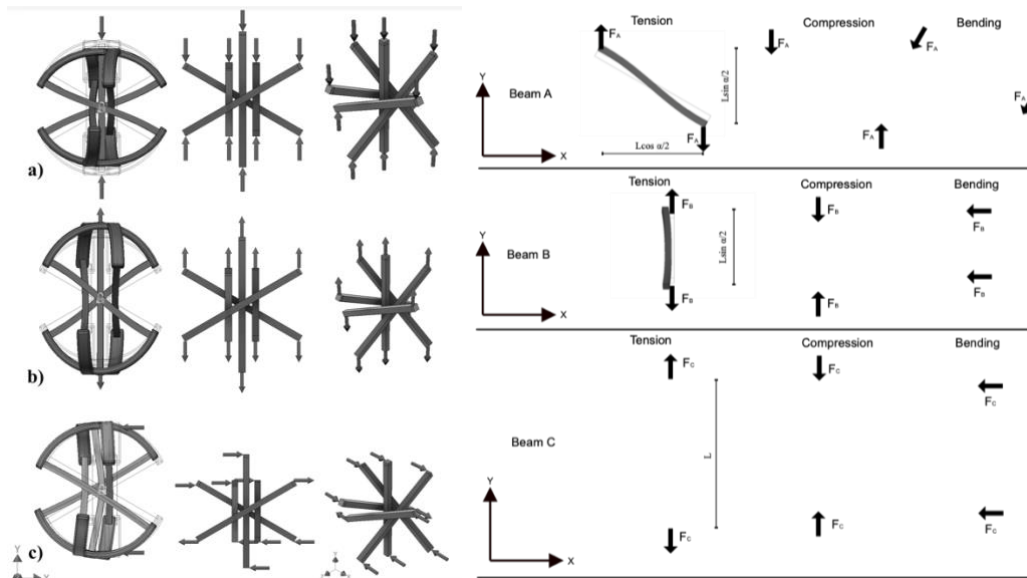


Figure 4.3 Loading Conditions of the Joint and the Individual Beams

The first 3 beams only have unique loading variations. The last 2 behave similarly to the first 2 due to the symmetry of the model. Figure 4.3 shows the orientation and position of the loads for these 3 beams for compression, tension and bending.

On Figure 4.4 are shown the results from the studies for tension a) and b) and bending c) and d). As it can be observed, in b), there is a rotation of the top platform due to the tensile forces. The results for compression are similar to the tension with the reversed direction of the rotation. The displacements corresponding to axial load ranging between 2 N and 20 N with the increment of 2 N are shown on the plots of Figure 4.9 a). On Figure 4.9 b) the displacements related to the transverse load are given, the range of which is 0.05 N to 0.2 N with the step size of 0.05 N.

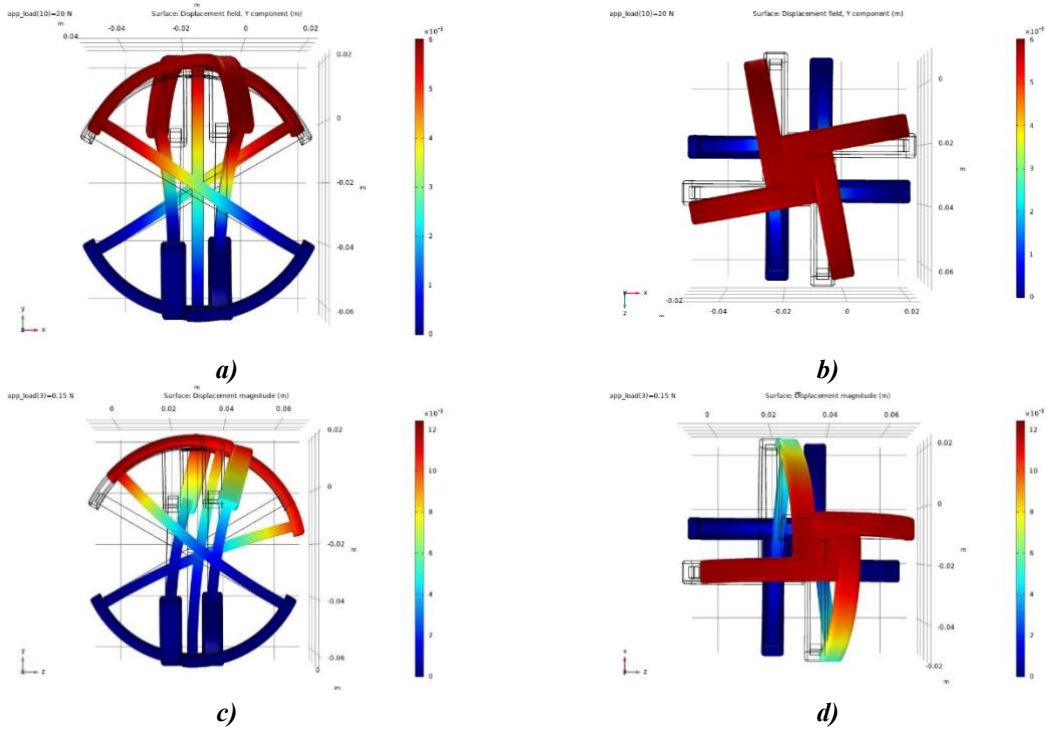
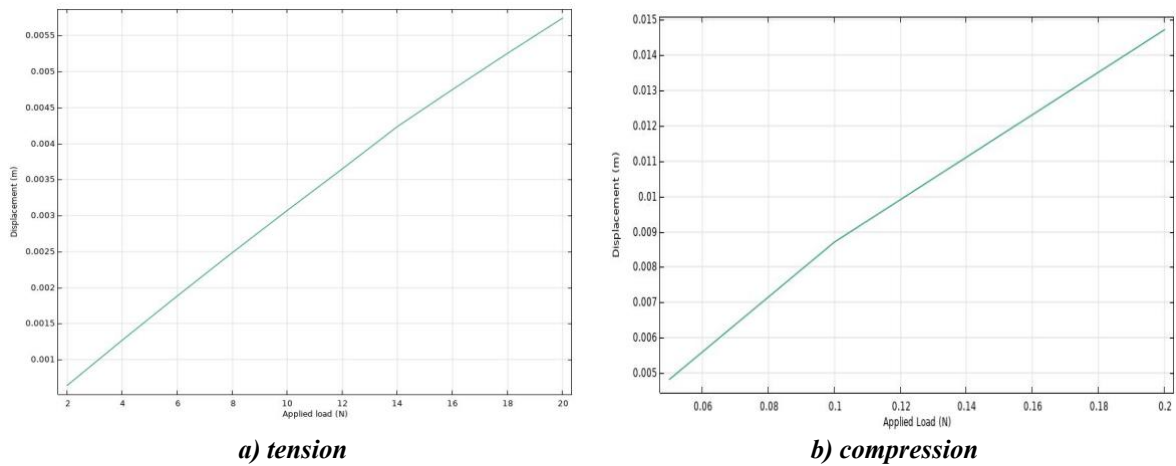


Figure 4.4 Strains Induced due to Axial and Transverse Loading

As illustrated in Figure 4.5, a nonlinear behavior of the model can be observed when large deformations occur due to the nonlinear properties of the joint.



a) tension **b) compression**
Figure 4.5 Displacement vs Load plot for axial loading

The FEA simulation studies yield conforming results to the physical behavior of the design. The proposed configuration of the cross-spring pivot provides greater rotational stability due to the additional center leaf placed along the axis of the joint. However, in transverse plane when axial forces applied additional rotation can be observed about Z-axis. Designing such compliant joint for specific applications can be improved by parameterization of center-shift phenomenon and characterizing the mechanical properties of the flexible 3D printing materials. The proposed design of a cross-spring joint has geometry similar to the ligaments of the human knee joint and therefore, its applications have been inspired by the function of the knee ligaments since their geometrical similarities such as precision adjustments unbalanced forces in small displacement sensitive instruments.

4.1.2 A Computational Model for 3D Printing of Orthoses Based on a Systematic Structural Analysis for Reverse Engineering Oriented Production

In [86] a framework for computational analysis and automatic generation of 3D compliant models suitable for applications in Orthoses is explained. The tool can generate solutions automatically for orthotic supportive device. A schematic representation of these supports is presented at Figure 4.6.

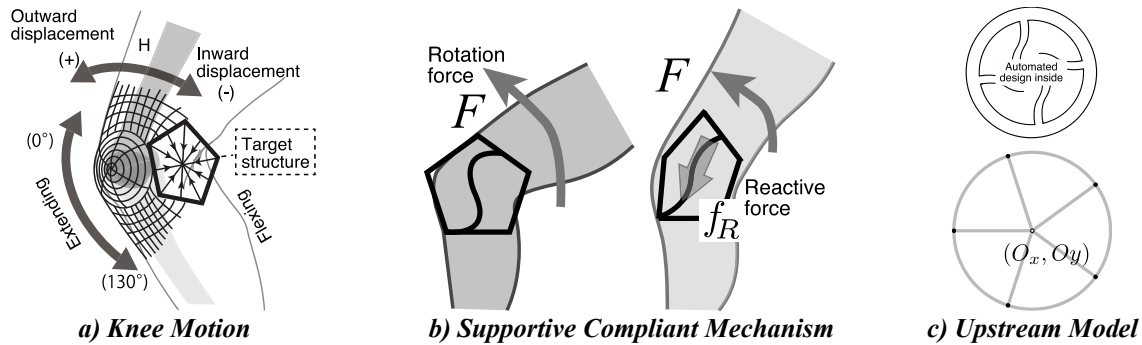


Figure 4. 6 Compliant Mechanism as a Knee Orthosis

A testing system was developed with a programmable actuator by the company Hebi Robotics [85] with displacement, velocity torque sensors (X series model) to replicate the basic knee flexion and extension. The actuator and the tested samples are shown in Figure 4.7 a) and b), respectively. By using the programmable actuator, the 2D plate-based orthosis part was examined, and necessary forces with respect to the displacement were automatically recorded. The automated experiment offers a quantitative validation.

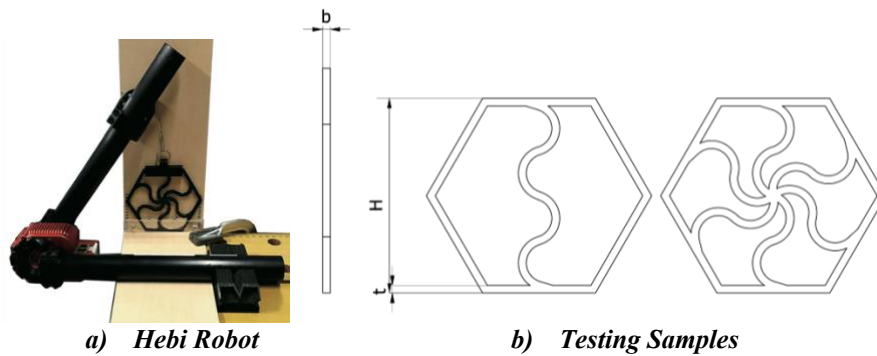


Figure 4. 7 Experimental Setup

The actuator with embedded sensors enables simultaneous control of displacement, velocity, and torque as well as three-axis inertial measurement and records of the values as temporal sequences every 10 [ms]. Temporal sequences of position (angle of the rotation), velocity and torque were performed and recorded by the actuator and the accumulated data can be analyzed for systematic comparison.

Figure 4.8 shows a comparison between data obtained from different designs, with hexagonal outer shape and with 1 or 3 “S” curved connecting part as compliant mechanisms.

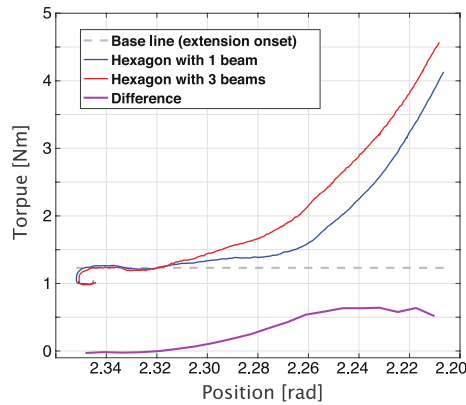


Figure 4. 8 Results Comparison of the Physical Test

Th tensile forces increased, and the force difference was saturated from the midpoint, which implies that the kinetic difference was 1 [Nm]. The result indicated that the tensile force can be varied depending on the number of beams and the design can easily be modified to adjust the target value of the resistance.

Focused on a supportive device for flexion and extension of the human knee, a compliant mechanism-inspired design was newly introduced and validated in the resistance of tensile loading force.

4.2 Flexible Bar Geometric Designs for Personalized Knee Orthoses Inspired by Compliant Mechanisms

In [87] the analysis and properties of flexible 3D Printed beams with applications in Orthoses is discussed.

4.2.1 Introduction

3D printed compliant mechanisms were recently highlighted not only for their traditional application, but also in the reverse engineering of human joint supportive devices. However, there is still a lack of systematic design principles for developing a custom-made adjustable orthotic device to fit the target body part requirements. In this study, a geometrical approach providing the target design by using a morphological replacement at the concentration of stress is proposed. This concept is verified in 3D printed orthotic devices to improve the knee joint function during recovery from an injury. It allows larger deformations of the beams to control the motion of the joint. Theoretical analysis and experiments demonstrate the flexibility and support during the flexion and extension of the knee. It implies the impact of the geometry in orthosis design.

4.2.2 Methodology

Flexible Beams and the 3D Printing Parameters for their Fabrication

Proposed beams were designed in Autodesk Inventor Professional [92]. . Initially, divided into four groups (A, B, C and D) based on common geometrical features. For the beams in Group A, geometry is removed from a simple beam annotated with 0. In Groups B, C and D, geometry is added to the beam as a half regular polygon with different number of the sides – square, hexagon and half circle, respectively. All models have common features - length $l=160$ mm and a square cross-section $a=10$ mm. As mentioned, the compliant hinging principle is varied. All variations and their groups are shown on Figure 4.9. The parameters that are unique for a given group are given on the figure as well. Once 3D printed, the physical pretotypes of the beams will be attached on the inner and outer sides of the knee forming a supportive device that provides guided flexion of the joint. Therefore, the beams have to match certain requirements such as compactness, providing lateral stability of the knee joint and supporting the knee flexion and extension.

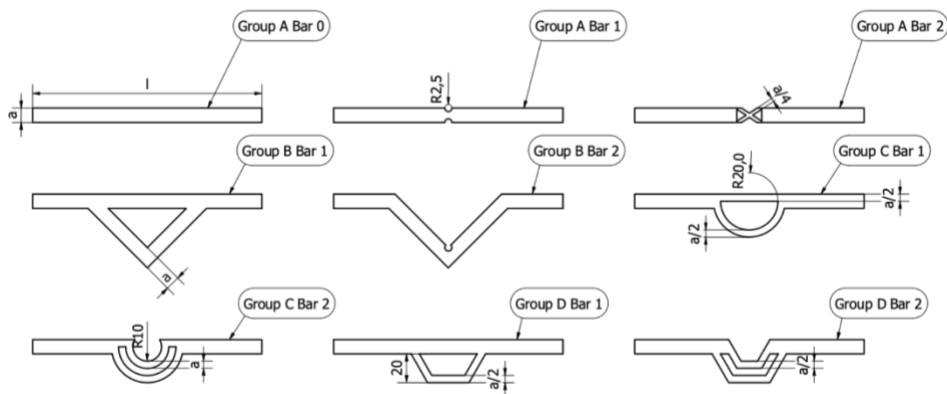


Figure 4. 9 Beam Groups

All beams were fabricated by using the Fused Deposition Modeling (FDM) technology on a 3D printer Anycubic i3 Mega [88] with a flexible Thermoplastic Polyurethane (TPU) filament called Ninjaflex available commercially at [89]. The samples were printed under the same condition and parameters, as shown in Table 4.1, the configurations of the slicing software Ultimaker Cura are illustrated [90]. The orientation for a sample on the 3D printing platform is also the same, the models are flat with their surface in the platform. As shown in Table 4.3, the samples were printed with infill density of 90% and infill pattern known as Cross 3D, which is described by the slicing software Ultimaker Cura in [91] as a strong 3D infill. It suggests that it is a robust infill suitable for 3D deformations.

In addition, the infill density percentage is highly important related to stiffness of the parts. In principle, the higher infill density, the stiffer the part is. However, with the increase of the infill density, the samples become heavier. Further, the time duration of the printing process increases as well. The increase is linear up to 90% and then it spikes significantly at a 100%. Therefore, 90% was chosen for infill density in this study to avoid unnecessary processing time with a certain strength.

Parameter	Values
3D printer	Anycubic i3 Mega
Slicing Software	Ultimaker Cura
3D printing Material	Ninjatek Ninja Flex TPU Filament
Printing Temperature [°C]	230 (Recommend for the material)
Platform Temperature [°C]	60
Supporting Material	No
Infill Density [%]	90
Infill Type	Cross 3D
Layer Height [mm]	0.1
Printing Speed [mm/s]	30

Table 4. 1 3D Printing Processes

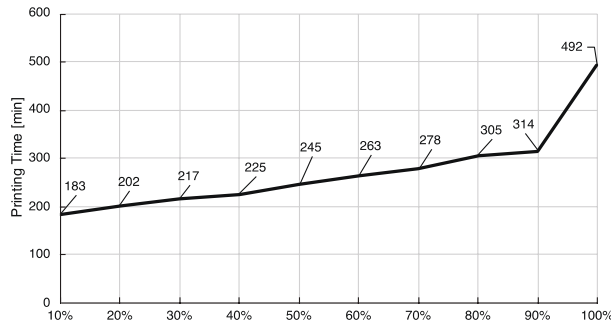


Figure 4. 10 Relationship between the 3D printing Infill Density and the Printing Duration

The example shown on Figure 4.10 is for Group A Bar 0 but applies for all samples.

Load Analysis of the Beams

The main requirement of the beams is to provide the lowest resistance support the motion during knee flexion (in plane bending while at the same time preventing lateral (out of plane) motion). In addition, the full range of motion of the human knee joint must be considered as well – from fully extended knee – 0° to fully flexed knee at 140° degrees. The designed compliant beam must provide deformation in this range. However, due to its symmetry, each side of the joint need to deform at about an angle of 70°.

The samples have been tested in non-linear environment using Autodesk Inventor Nastran [92, 93].

The models illustrated in Figure 4.11 represent a schematic view of the loading conditions. The members are fixed in one end and at the other a roller support is used. An equal for all models force is applied at the middle where the articulation occurs.

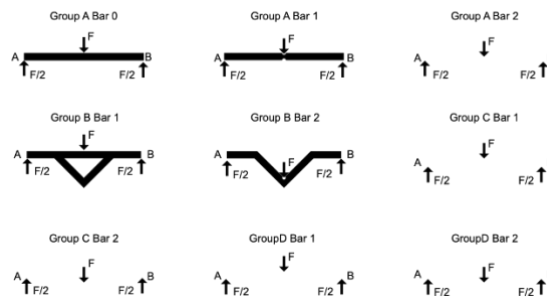


Figure 4. 11 Loads on the Beams

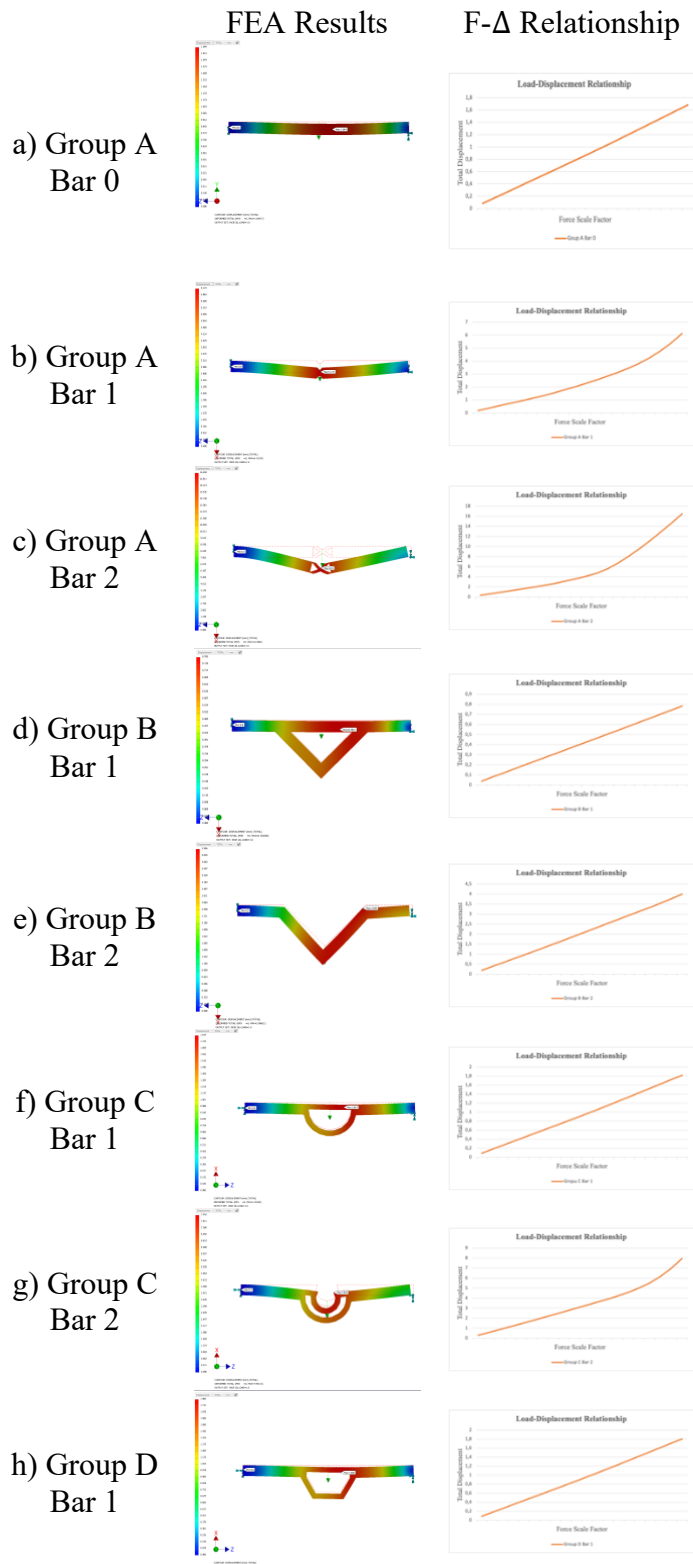
The results of the FEA analysis will show which bars deform the most under the same boundary conditions. The beams realizing the highest values of the deformations are suitable candidates as a knee assistive device.

4.2.3 Results

All beam models were subjected to a Finite Element Analysis in the Non-linear static stress environment of Autodesk Inventor Nastran where a 3-point bending test was conducted on the samples. The study accounts for the large deformations and uses a non-linear elastic material. All beams are loaded with the same force $F=150$ [N] in negative Y direction as shown on Figure 4.23. The mechanical properties of the material are based on the Ninjaflex TPU filament – Young’s Modulus is 12 [MPa], Tensile Strength 26 [MPa] and Poisons Ratio is 0.35. The simulation of each sample includes 20 increments. The purpose of this study is to show the beams with the highest deformations with the same loading applied based on the geometry while accounting for the non-linearities from large deformations of the model and the

anisotropic material. Figure 4.11 shows the setup of the analysis and the results for the displacements.

The plots on Figure 4.12 summarize the results from the analysis for the stress and the displacements of the beams during the FEA bending test. The values are arranged from the smallest to the largest.



i) Group D
Bar 2

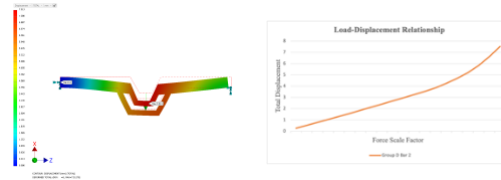


Figure 4. 12 Non-linear Static Stress Analysis of the Bars with the Largest Deformations

As it can be observed in Figure 4.13, the samples that experienced the highest values of the stress and the displacements are from Group A bars 3, 2 and 4. The lowest values belong to samples from Group B – bars 1 and 3. Similarly, the displacements with highest values are again members from Group A Bar 2 and Group C Bar 2 respectively and the lowest – Group D bars 2.

As it is expected, the highest deformations lead to the highest levels of the stress in the samples.

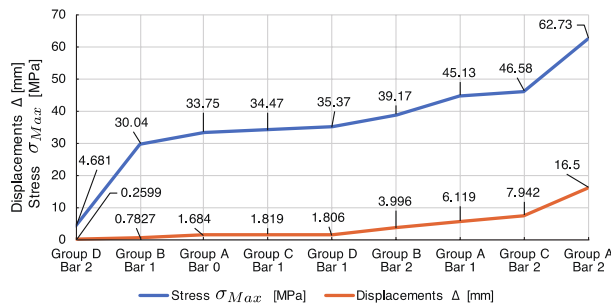


Figure 4. 13 Mechanical Behaviors of the Bars Based on the Geometry

For the samples to be applicable for an Orthotic device, a good balance of the stress and the strain (displacements) relationship is required. Therefore, possible candidates are Group A Bar 2 and Group C Bar 2.

The force-displacement relationships for all beams after the simulations are illustrated on Figure 4.14. The non-linear behavior of the models can be observed from the plots. For some beams such as Group A Bar 0, Group B Bar 1 and Group D Bar 2, the load of 150 N was not significant enough to deform them out of the linear elastic region.

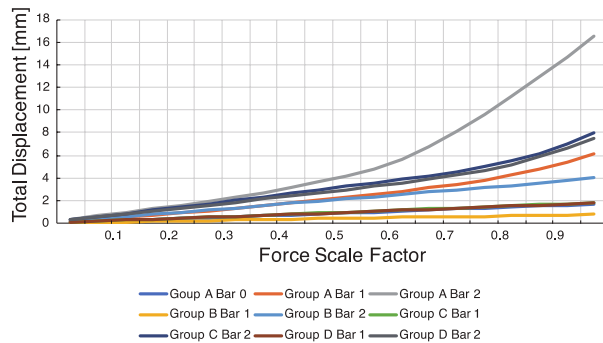


Figure 4. 14 Non-linear Deformation of the Bars – FEA Results

Figure 4.15 illustrates the measured 3D Printing time in minutes. It can be observed that Group B Bar 1 takes more 2 hours longer than the other samples.

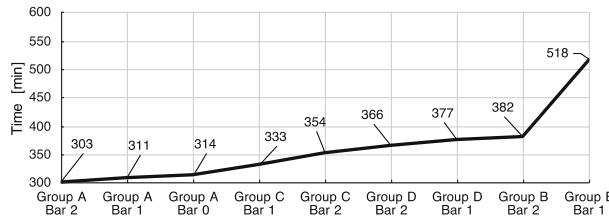


Figure 4.15 3D Printing Time of the Samples Mass of the Samples

As it can be observed from the Table 4.2, Bars 1 and 2 from Group A and Bar 2 from Group C are the models with most points and therefore most appropriate for the task. To support a smooth knee flexion and extension, a large degree of the displacement is necessary. Group C Bar2 has a flat planar geometry that helps prevent twisting motion.

Name	Displacements	Out of Plane Motion
Group A Bar 0	X	X
Group A Bar 1	✓	X
Group A Bar 2	✓	X
Group B Bar 1	X	✓
Group B Bar 2	X	✓
Group C Bar 1	X	✓
Group C Bar 2	✓	✓
Group D Bar 1	X	✓
Group D Bar 2	X	✓

Table 4.2 Evaluation of the Samples

4.2.4 Discussion

In this research the application of the flexible compliant beams fabricated by using the advancements in the Additive Manufacturing in the field of orthopedics as a knee supportive device is investigated.

In order to achieve that, 9 models were developed and analyzed in non-linear studies accounting for the large displacements the supports have to undergo in a real working environment. However, the simulations are not used to provide precise values of the stress-displacement relationships but to limit the models with less flexible properties due to their geometry.

It is important to mention, the out of plane deformations that have to be eliminated to provide a lateral stability of the knee were not included in the FEA studies. They are subject to the future development of the models.

After the evaluation process of the samples, due to its better out of plane stability Bar 2 from Group C was implemented in such a device 3D Printed from a material PPGW (Polypropylene Glass Wool). The prototype support is shown on Figure 4.16 a) extended and b) flexed knee. It allows free motion (bending) and stabilizes the joint during walking.

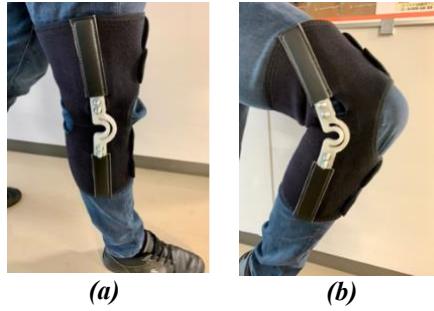


Figure 4. 16 Physical Prototype Used in Orthotic Support

4.2.5 Physical Tests and Comparison of the Models

As discussed above, Group C Bar 2 has been chosen and fabricated. Additionally, to determine the properties of the model, a bending test simulating the knee flexion has been conducted with the help of the artificial leg illustrated at Figure 4.18.



Figure 4. 17 Artificial Leg for Simulating Knee Flexion

The experimental setup is as follows: the supportive device shown on Figure 4.17 was attached to the artificial leg from Figure 4.18 and the leg was bent. The force was recorded by a force gauge as described on Figure 4.19.

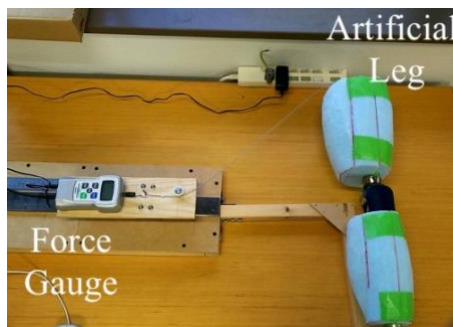


Figure 4. 18 Artificial Leg Experimental Setup

Figure 4.20 presents a model of the experimental setup with the parameters of interest.

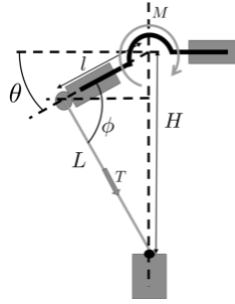


Figure 4.19 Model of the Experimental Setup

The force of the artificial leg was recorded without any supportive device attached. After, the supportive device was added, and the force was obtained once again. The loading on the leg was substituted from the combined loading of the leg and the supportive device to determine the force needed to deform only the support.

Important parameters here are the moment M generated around the bending axis and the tension T in the wire.



$$\sin\theta = \frac{H^2 + l^2 - L^2}{2lH} \quad (4.1)$$

$$\varphi = \theta + \arccos \frac{l \cos\theta}{L} \quad (4.2)$$

$$M = Tl \sin\varphi \quad (4.3)$$

where: L is the length associated with the lower limb (the tibia), l is the length of the thigh (the femur), φ is the bending angle and θ is the angle between the femur and the horizontal axis (for the measurement purposes of this experiment $\theta < 90^\circ$).

Several models were tested and compared during this experiment as described at Table 4.3.

Name	Description	Material	Image
Genu Direxa (M)	Model of the company Ottobok	-	
Genu Airexa	Model of the company Ottobok	-	

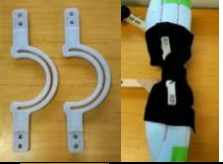






ArizonoR50th5	$R_1=50 \text{ mm}$ $R_2=40 \text{ mm}$ $\theta =5^\circ$	PPGW	
Arizonoa25b50th5	$a=50 \text{ mm}$ $b=25 \text{ mm}$ $\theta =5^\circ$	PPGW	
ArizonoR50th5BI	$R_1=50 \text{ mm}$ $R_2=40 \text{ mm}$ $\theta =5^\circ$ Inside attachment	PPGW	
ArizonoNewA	$R =50 \text{ mm}$ $a=50 \text{ mm}$ $b=40 \text{ mm}$ $\theta =15^\circ$	PPGW	
ArizonoNewB	$R =50 \text{ mm}$ $a=50 \text{ mm}$ $b=40 \text{ mm}$ $\theta =15^\circ$	PPGW	
ArizonoNewC	$R_1=50 \text{ mm}$ $R_2=40 \text{ mm}$ $R_3=30 \text{ mm}$ $\theta =15^\circ$	PPGW	
ArizonoNewD	$a=60 \text{ mm}$ $b=30 \text{ mm}$ $\theta =15^\circ$	PPGW	

Table 4. 3 Description of the Tested Models

On Figure 4.20 below are illustrated all samples and their main parameters.

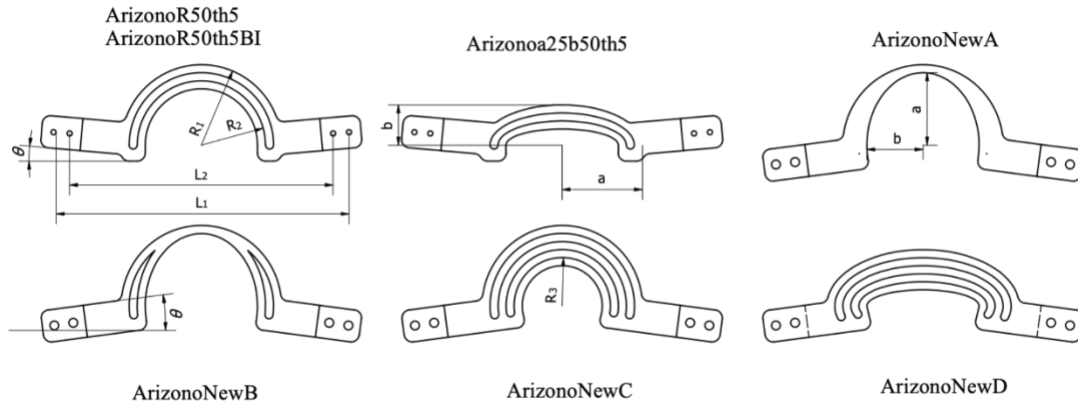


Figure 4. 20 Sample Models

where R_1 , R_2 and R_3 are the radiuses from the biggest half circle to the smallest, respectively; a and b are the bigger and smaller radiuses of the elliptical models and θ is the angle between the ages of the attachment arms.

The results of the experiment are plotted on Figure 4.21.

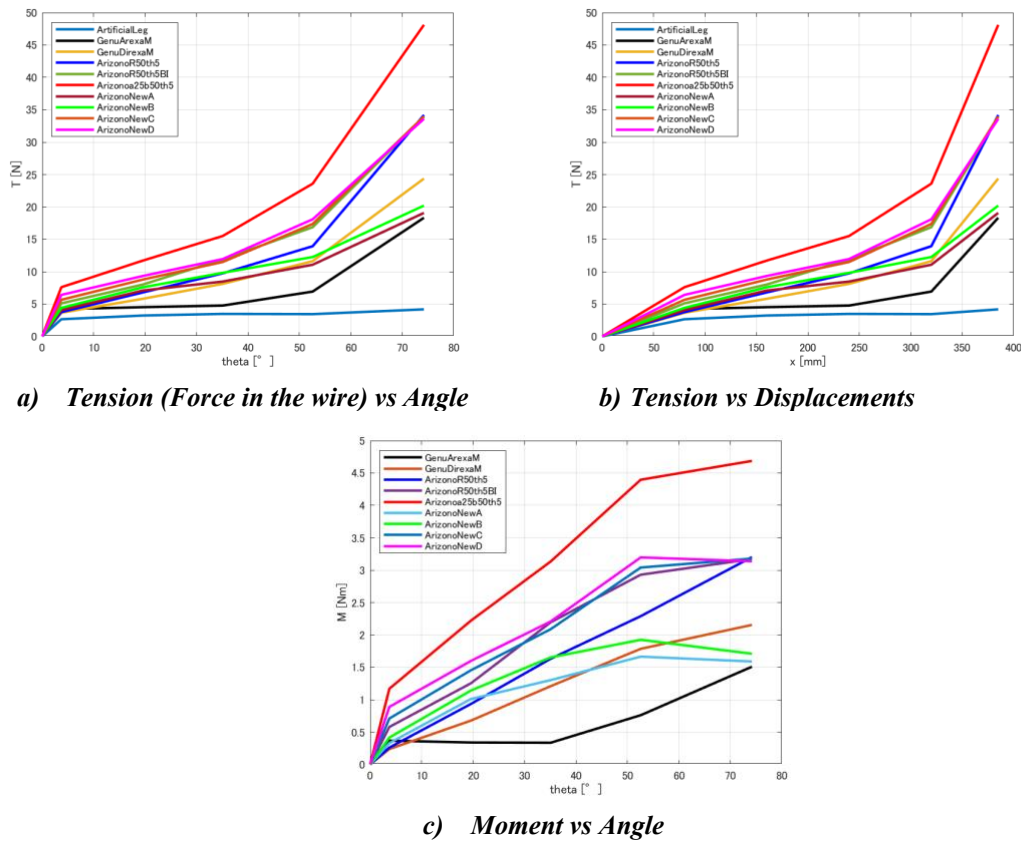


Figure 4. 21 Comparison of the Tested Samples

As it can be observed from the plots, the already existing solutions provided by the industry leader Ottobok (Genu Direxa (M) [94] and Genu Airexa [95]), and the 3D printed models have varied flexibility that can graded and organize to enhance the rehabilitation process and even make it safer. That means the 3D printed orthotic devices can be used in the rehabilitation process as a subsequent of the harder supports. This way the gap between the currently available devices can be narrowed down by including the soft 3D printed options. The recovery of the patients is a very gradual process of increasing the level of activity and the range of

motion of the joint. However, the existing solutions cannot tackle this progression fully due to the flexibility and adjustability limitations. The proposed designs are based on modulus principle and options with different stiffness/flexibility can be easily replaced. In addition, its comparable cost makes it strong candidate to fill in the existing void and compliment the industry provided solutions.

Figure 4.22 represents the moment that the supportive devices will offload from the knee joint during walking gait according to Table 3.2 and reference [1]. The highest level of support these devices provide occurs at around 70 % of the gait which is part of the swing, a transition between the initial and terminal phases. From the terminal portion of the stance phase at 50% to the terminal of the swing phase at 90%, the maximum moments during walking gait are 14.4 N and -0.26 N, respectively.

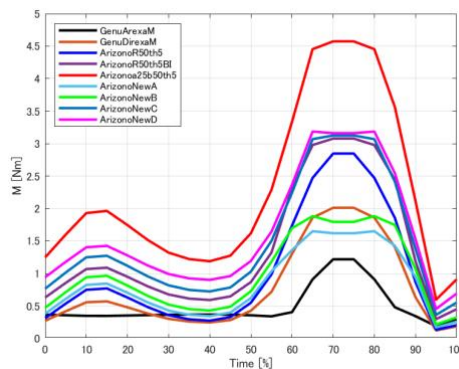


Figure 4. 22 Moment vs Walking Gait Phase

Table 4.4 summarizes the maximum values that the support can offload during the swing phase of the walking gait.

Name	Offload, Nm	Time, %
Genu Direxa (M)	1.9	70, 75
Genu Airexa	1.14	70, 75
ArizonoR50th5	2.82	70
Arizonoa25b50th5	4.55	70
ArizonoR50th5BI		
ArizonoNewA	1.65	65, 80
ArizonoNewB	1.9	65, 80
ArizonoNewC	3.09	70
ArizonoNewD	3.14	70, 75

Table 4. 4 Maximum Offloading of the Supports

4.2.6 Implementation of the Compliant Mechanisms in the Rehabilitation Protocol of Athletes with ACL Complications

As already discussed, the 3D printed models can be used as a set one after the other starting with a stiffer option and gradually increasing the flexibility by replacing the device with different module. The models with varied flexibility can be organize and implemented in a way that will provide safer environment for the rehabilitation process. They can be applied as a subsequent of the harder supports. The recovery of the athletes is a slow and gradual process of increasing the level of activity and the range of motion of the joint. However, the existing solutions cannot reflect on this progression fully due to the flexibility and adjustability limitations. The plot on Figure 4.23 clearly shows the distribution of the moments and

compatibility of the supports. By varying the parameters such as the Radius of the curvature and the number of flexures, more individual solutions could be generated.

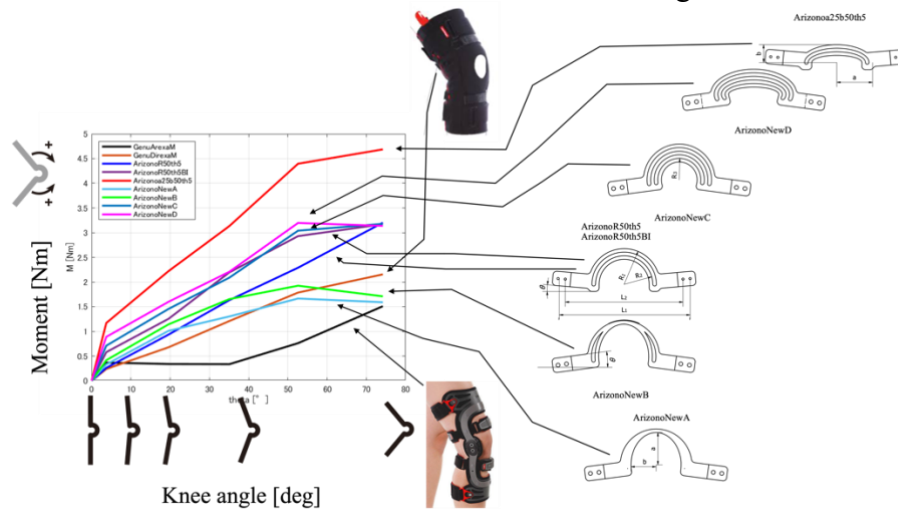


Figure 4. 23 Grading the Models Based on their Peak Moments

It is recommended that for initial peak moments shown on Figure 4.24, the supports are used for improving the resisted knee flexion through concentric contractions and resisted knee extension eccentrically. After the ROM and the quadriceps strength improves, the patient can transition to a device with a greater stiffness in order to further increase the muscular strength during knee flexion and extension. When the patient can perform full ROM controlled knee flexion with the stiffest support, they can transition to another exercise such as the squat pattern. For the squat, the opposite approach could be taken. The patient starts with the stiffest support that will provide the highest level of stability and gradually transitions towards the more flexible options until they no longer need any additional assistance and are capable of performing the motion on their own.

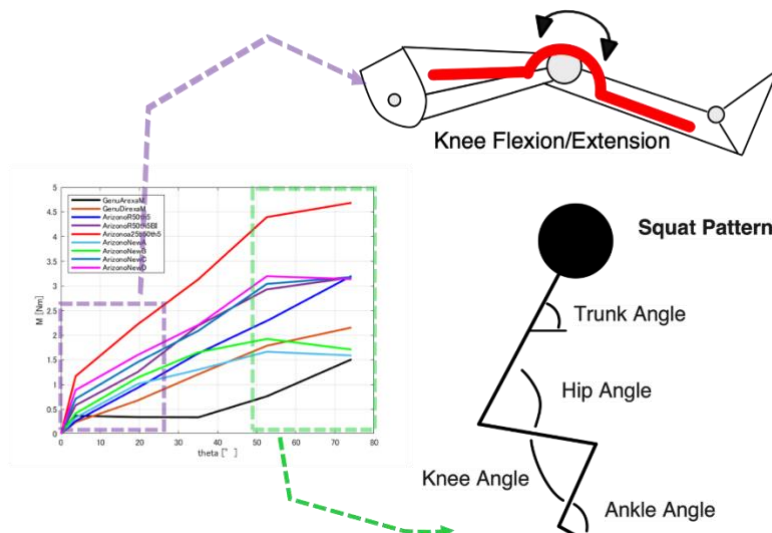


Figure 4. 24 Rehabilitation Implementation of the Supportive Devices

Additional categorization if the devices can be made based on the task completion (Table 3.3) as discussed in [82] instead of the time of the recovery. Table 4.5 shows the first 5 tasks and the prescribed devices for them.



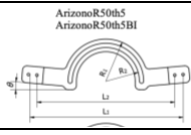


Task №	Task Category	Description	Strength Level	ROM	Device
1	Walking	Walking without crutches	Good quad recruitment	Full extension	 ArizonoNewA
2	Bilateral Squat	Squat to 90° with less than 20% asymmetry	50% BW single leg leg press	Full extension, flexion >90°	 ArizonoNewB
3	Single Leg Squat	Single leg squat to 90°	80% BW single leg leg press	120° flexion	 ArizonoR50thS ArizonoR50thSBI
4	Bilateral Landing	Bilateral landing control from submaximal jump	100% BW single leg leg press or 150% BW double leg leg press/squat	>130° flexion	 ArizonoNewC
5	Running	Treadmill running with 8 km/h	125% BW single leg leg press/squat and/or Isometric extension > 70% Limb Symmetry Index (LSI)	>130° flexion	 ArizonoNewD

Table 4. 5 Task Based Protocol for Rehabilitation with Prescribed Devices

After the patient fills confident that they can complete a task with the help of the assistive devices, they can remove them and try freely to perform the task without any external support.

4.2.7 Summary of the study

The results of this work analyse the mechanical behavior of 3D Printed flexible beams with application as an orthotic device. The bars use their compliance to execute the motion and have different hinging mechanism. A non-linear finite element analyses accounting for the anisotropic material and the large deformations of the flexible models were conducted on all beams to determine the most appropriate for the application. In the selection process the 3D Prating time and the mass of the samples were included. Plots of the results were provided. An evaluation table ranking the criteria was created to objectively determine the beams with most applicable behavior.

Advantages of the designed beams are the low-cost, light weight and compactness in comparison to existing solutions that are hardly affordable and complicated. It allows for simple attachment and replacement with a support with different stiffness depending on the stage of the healing process of the patient.

The most suitable model was redesigned, and several variations were created and printed from PPGW filament. All samples have common parameters such as length and cross-section but some features as the radius of the arc and the number of the flexures are varied across the models. They were tested in a physical setup with an artificial leg that represents the human

knee flexion and extension. The force was recorded by a force gauge and converted into bending moment. The models for all samples were ranked. Rehabilitation recommendations about the implementation of the models based on their stiffness were provided. The combination of all devices as a set will allow smoother and safer recovery process.

Proposed knee orthotic devices are useful for rehabilitation process of athletes. Especially in the enhancement of muscle force in training by gradual increase in range of motion by adding resistance from the devices.

In the future, the evaluation table will be extended including more parameters such as various cross-section geometries, infill patterns and densities and multi-material assemblies combining flexible and stiff materials in different areas of the supportive device. The axial loading caused by the ground reaction force has to be considered in the future development. More tests need to be conducted regarding knee torsion and overextension.

Proposed knee orthotic devices are useful for rehabilitation process of athletes, especially in the enhancement of muscle force in training. They allow progression by gradual increase in range of motion by adding resistance from the devices.

Furthermore, there is a potential to design a new rehabilitation program with the proposed devices including a walking/running protocols.

The constantly increasing capabilities of the Additive Manufacturing processes and 3D Printing more specifically allow for fabricating complex geometries with controlled stiffness for the first time providing an opportunity for meeting the personal requirements in the field of orthoses – the most important link of the patient-doctor relationship aiming for improving the quality of life.

5 Discussion

5.1 Determining the Elastic Properties of Flexible 3D Printed Beams with Variable Infill Densities and Patterns

5.1.1 Introduction and Background

Flexible non-linear 3D printed materials are rapidly gaining popularity in various engineering applications such as soft robotics, actuators, medical devices, etc. Due to their wide applicability, there is an increased research interest in characterization of their mechanical properties and performance. Unlike the conventional manufacturing processes, 3D printing has an additive character and allows for the geometry to be controlled from inside. The internal geometry and density corresponding to a given model can be tuned to a desired stiffness. In this study we investigate the effect of the infill percentage and infill geometry on the mechanical properties of 3D printed samples from flexible material by using a desktop type FDM 3D printer. The analyzed samples have the same shape and geometry – a beam with a square cross-section but the infill percentage is varied from 10 % to a 100 % with an increment of 15 %. The effects of three different types of infill geometries– rectangular, square and honeycomb have also been analytically determined. The approach for the analytical formulation adopts the methodology for calculating the in-plane properties and stiffnesses in cellular solids. The results for the mechanical properties for the different infill densities and infill geometries have been compared for all configurations. Despite the common external geometry of all beams, there is a significant change in their stiffness with the variation of the infill patterns and densities. Finally, a non-linear FEA study for the fully solid beam was conducted and compared with the analytical results. The method, used in this study can be applied for optimization of the stiffness to weight ratio during the design process of flexible 3D printed parts undergoing larger deformations.

Stiffness of 3D printed parts are very hard to determine due to the variation in the internal geometry of various infill patterns. This can only be obtained experimentally and there is limited approach to systematically derive the mechanical properties analytically. Controlling the internal structure allows optimizing the desired stiffness to mass ratio for 3D printed parts. In this work we derive and compare the mechanical properties of three different infill patterns and seven different infill densities.

Table 5.1 shows the research background on the topic. As it can be observed, the mechanical properties of the 3D printing materials have been explored previously in the literature, however, these studies are mainly empirical and there is a lack of more systematic approach for analyzing the behavior of these structures.

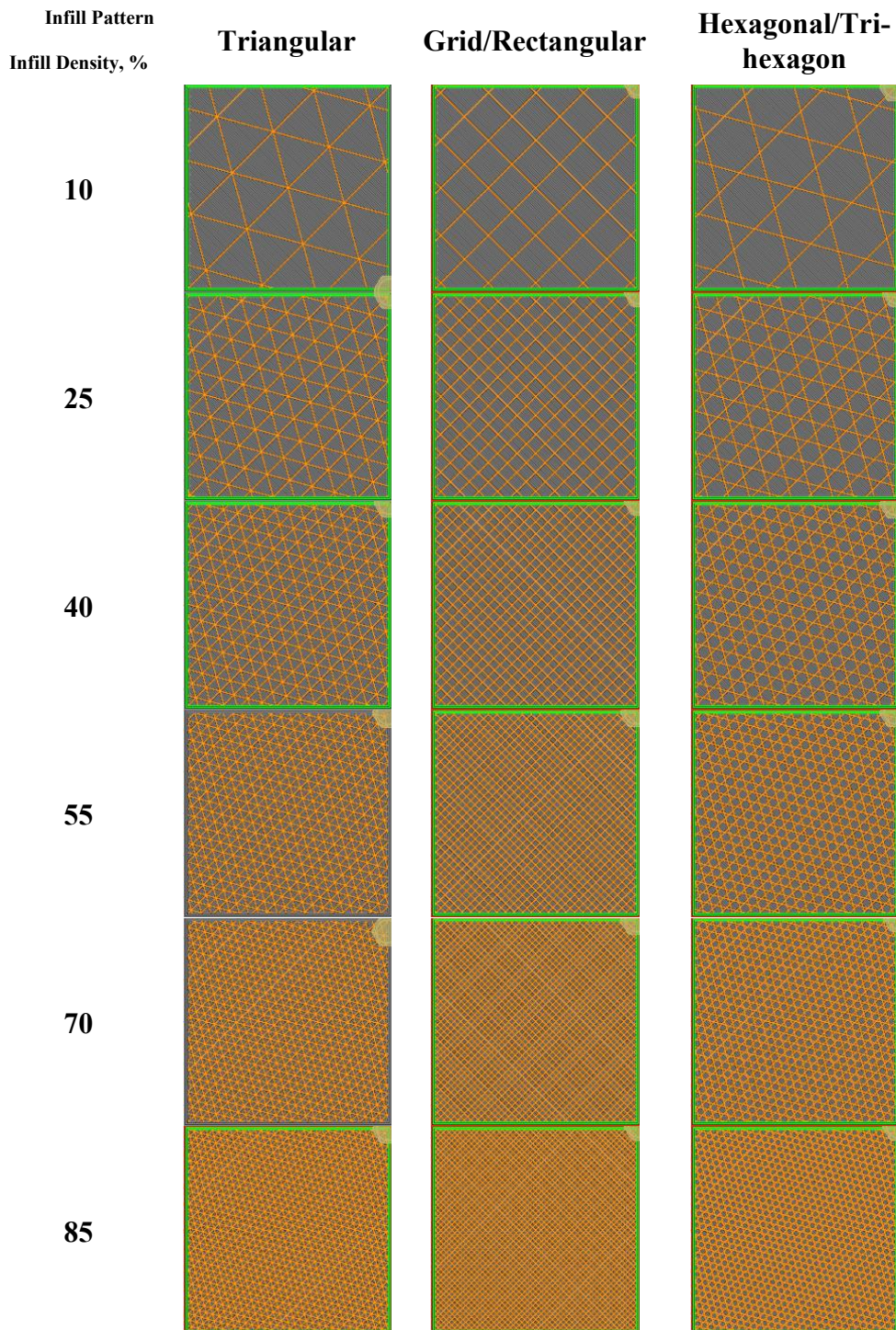
Study	Subject	Method
Aveen et al., 2018 [4]	PLA Properties	Tensile /Bending Tests
Catana et al., 2021 [5]	PLA Properties	Tensile /Bending Tests
Ahmed et al., 2016 [6]	PLA-ABS Comparison	Bending Test
Brčić et al., 2021 [7]	PLA-ABS Comparison	Bending Test
Johnson & French, 2018 [9]	Infill Density	Tensile Test
Fernandez-Vicente et al., 2016 [11]	Infill Geometry	Tensile Test
Galeta et al., 2016 [12]	Infill Geometry	Tensile Test

Letcher & Waytashek, 2014 [13]	Infill Orientation	Tensile /Beding Tests
Farbman & McCoy, 2016 015 [15]	Infill Density and Geometry	Tensile Test/FEA

Table 5. 1 Research Background on the 3D Printing Materials

51.2 Methodology

Table 5.2 illustrates all possible combinations of infill patterns and densities that were compared in this study.



100

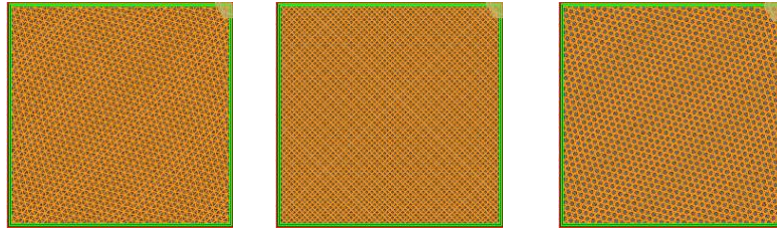


Table 5. 2 Combinations of infill density and infill patterns

Flexible 3D Printed Samples and Printing Parameters

As discussed above, beams, fabricated from a flexible 3D Printing filament were designed with variable infill density – from 10% to 100% with step of 15% as shown on Figure 5.1.

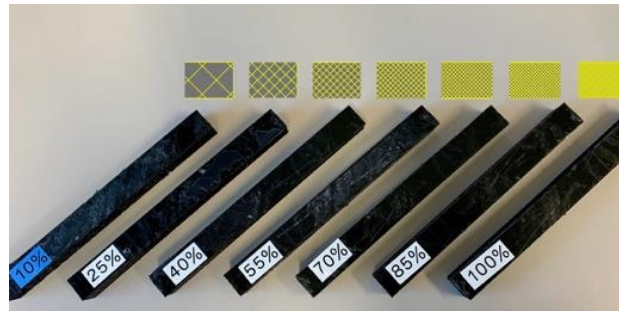


Figure 5. 1 3D Printing Samples with Variable Infill Density

The samples were designed in Autodesk Inventor Professional 2021. For preparing the models for 3D Printing, a slicing software Ultimaker Cura. The 3D Printing parameters are shown in Table 5.3. The 3D Printer is Anycubic i3 Mega. The flexible TPU materials is Ninja Flex from a company called NinjaTek. This material is flexible in nature and is chosen due to its mechanical properties. The nozzle temperature settings were used as recommended by the manufacturer and shown in the Table 5.4 is 230 °C. The pattern of the infill is grid – described by Ultimaker Cura as 2D strong infill.

Parameter	Value
3D Printer	Anycubic i3 Mega
Slicing Software	Ultimaker Cura
3D Printing Material	Ninjatek Ninja Flex TPU Filament
Printing Temperature [°C]	230
Platform Temperature [°C]	60
Supporting Material	No
Infill Density, %	10, 25, 40, 55, 70, 85, 100
Infill Type	Grid
Layer Height, [mm]	0.15
Printing Speed, [mm/s]	50

Table 5. 3 3D Printing Parameters for the Samples

Parameter	Value
Extruder Temperature, °C	225-250
Platform Temperature, °C	Room-50
Top/Bottom Layer Speed, mm/s	10-20
Infill/Shell Speed, mm/s	15-35
Tensile Strength, Yield, MPa	4
Tensile Strength, Ultimate, MPa	26
Tensile Modulus, MPa	12
Elongation at Yield, %	65
Elongation at Break, %	660
Melting Point, °C	216

Table 5. 4 Properties of the 3D Printing Flexible Filament

Defining the Modulus of Elasticity for the Different Infill Geometries and Densities

A. Infill Pattern

Infill patterns (geometries), explored in this research and available in Ultimaker Cura are represented as cellular solids [83]. The infill types, generated by the slicing software are shown on Figure 5.2.

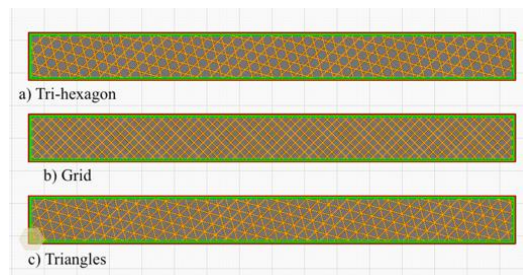


Figure 5. 2 Infill Geometries in the Slicing Software

To analyse the various patterns, they have been modelled as cellular solids as illustrated on Figure 5.3.

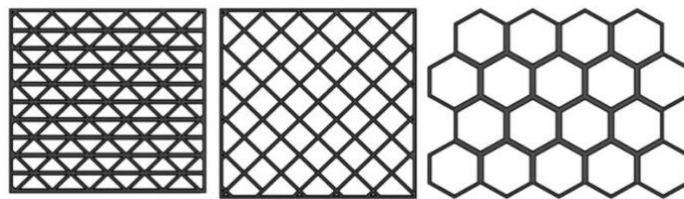
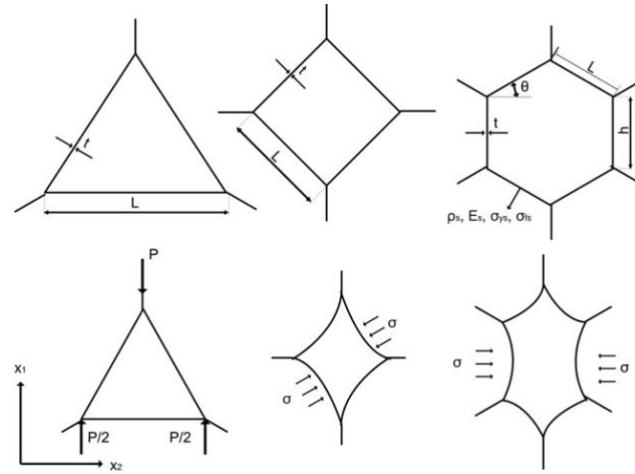


Figure 5. 3 Modeling the Infill Patterns as Cellular Solids

The parameters of a single cell for all types of infill as well as the deformations are shown on Figure 5.4.



a) triangular b) rectangular c) honeycomb cell
Figure 5. 4 Parameters of the Cells

Figure 5.4 shows common cell types of cellular solids also used in this work to model the infill patterns. Triangular cells shown on Figure 5.4 a), the following characteristics:

- Behave like a truss.
- Analysed as pin joints (no moments at the nodes).
- Only axial loads along the members.
- Forces in each member are proportional to P.

$$E^* \propto \frac{P E_s b t}{b P l} = C E_s \left(\frac{t}{l} \right) \quad (5.1)$$

where: C is a constant related with the cell geometry, for equilateral triangle, C=1.15.

Figure 5.4 b) shows rectangular cells that represent the grid infill type.

Those in the diagonal direction, called E_{45}^* , are given by:

$$E_{45}^* = 2 E_s \left(\frac{t}{l} \right)^3 \quad (5.2)$$

The Young's modulus can be obtained from the limit of the equations for hexagonal cells when $h=0$ and $\theta=45^\circ$.

On Figure 5.4 c) are shown regular hexagonal cells. The modulus of elasticity for that type of cells can be obtained by the following equation:

$$E_1^* = E_s \left(\frac{t}{l} \right)^3 \cdot \frac{\cos \theta}{(h/l + \sin \theta) \sin^2 \theta} \quad (5.3)$$

where:

- Properties of the solid: Young's Modulus of the solid E_s ;
- $\left(\frac{t}{l} \right)^3$ related to the relative density (volume fraction of the solid).
- $(h/l + \sin \theta) \sin^2 \theta$ factor that depends on cells geometry.

For regular hexagonal honeycomb: $\frac{h}{l} = 1$; $\theta = 30^\circ$:

$$E_1^* = \frac{4}{\sqrt{3}} E_s \left(\frac{t}{l}\right)^3 \quad (5.4)$$

B. Infill Density

Infill density of the beams is a parameter related to the relative density.

- Density of the cellular material, ρ^* ;
- Density of the solid material, ρ_s .

$$\frac{\rho^*}{\rho_s} = \frac{M_s}{V_t} \cdot \frac{V_s}{M_s} = \frac{V_s}{V_t} = \frac{\left(\frac{t}{l}\right) \left(\frac{h}{l} + 2\right)}{2 \cos \theta \left(\frac{h}{l} + \sin \theta\right)} \quad (5.5)$$

where: M_s is the mass of the solid, V_t and V_s are the total volume and the volume of the solid respectively.

Volume Related Parameters:

To determine the volume of the solid V_s each, beam the following 3D Printing limitations have to be considered:

1. Calculating the volume of the shell (the side walls and top and bottom layers) made out of solid material (100% infill);
2. Layer thickness.
3. Top and bottom layer thickness.
4. Least thickness for the top and bottom layers.
5. Number of the top and bottom layers (layer thickness divided by the layer height).
6. Diameter of the nozzle (theoretically, the thinnest layer can be printed with the diameter of the nozzle).
7. Wall thickness (side walls of the model).

The stiffness is calculated in (6). It is a function of the Elasticity E and the strain ε .

$$\sigma_1 = E\varepsilon = \frac{P}{A} = \frac{P}{(h + l \sin \theta)b} \quad (5.6)$$

where: P is the applied loading, A is the area on which the load is applied; b is the thickness of the 3D printed layer. The strain in the samples is expressed by (5.7).

$$\varepsilon_1 = \frac{\delta \sin \theta}{l \cos \theta} \quad (5.7)$$

$$\delta = \frac{(2)P \sin \theta (l/2)^3}{3E_s I} = \frac{P \sin \theta l^3}{12E_s I} \quad (5.8)$$

$$I = \frac{bt^3}{12} \quad (5.9)$$

where: δ is the deflection of the sample; l is the length of the side of the sample (shown on Figure 5.4); E_s is the Modulus of Elasticity of the material; I is the moment of inertia.

5.1.3 Results and Discussion

5.1.3.1 Analytical Results

To determine the geometrical constraints of the beam, the below parameters are used

1. Material: Ninjatek Ninjaflex TPU filament.
2. Square cross-section of $a= 0.015$ m and length $l= 0.15$ m.
3. Layer thickness (equal to the depth b): 0.15 mm.
4. Top layer thickness: 1.2 mm.
5. Bottom layer thickness: 1.2 mm.
6. Number of the top and bottom layers: 8.
7. Diameter of the nozzle (equal to the thickness of the wall): 0.3 mm.

Wall thickness: 1.2 mm.

After solving (5.5) for the relative density and $\frac{t}{l}$, if $\frac{h}{l} = 1$ and E of the material is 12 MPa, for triangular cells (patterns) $\theta = 60^\circ$; for rectangular - $\theta = 45^\circ$; for hexagonal - $\theta = 30^\circ$, the results for the Elasticity for the 3 types of infill and 7 densities are calculated. The applied loading, used for the analytical part as well as the FEA analysis is 5 N.

Figure 5.5 a) shows parameters affected by the infill percentage directly. All samples are printed with the same regimes. After, the 3D printing time and the mass of the completed specimens is measured. As it can be observed, the duration of the printing process is increasing in a linear fashion up until 90% but gets significantly higher (more than 2 times) for 100% infill. Similarly, the mass of the models and their density progresses linearly to 90% and the increase from 90% to a 100% is with a greater increment. Therefore, to save time and materials and to make the parts lighter, it can be recommended for models with only visual value to be printed with infill percentages lower than a 100%.

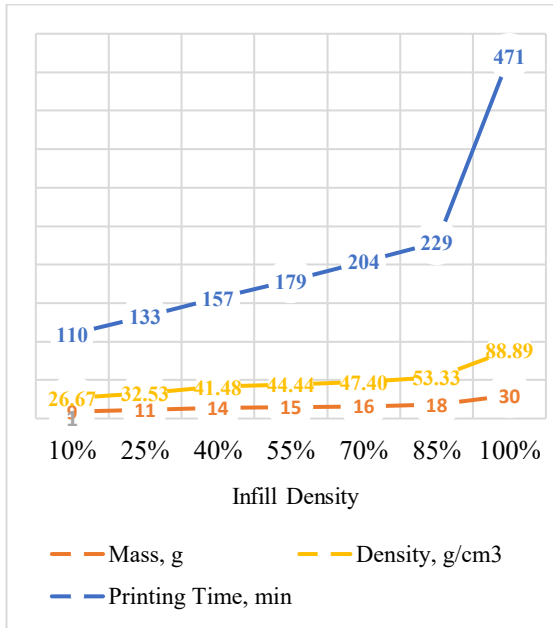
As expected, on Figure 5.5 b) the relative elasticity of the samples increases with the increase of the infill. In addition, it was also expected that the highest values will be for the triangular infill pattern due to the parameter $\frac{t}{l}$ related to the relative density (volume fraction of the solid).

The volume fraction of the solid for rectangular and hexagonal infill patterns is raised on the third power which leads to lower values of their elasticity moduli. However, that is not the case because with the increase of the infill density, length l (illustrated on Figure 4.23 and used in equation (5.8) to calculate the deflection) is decreasing. This is due to the fact that more cells have to fit in a given volume by increasing the infill density and the only way is by making the cells smaller (smaller l).

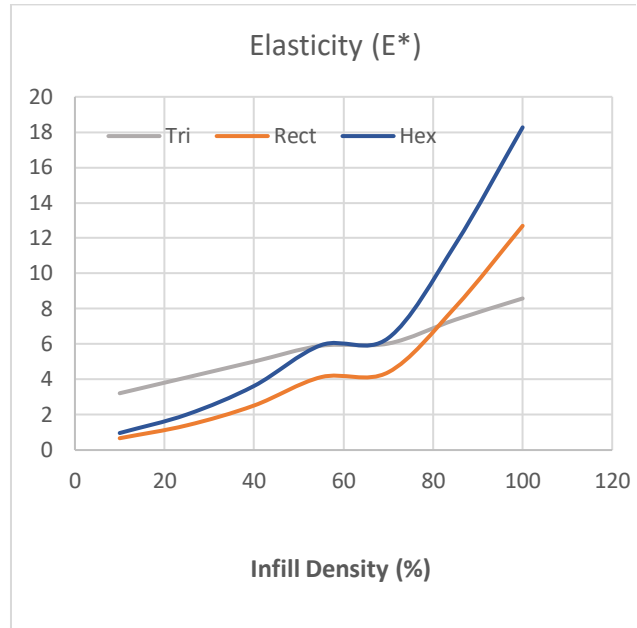
On Figure 5.6 a) the values of the strain are shown. As expected with the increase of the infill, the strain decreases which makes the parts produced with higher infill density stiffer. Here, the highest strain values are for the triangular infill pattern and the highest – for the hexagonal. Similar trend can be observed for the stiffness. It raises with the infill density and is the highest for the hexagonal pattern (Figure 5.6 b)).

5.1.3.2 Finite Element Analysis Results

FEA simulation was conducted on a beam of similar dimension and mechanical properties of Ninja Flex was used as given in manufacturer specification. The simulation study was conducted in COMSOL and the stresses and displacements corresponding to a tip load is illustrated in Figure 5.7. The non-linear behaviour of the beam can be seen in figure 5.7 b) where the load has been varied from 0.5 N to 5 N with an interval of 0.5 N. The FEA analysis aims to represent the stress for a beam with 100% infill density. The results of the deformation from this study for 5 N force are 0.075 mm are similar to the values of the deflection for 100% infill density and rectangular pattern – 0.0704 mm.

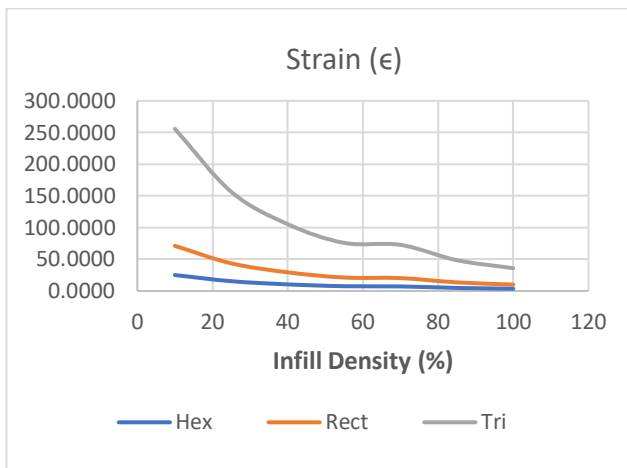


(a) Impact of the Infill Density on the 3D Printing Parameters

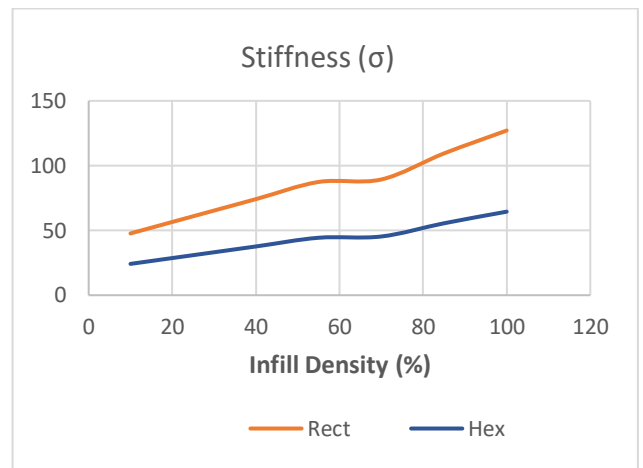


(b) Relative Density-Modulus of Elasticity Relationship

Figure 5. 5 Impact of infill-density on 3D Printing Parameters and Modulus of Elasticity (analytical).

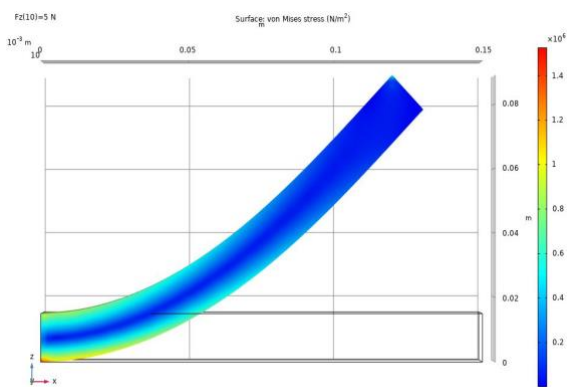


a) Strain

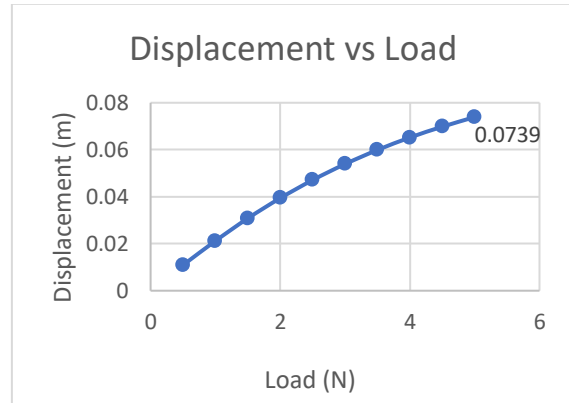


b) Stiffness

Figure 5. 6 Impact of infill-density on 3D Printing Parameters and Modulus of Elasticity (analytical)



(a) Stresses on the Beam (5N)

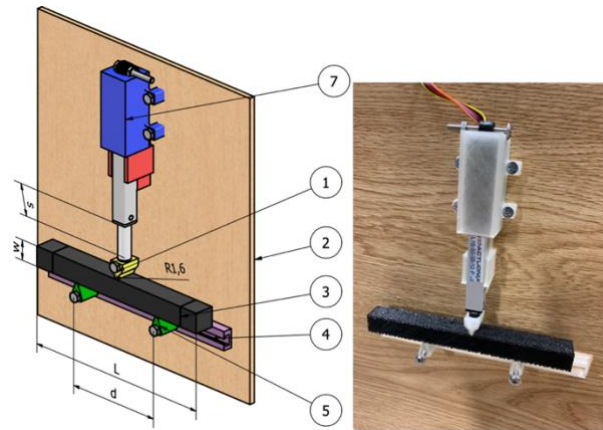


(b) Displacements of the tip (0.5N – 5N)

Figure 5. 7 Stresses and Displacements of the beam from COMSOL FEA analysis.

5.1.3.3 Experimental Setup

An experimental setup for three-point bending test of the TPU 3D Printed samples was created. Figure 5.8 a) illustrates the setup and its components as follows: 1-Loading Roller; 2-Plate; 3-Sample; 4-Support Guiding Mechanism; 5-Support; 6-Linear Actuator; 7-Holder. Figure 4.19 b) shows an image of the actual setup.



a) Components b) Image of the Physical Setup
Figure 5. 8 Experimental Setup

The bending of the beam (pushing force) is realized by a linear motor (miniature actuator series L16 [64] a control board described in [75] from the company Actuonix. The motor has gear ratio of 35:1, maximum force of 50 N and maximum back drive force of 31 N. The stroke of 50 mm and the mechanical backlash is 0.25 mm. The input voltage of the motor is 12 V. The actuator can be calibrated by using a strain gauge (push pull scale).

The beam (3) is positioned on two adjustable supports (4) which can be translated in Z direction and the distance d between them can be varied. A roller (1) with the same radius R as the supports attached to the motor (6) applies the loading in the middle of the beam.

Components with positions (1, 4, 5 and 7) are 3D Printed from a PLA material.

After the calibration of the motor, during the bending experiment, the values of the current and the displacements (the stroke of the motor s) are recorded at each step.

By using the current-force relationships, obtained by the strain gauge for the motor, the current is converted into an applied force acting on the beam. The force-displacement diagram is plotted and after calculating the modulus of elasticity, converted into a stress-strain relationship plot illustrating the mechanical behavior of the Ninjaflex TPU material.

To calculate the behavior of the beam within the framework of the proposed experiment, the following algorithm can be used:

1. Calculating beam characteristics (geometry, moment of inertia).
2. Measuring the current-force characteristics of the linear actuator.
3. Determining the displacements (from the linear motor actuation).
4. Converting the current values from the linear actuator into applied external force (P) acting on the beam.
5. Calculating the Modulus of Elasticity from equations 7 and 8.
6. Obtaining the force-displacement response plots.
7. Converting the values of the force-displacements curves into stress-strain relationship for the TPU material.

5.1.4 Summary

In this study we investigate the influence of the infill patterns and infill densities on the mechanical properties of samples fabricated from flexible TPU filament by implementing the cellular solid model. The results are obtained analytically for 3 common types of infill geometries – triangular, rectangular, and hexagonal and for 7 infill percentages – 10, 25, 40, 55, 70, 85 and 100. The values of the deflection, strain, elasticity, and stress for all 21 combinations are presented. The relative elasticity increases as the infill percentage increases and is the highest for the hexagonal infill pattern. The values for rectangular and triangular patterns are close to each other with lowest modulus of elasticity calculated for the triangular. The values of the strain, as expected, with the increase of the infill, the strain decreases. The highest strain values are for the triangular infill pattern and the highest – for the hexagonal. Similarly for the stiffness, it raises with the infill density and is the highest for the hexagonal pattern.

The deformation is compared to a non-linear FEA analysis for a beam from 100% infill density with the same properties of NinjaFlex filament. From the simulation is obvious that the deflection is close to the values for rectangular pattern with 100% infill.

It is important to note, that the results obtained analytically should be verified with an experimental data of beams fabricated from the same NinjaFlex material and parameters.

This methodology can be applied in the design process of flexible parts with controlled elasticity and optimized mass to stiffness ration while at the same time preserving the outer geometry of the models.

5.2 Varying the Infill Density of the Models

Another approach to optimize the stiffness of the beams is by varying their infill density (percentage). This is method is illustrated on Figure 5.9 and discussed in more details in the next chapter.

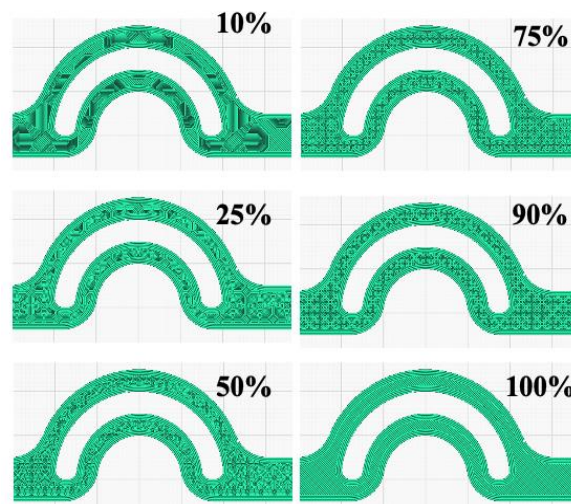


Figure 5. 9 Variation of the Infill Density

This approach can be further enhanced by using a “Topology Optimization” tool embedded in the CAD modeling software. An example step by step implementation of this method is presented at Figure 5.10 below.

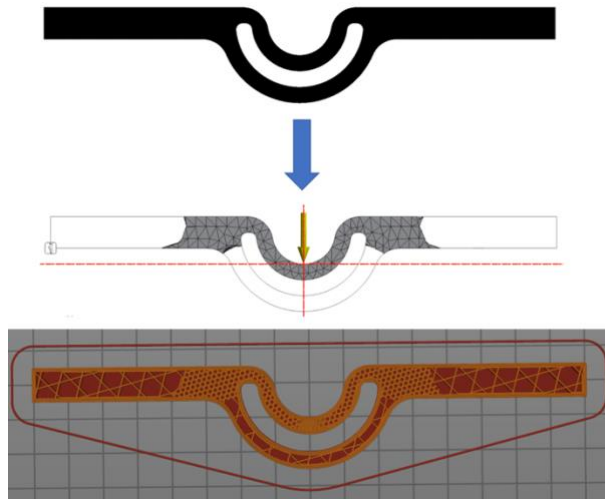


Figure 5.10 Topology Optimization for Orthotic Device Fabrication

5.3 Out of Plane Motion

So far, this chapter investigates the in-plane motion – flexion and extension of the knee and in particular, the flexion in more details. However, it is very important to consider the other degrees of freedom of the joint that could occur during the recovery and prevent them such as: overextension of the knee, in-wards and out-wards bending (knee valgus) and flexion of the knee at the initial stage of the recovery.

To address all these requirements, new modifications of the device were developed. As part of the future plans, the models need further improvements to prevent lateral deformations.

As an example of a way to improve the lateral stiffness is shown on Figure 5.11 a) by replacing the square cross-section with an “I-type beam” cross-section. To increase the range of motion the samples are redesigned as illustrated in b). Figure 5.11 c) and d) represent a multi-material assemblies of the beams combining a stronger PPGW and a more elastic TPU filament to provide a larger lateral stability and higher control over the stiffness.

Another unique opportunity can be provided by the additive processes and the infill density variability contributes to allow a local control of the stiffness of the model. A combination of those factors will increase the potential of the additive manufacturing for customizable solutions to fit for individual requirements.

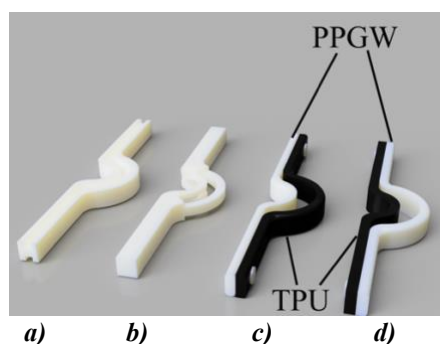


Figure 5.11 3D Representation of the Beam

Proposed models on Figure 5.11 c) and d) have been 3D Printed as a combination of TPU and PLA filaments and after that assembled. The results are illustrated on Figure 5.12.

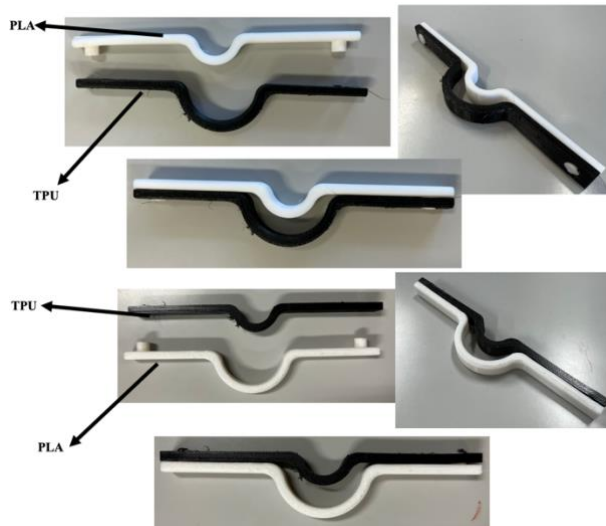
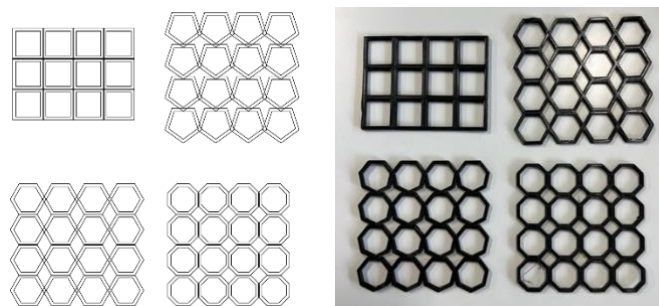


Figure 5.12 Material Combination

5.4 Development of a Regular Polygon Mesh Applied as an Orthotic Wearable for the Knee Joint

On Figure 5.11 are presented several examples of grid structures made from regular polygons with different number of the sides. On Figure 5.13 a) all models are shown in a drawing view. On Figure 5.13 b), the models are 3D Printed from a flexible TPU material.



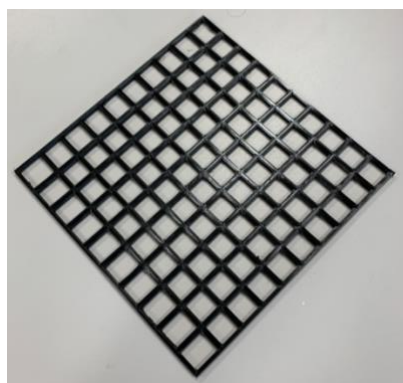
a) Drawing View

b) 3D Printed

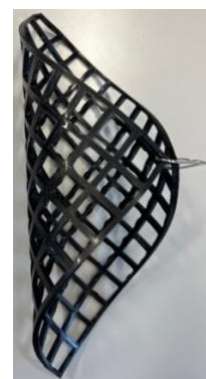
Figure 5.13 Grid structures Variations

After the flexibility of the mesh is determined by using some of the above-mentioned methods, the mesh can be combined with the flexible beams discussed in the previous section to provide a fully customized solution depending on patients' specific requirements and diagnose.

This design is inspired by Origami style foldable flat surfaces. It has the advantage that can be 3D Printed flat relatively quickly and afterwards folded and wrapped around the knee. See Figure 5.14.



a) Flat Orientation for 3D Printing



b) Wrapping the Mesh around the Knee

Figure 5. 14 Planar Mesh Structure

This chapter summarizes the future plans and development of the compliant 3D Printed wearables. It introduces several optimization strategies applicable in the framework of the project such as:

- Analyzing the inside structure of the parts (infill) as a cellular solid, where the modulus of elasticity of different infill patterns (geometries) and densities (percentages) are discussed.
- Control the regional infill density of the parts – decreasing the amount of material at places where the stress concentration is lower and increasing at locations with higher levels of the stress. The method has been further expanded by the introduction of Topology Optimization of the parts and combining the optimized parts with the initial geometry printed with a lower amount of infill.
- Presenting origami inspired flat grid structures that consist of regular polygons with different number of the sides. These patterns can be 3D Printed flat which simplifies the fabrication process and afterward attached to the knee wearable device. The approach provides an extra level of customization to the supportive device.
- Finally, an example of two four-bar mechanisms combined as an end effector is given. Here, the pin joints are replaced with a compliant flexures and the entire model relies solely of the deformation to execute the motion of manipulating with objects combined with the friction between the jaws and the object itself in order to hold it without dropping and breaking it.

6 Conclusion

This work aims to explore, analyze, and summarize the custom-built orthotic knee wearable solutions and provide low-cost alternatives with high level of personalization according to the patients' conditions.

The demand for such devices has been established in Sections 1 and 2 where the current solutions were investigated. It is clear from the literature review section that there is a gap for custom-made cost-efficient devices that can meet patients' needs and help accelerate the healing process. Especially amongst the athlete population, there is an unaddressed issue of transitioning between various supportive devices during the recovery process. This is a period when after an injury, the healing process takes place with different pace depending on the severity of the injury and the lifestyle of the patient. Therefore, not all joint related issues are equal, and they should be treated individually. That means that there is a high demand for customization in the field of Orthopedics in the creation of supportive devices that can adjust accordingly to the necessities of the users and the stage of the injury/rehabilitation.

In the "Literature Review" some possible candidates to address those issues and their development are discussed. From one hand, 3D Printing is highly suitable for the realization of complex geometry and custom designs in all fields of Engineering and beyond. On the other hand, Compliant Mechanisms, their capabilities, variations, and implementation are explained. They can perform motion without being made from multiple moving parts but as a single unit that deforms under an external loading. Combining the advancements in CAD design, FEA analysis, 3D Printing being more and more reliable, accessible, and accurate, the new 3D Printing filaments with enhanced mechanical properties and lastly the potential of the Compliant Mechanisms, leads to unlimited new opportunities restricted only by the imagination of the makers. That is also true and applicable in the of Orthotic devices and wearables. Some additional specifications that can be fulfilled for the device by using the above techniques are:

- Adaptivity – some portions of the device can be replaced with structures with a different flexibility depending on the stage of the healing process.
- Designing specific segments of the device individually from each other for further personalization.
- Ergonomics – for instance using 3D scanning of the patients' joint to determine and fabricate the most suitable shape for them.
- Light weight and compactness.

Such concept of creating a supportive device by using flexible 3D Printing of a compliant mechanisms is developed in Sections 3 "Methodology" and 4 "Results".

Section 3 gives the methods used to develop the Orthotic knee joint supportive device based on a compliant mechanism.

The biomechanics of the knee is explored during various common daily activities such as walking, stair descent and ascent and sit-to-stand. The parameters that influence the motion are discussed. A summary of the loading on the knee joint during the different activities is provided. The rehabilitation protocol for athletes is described. A ten-task based progression is introduced and the requirements of how to transition from one exercises to the next is discussed based on the level of recovery of the patients.

Next, a methodology based on the cellular solids' analysis was presented. The main objective is to represent the 3D Printing inner structure as a honeycomb or a foam. 3D Printing and Additive Manufacturing processes allow the unique advantage to control the geometry of the model from inside called infill density and its pattern. If these are properly optimized, that can lead to stiffer and at the same time lighter parts while keeping the outer geometry unchanged

and saving material and time for printing. For those reasons improving not only the design of the models but also their infill is a crucial process that will be more and more emphasized in the near future by researchers and engineers.

The guidance for analyzing the infill pattern and density based on a honeycomb model is discussed here. It describes the cells as honeycombs – regular polygons with different number of the sides – triangular, square, and hexagonal. The methodology calculates the moduli of elasticity for different geometries and relative densities. After that, the stress and strain that occurs in the cell walls due applied loading is explained.

This approach is especially practically valuable for analyzing the stiffness/ flexibility of 3D Printed structures and even flexible 3D Prints.

Implementing this algorithm into the design of compliant mechanisms and further, into the design of the Orthotic knee support, allows an extra level of customization where more parameters can be taken under consideration such as the weight of the patient, physical activity, age, speed of the recovery and more making this tool very powerful in analyzing parts with controllable elasticity.

Section 4 describes the results of this study. At first the compliant cross-spring pivot has been modified into spatial mechanism that simulates a universal joint. This joint consists of two mutually perpendicular cross-spring pivots and has two rotations around two orthogonal axes. The design can be implemented as stabilizing mechanism or for actuating precise positioning tools. This model is similar to the ligaments of the human knee joint and, therefore, its application has been insured by their stabilizing functions attaching the bones to each other.

In addition, the proposed concept consists of two materials – flexible TPU for the beams that will deform to execute the motion, and solid PLA for the platforms that will connect to other objects. By using this approach, one of the advantages of the complaint mechanisms to avoid the assembly process is eliminated, but another benefit is introduced – varying different material pairs and combinations regarding the application needs. A non-linear analysis was conducted, and the results were described. A monolithic model printable as a single unit was developed and 3D Printed to demonstrate the prototyping capabilities of 3D Printing.

It is important to note, this joint, in its 3-dimensional variation, cannot be implemented in the compliant supportive device. It is rather an illustration of the progress of the additive processes, and it can have various applications related with precise positioning and/or as a universal joint, or a robotic manipulator orientation. For the purposes of the knee wearable device, a more conventional planar version of the compliant cross-spring pivots is more suitable and discussed in the later chapters.

Also in this section, an algorithm for automatically generating solutions of 2-dimensional plates with different number of the springs was developed and applied. These plates will be used as part of the supportive device responsible for flexing and extending the knee. The generated models were converted into CAD files and the geometry was post processed. After that a 3rd dimension, thickness was added to the design. Next, a FEA simulation was applied to compare the behavior of models with different number of springs. The concepts were 3D Printed from a flexible filament and an experiment was carried by using a robotic arm to apply tensile stress to the samples. The results were recorded, and the force-displacement relationships were obtained.

At last, but not least, the behavior of compliant beams with different geometry that determines their properties is introduced by using non-linear FEA and parameter comparison charts. Beams with different geometry were designed and 9 of these variations were 3D Printed from flexible TPU filament and simulated in non-linear environment. These beams will be installed at the sides of the supportive device, so they have to provide controlled motion of the knee in flexion and extension and at the same time, limit the lateral deviation of the joint. The beams were designed to have some common features such as cross-sectional area and length, but

different geometry of the compliant hinge. After that the beams were compared by the duration of the 3D Printing, their mass, the stress and the lowest resistance during motion (the highest displacements at a given force value).

A prototype of one of the models with best performance was fabricated, 3D Printed from a material called PPWG and later implemented into a passive wearable device for the knee. More prototypes on the same base were developed and tested with the help of an artificial leg that represents the knee flexion and extension. The new prototypes were implemented on the artificial leg and the force was recorded with a force gauge and then converted to bending moment for all samples. The moments were plotted with respect to the angle of deformation and the results were categorized and compared to these of existing orthotic devices. All models were grouped and their implementation into the rehabilitation protocol was discussed. These knee orthotic devices based on proposed 3D printed compliant mechanisms provide motion assistance and loading force with offload from 0.75 to 2 [Nm] as individual maximum values depending on their shapes. Proposed 3D printed compliant mechanisms were designed to move in the 2D plane (ROM: 0~75 degree) to restrict knee motions without overextension, torsion and valgus of the knee. Especially for the overextension, two materials with different elasticity can be combined in a single device. Restrictions in ROM were theoretically verified and examined. More tests of the real devices attached to patients are required.

Relatively low cost and harmless materials opens a new horizon for the support device for patients with ACL complications including athletes.

Some new concepts for the future development and optimization of the beams were proposed such as multi-material combination which will allow greater lateral stability due to the rectangular cross-section and at the same time, controlled flexibility in the main direction.

The “Discussion” Section summarizes the future plans and directions of this study. The cellular solid implementation is extended and the various moduli of elasticity for samples with varied infill density and infill geometry were calculated. The results were compared and the relation of the relative density to the elasticity and therefore to the stress was plotted. Seven beams with the same geometry were 3D Printed and used to illustrate the change in behavior when the infill is modified. A testing setup with a linear actuator to apply the constant loading was developed as well.

The second stage of the future work will include the local control of the infill percentage and pattern. If the properties discussed above are verified by an experiment, then the flexibility could be controlled independently in the different areas of the same part to make it stronger and lighter at the same time. This way the amount of the used material will be decreased which will lead to decreased printing duration and cost-efficiency. The approach can be also combined with Topology Optimization for further enhancement of the designs.

The opportunities that are presented by the progress of software and additive technologies and materials is limitless and will allow for greater level of customization and optimization at each stage of the design and manufacturing process as part of the product lifecycle. That will lead to shorter and more efficient prototyping phase and greater diversity of the product line ups.

The impact of this progress redefines the Engineering and Research fields and what was previously considered “impossible”.

References

1. L. Zhang, G. Liu, B. Han, Z. Wang, Y. Yan, J. Ma and P. Wei, “Knee Joint Biomechanics in Physiological Conditions and How Pathologies Can Affect It: A Systematic Review,” *Applied Bionics and Biomechanics*, 2020, Article Number 7451683.
2. Cruciate Ligament Tear (<https://www.ottobock.com/en-au/situation/diagnoses-and-symptoms/cruciate-ligament-tear>) – 2022/04/06.
3. Megaro, V., Zender, J., Bacher, M., Coros, S., Cross, M., Thomaszewski, B., “A Computational Design Tool for Compliant Mechanisms,” *ACM Transactions on Graphics*, Vol. 36, No. 4, Article 82, July 2017.
4. K. P. Aveen, F. V. Bhajathari and S. C. Jambagi, “3D Printing & Mechanical Characterisation of Polylactic Acid and Bronze Filled Polylactic Acid Components,” *IOP Conf. Ser.: Mater. Sci. Eng.*, 2018, 376 012042.
5. Catana, D.; Pop, M.-A.; Brus, D.-I. Comparison between the Test and Simulation Results for PLA Structures 3D Printed, Bending Stressed. *Molecules* 2021, 26, 3325. <https://doi.org/10.3390/molecules26113325>
6. M. Ahmed, M. R. Islam, J. Vanhoose, L. Hewavitharana, A. Stanich and M. Hossain, “Comparisons of Bending Stiffness of 3d Printed Samples of Different Materials,” *IMECE2016-65119*, 204.
7. M. Brčić, S. Krčanski and J. Brnić, “Rotating Bending Fatigue Analysis of Printed Specimens from Assorted Polymer Materials,” *Polymers* 2021, 13(7), 1020. <https://doi.org/10.3390/polym13071020>
8. P. Piatek, K. Rajkowski, K. Cieplak, M. Sarzyński, J. Małachowski, R. Woźniak and J. Janiszewski, “Deformation process of 3D printed structures made from flexible material with different values of relative density,” *Polymers*, 2020, 12(9), 2120. <https://doi.org/10.3390/POLYM12092120>
9. G.A. Johnson and J. J. French, “Evaluation of Infill Effect on Mechanical Properties of Consumer 3D Printing Materials,” *Advances in Technology Innovation*, 3(4), 2018, pp.179–184.
10. K. L. Alvarez C., R. F. Lagos C. and M. Aizpun, “Investigating the influence of infill percentage on the mechanical properties of fused deposition modelled ABS parts,” *Ingeniería e Investigación*, 36(3), 2016, 110–116. <https://doi.org/10.15446/ing.investig.v36n3.56610>
11. M. Fernandez-Vicente, W. Calle, S. Ferrandiz, and A. Conejero, “Effect of Infill Parameters on Tensile Mechanical Behavior in Desktop 3D Printing,” *3D Printing and Additive Manufacturing*, 3(3), 2016, 183–192. <https://doi.org/10.1089/3dp.2015.0036>
12. T. Galeta, P. Raos, J. Stojčić, and I. Pašić, “Influence of structure on mechanical properties of 3D printed objects,” *Procedia Engineering*, 149, 2016, pp.100–104. <https://doi.org/10.1016/j.proeng.2016.06.644>
13. T. Letcher, and M. Waytashek, “Material property testing of 3D-printed specimen in pla on an entry-level 3D printer,” *ASME International Mechanical Engineering Congress and Exposition, Proceedings (IMECE)*, 2014, 2A. <https://doi.org/10.1115/IMECE2014-39379>
14. L. Baich, G. Manogharan, and H. Marie, “Study of infill print design on production cost-time of 3D printed ABS parts,” *International Journal of Rapid Manufacturing*, 5(3/4), 2015, 308. <https://doi.org/10.1504/ijrapidm.2015.074809>
15. D. Farbman, and C. McCoy, “Materials testing of 3D printed ABS and PLA samples to guide mechanical design,” *ASME 2016 11th International Manufacturing Science and Engineering Conference, MSEC*, 2016, 2. <https://doi.org/10.1115/MSEC2016-8668>
16. J. Xiao, and Y. Gao, “The manufacture of 3D printing of medical grade TPU,” *Progress in Additive Manufacturing*, 2(3), 2017, 117–123. <https://doi.org/10.1007/s40964-017-0023-1>

17. B. P. Trease, Y. M. Moon, and S. Kota, "Design of large-displacement compliant joints," *Journal of Mechanical Design, Transactions of the ASME*, 127(4), 2005, 788–798. <https://doi.org/10.1115/1.1900149>
18. L. Liu, S. Bi, Q. Yang, and Y. Wang, "Design and experiment of generalized triple-cross-spring flexure pivots applied to the ultra-precision instruments," *Review of Scientific Instruments*, 85(10), 2014. <https://doi.org/10.1063/1.4897271>
19. A. Ion, D. Lindlbauer, P. Herholz, M. Alexa, and P. Baudisch, "Understanding metamaterial mechanisms," *Conference on Human Factors in Computing Systems – Proceedings*, 2019, 647:1-14. <https://doi.org/10.1145/3290605.3300877>
20. X. Pei, J. Yu, G. Zong, S. Bi and H. Su, "The modeling of cartwheel flexural hinges," *Mech. Mach. Theory* 44 (10), 2009, 1900–1909.
21. S. Henein, P. Spanoudakis, S. Droz, L. I. Myklebust and E. Onillon, "Flexure pivot for aerospace mechanisms," *Proceedings of the 10th European Space Mechanisms and Tribology Symposium*. San Sebastian, Spain, 2003.
22. J. A. Haringx, "The cross-spring pivot as a constructional element," *Flow Turbul. Combust.* 1 (1), 313–332, 1949
23. L. A. Gonçalves Junior, R. Theska, H.A. Lepikson, A.S. Ribeiro Junior, S. Linß and P. Gräser, "Theoretical and experimental investigation of performance characteristics and design aspects of cross-spring pivots," *International Journal of Solids and Structures*, Vol.185-186, 2020, pp.240-256.
24. M. Murphy, A. Midha and L. Howell, "The Topological Synthesis of Compliant Mechanism," *Mech. Mach. Theory* Vol.31, No. 2, pp. 185-199, 1996, 0094 114X(95)00055-0.
25. N. T. Pavlovic, N. D. Pavlovic, "Compliant mechanism design for realizing of axial link translation," *Mechanism and Machine Theory* 44, 2009, 1082–1091.
26. Y. Jingjun, P. Xu, Z. Shanshan, B. Shushing and Z. Guanghua, "A new large-stroke compliant joint & micro/nano positioner design based on compliant building blocks," *ASME/IFTOMM International Conference on Reconfigurable Mechanisms and Robots*, 2009, pp. 409*41
27. B. Jensen and L. Howell, "The modeling of cross-axis flexural pivots," PII: S0094-114X(02)00007-1, *Mechanism and Machine Theory* 37, 2002, 461–476.
28. K. Marković and S. Zelenika, "Characterization of cross-spring pivots for micropositioning applications," doi: 10.1117/12.2178490, *Proc. of SPIE* Vol. 9517 951727-2.
29. R. Chen, L. Chen, B. Tai, Y. Wang, A. Shih and J. Wensman, "Additive Manufacturing of Personalized Ankle-Foot Orthosis," *Proceedings of NAMRI/SME*, Vol. 42, 2014.
30. Y. Lin, L. Huang, C. Chen, "Strength Evaluation and Modification of a 3D Printed Anterior Ankle Foot Orthoses," *Appl. Sci.* 2020, 10, 7289; [doi:10.3390/app10207289](https://doi.org/10.3390/app10207289).
31. K. W. Lin, L. W. Chou, Y. T. Su, S. H. Wei and C. S. Chen, "Biomechanical Effect of 3D-Printed Foot Orthoses in Patients with Knee Osteoarthritis," *Appl. Sci.* 2021, 11, 4200. <https://doi.org/10.3390/app11094200>
32. B. D. M. Chaparro-Rico, K. Martinello, S. Fucile and D. Cafolla, "User-Tailored Orthosis Design for 3D Printing with PLACTIVE: A Quick Methodology," *Crystals* 2021, 11, 561. <https://doi.org/10.3390/cryst11050561>
33. S. Santos, B. Soares, M. Leite and J. Jacinto, "Design and development of a customised knee positioning orthosis using low cost 3D printers," *Virtual and Physical Prototyping*, 12(4), 2017, 322–332. <https://doi.org/10.1080/17452759.2017.1350552>
34. Y. J. Choo, M. Boudier-Revéret and M. C. Chang, "3D printing technology applied to orthosis manufacturing: Narrative review," *Annals of Palliative Medicine*, 9(6), 2020, 4262–4270. <https://doi.org/10.21037/apm-20-1185>

35. J. C. D. dos S. F. Hensen, J. A. Foggatto, L. Ulbricht, and A. M. W. Stadnik, "Additive manufacturing of customized lower limb orthoses – A review," *International Journal for Innovation Education and Research*, 6(10), 2018, 141–152. <https://doi.org/10.31686/ijer.vol6.iss10.1175>
36. Y. A. Jin, J. Plott, R. Chen, J. Wensman, and A. Shih, "Additive manufacturing of custom orthoses and prostheses - A review," *Procedia CIRP*, 36(July), 2015, 199–204. <https://doi.org/10.1016/j.procir.2015.02.125>
37. T. J. Wallin, J. Pikul, and R. F. Shepherd, "3D printing of soft robotic systems," *Nature Reviews Materials*, vol. 3, pp. 84–100, 2018.
38. B. Berman, "3-D printing: The new industrial revolution," *Business Horizons*, vol. 55, no. 2, pp. 155–162, 2012.
39. F. Hu, L. Li, Y. Liu and D. Yan, "Enhancement of Agility in Small-Lot Production Environment Using 3D Printer," *Industrial Robot and Machine Vision, International Journal of Simulation: Systems, Science & Technology*, vol. 17, no. 32, pp. 1–6, 2016.
40. Y. Wang, Q. Tan, F. Pu, D. Boone and M. Zhang, "A Review of the Application of Additive Manufacturing in Prosthetic and Orthotic Clinics from a Biomechanical Perspective," *Engineering*, vol. 6, no. 11, pp. 1258-1266, 2020.
41. P. S. P. Teng, K. F. Leong, P. W. Kong, B. J. Halkon, and P. Y. Huang, "The use of rapid prototyping in the design of a customised ankle brace structure for ACL injury risk reduction," *Virtual and Physical Prototyping*, vol. 8, no. 4, pp. 241–247, 2013.
42. H. Kim and S. Jeong, "Case study: Hybrid model for the customized wrist orthosis using 3D printing," *Journal of Mechanical Science and Technology*, vol. 29, no. 12, pp. 5151–5156, 2015.
43. G. Baronio, S. Harran and A. Signoroni, "A Critical Analysis of a Hand Orthosis Reverse Engineering and 3D Printing Process," *Applied Bionics and Biomechanics*, vol. 2016, article ID 8347478, 2016.
44. J. T. Kate, G. Smit and P. Breedveld, "3D-printed upper limb prostheses: a review," *Disability and Rehabilitation: Assistive Technology*, vol. 12, no. 3, pp. 300–314, 2017.
45. Y. H. Cha, K. H. Lee, H. J. Ryu, I. W. Joo, A. Seo, D. H. Kim and S. J. Kim, "Ankle-Foot Orthosis Made by 3D Printing Technique and Automated Design Software," *Applied Bionics and Biomechanics*, vol. 2017, article ID 9610468, 2017.
46. H. R. Weiss, N. Tournavitis, X. Nan, M. Borysov and L. Paul, "Workflow of CAD / CAM Scoliosis Brace Adjustment in Preparation Using 3D Printing," *The Open Medical Informatics Journal*, vol. 11, no. 1, pp. 44–51, 2017.
47. S. Santos, B. Soares, M. Leite and J. Jacinto, "Design and development of a customised knee positioning orthosis using low cost 3D printers," *Virtual and Physical Prototyping*, vol. 12, no. 4, pp. 322–332, 2017.
48. K. Wang, Y. Shi, W. He, J. Yuan, Y. Li, X. Pan and C. Zhao, "The research on 3D printing fingerboard and the initial application on cerebral stroke patient's hand spasm," *BioMed Eng OnLine*, vol. 17, article ID 92, 2018.
49. H. Lal and M. K. Patralekh, "3D printing and its applications in orthopaedic trauma: A technological marvel," *Journal of Clinical Orthopaedics and Trauma*, vol. 9, no. 3, pp. 260–268, 2018.
50. K. W. Lin, C. J. Hu, W. W. Yang, L. W. Chou, S. H. Wei, C. S. Chen and P.C, Sun, "Biomechanical Evaluation and Strength Test of 3D-Printed Foot Orthoses," *Applied Bionics and Biomechanics*, vol. 2019, article ID 4989534, 2019.
51. S. Chunhua and S. Guangqing, "Application and Development of 3D Printing in Medical Field," *Modern Mechanical Engineering*, vol. 10, pp. 25–33, 2020.

52. D. Zhang and X, Zhang, "Rehabilitation Brace Based on the Internet of Things 3D Printing Technology in the Treatment and Repair of Joint Trauma," *Journal of Healthcare Engineering*, vol. 2021, article ID 6663892, 2021.
53. D. F. Redaelli, V. Abbate, F. A. Storm, A. Ronca, A. Sorrentino, C. De Capitani, E. Biffi, L. Ambrosio, G. Colombo and P. Fraschini, "3D printing orthopedic scoliosis braces: a test comparing FDM with thermoforming," *The International Journal of Advanced Manufacturing Technology*, vol. 111, pp. 1707–1720 , 2020.
54. C. Elliot, V. Gayathry, A. Pannertamil, D. B. Thiyam, P. Chezhiyan, M. Benisha, M. Anisha and R. Thandaiah Prabu, "Customized Knee Brace for Osteoarthritis Patient Using 3D Printing A Customized Knee Brace Using 3D Printing: A Customized Knee Brace Using 3D Printing," *Proc. 2021 Third International Conference on Intelligent Communication Technologies and Virtual Mobile Networks (ICICV)*, pp. 1300–1303, 2021.
55. C. Sheehan and E. Figgins, "A comparison of mechanical properties between different percentage layups of a single-style carbon fibre ankle foot orthosis," *Prosthetics and Orthotics International*, vol. 41, no. 4, pp. 364–372, 2017.
56. Y. C. Lin, L. Y. Huang and C. S. Chen, "Strength Evaluation and Modification of a 3D Printed Anterior Ankle Foot Orthoses," *Applied Sciences*, vol. 10, no. 20, article ID 7289, 2020.
57. N. Lobontiu, "Compliant Mechanisms: Design of Flexure Hinges", CRC Press, 2002.
58. M. Huber, M. Eschbach, H. Ilies, K. Kazerounian, "Case study: Novel Quasi-Passive Knee Orthosis with Hybrid Joint Mechanism," *Kecskem'ethy A., Geu Flores F. (eds) Interdisciplinary Applications of Kinematics. Mechanisms and Machine Science*, vol. 26, Springer, 2015.
59. S. Jun, X. Zhou, D. K. Ramsey, and V. N. Krovi, "Smart Knee Brace Design With Parallel Coupled Compliant Plate Mechanism and Pennate Elastic Band Spring," *ASME. J. Mechanisms Robotics*, vol. 7, no. 4, article ID 041024, 2015.
60. J. B. Ring and C. Kim, "A Passive Brace to Improve Activities of Daily Living Utilizing Compliant Parallel Mechanisms," *Proc. ASME 2016 International Design Engineering Technical Conferences and Computers and Information in Engineering Conference*, article ID V05AT07A015, 2016.
61. R. A. Bos, D. H. Plettenburg and J. L. Herder, "Exploratory design of a compliant mechanism for a dynamic hand orthosis: Lessons learned," *Proc. 2017 International Conference on Rehabilitation Robotics (ICORR)*, pp. 603–608, 2017.
62. R. Miclus, A. Repanovici and R. Nadinne, "Biomaterials: Polylactic Acid and 3D Printing Processes for Orthosis and Prosthesis," *Materiale Plastice*, vol. 54, pp. 98–102, 2017.
63. S. A. Srikanth and R. Bharanidaran, "Design Of A Compliant Mechanism Based Prosthetic Foot," *International Journal of Mechanical and Production Engineering Research and Development (IJMPERD)*, ISSN (P): 2249-6890; ISSN (E): 2249-8001, vol. 7, no. 3, pp. 33–42, 2017.
64. C. M. Racu and I. Doroftei, "Compliant Mechanism for Ankle Rehabilitation Device. Part I: Modelling and Design," *The 8th International Conference on Advanced Concepts in Mechanical Engineering*, IOP Publishing, IOP Conf. Series: Materials Science and Engineering, vol. 444, article ID 052014, 2018.
65. C. M. Racu and I. Doroftei, "Compliant Mechanism for Ankle Rehabilitation Device Part II: Op- timization and Simulation Results," *The 8th International Conference on Advanced Concepts in Mechanical Engineering*, IOP Publishing, IOP Conf. Series: Materials Science and Engineering, vol. 444, article ID 052014, 2018.

66. P. Bilancia, S. P. Smith, G. Berselli, S. P. Magleby and L. L. Howell, “Zero Torque Compliant Mechanisms Employing Prebuckled Beams,” *Journal of Mechanical Design*, vol. 142, no. 11, article ID 113301, 2020.
67. H. Sawada, “Upstream Design and 1D-CAE,” *Journal of System Design and Dynamics*, vol. 6, no. 3, pp. 351–358, 2012.
68. L. Zhang, Y. Liu, R. Wang, C. Smith and E. Gutierrez-Farewik, “Modeling and Simulation of a Human Knee Exoskeleton’s Assistive Strategies and Interaction,” *Frontiers in Neurorobotics*, 2021, 15 620928.
69. J. Vantilt, K. Tanghe, M. Afschrift, A. Bruijnes, K. Junius, J. Geeroms, E. Artbelien, F. Groote, D. Lefeber, I. Jonkers and J. Schutter, “Model-based control for exoskeletons with series elastic actuators evaluated on sit-to-stand movements,” *Journal of Neuroengineering and Rehabilitation*, 2019, Jun 3;16(1):65.
70. S. Schrade, Y. Nager, A. Wu, R. Gassert and A. Ijspeert, “Bio-inspired control of joint torque and knee stiffness in a robotic lower limb exoskeleton using a central pattern generator,” *IEEE*, 2017, Jul;2017:1387-1394.
71. R. McGrath, M. Ziegler, M. Pires-Faernandes, B. Knarr, J. Higginson and F. Sergi, “The effect of stride length on lower extremity joint kinematics at various gait speeds,” *PLoS One*, 2019, Feb 22;14(2):e0200862.
72. K. Gui, H. Liu and D. Zhang, “A generalizes framework to achieve coordinated admittance control for multi-joint lower limb robotic exoskeleton,” *IEEE*, 2017, Jul;2017:228-233.
73. K. Mankala, S. Banala and S. Agrawal, “Novel swing-assist um-motorized exoskeletons for gait training,” *Journal of Neuroengineering and Rehabilitation*, 2009, Jul 3;6:24.
74. P. E. Nikravesh, *Planar Multibody Dynamics: Formulation, Programming with MATLAB, and Applications*, 2nd edn., CRC Press, Boca Raton, 2018.
75. K. Komoda and H. Wagatsuma, Energy-efficacy comparisons and multibody dynamics analyses of legged robots with different closed-loop mechanisms, *Multibody System Dynamics* 40, 2017, pp. 123–153.
76. 3D Printed Orthoses Could Help out Children with Cerebral Palsy (<http://www.openbiomedical.org/3d-printed-orthoses-could-help-out-children-with-cerebral-palsy/>) – 2022/04/14.
77. Designing Orthotics for Young Patients with Cerebral Palsy (<https://wp.nyu.edu/connect/2019/04/22/makerbrace/>) – 2022/04/14.
78. Safe Landing Garment (<https://www.visualatelier8.com/fashion/safe-landing-garment-by-hubert-chen>) – 2022/04/14. Safe Landing Garment (Demonstrational Video) (<https://vimeo.com/306602996>) – 2022/04/14.
79. 3D Printed Flexible mesh for Knee and Ankle Support (<https://3dprintingindustry.com/news/the-mit-scientists-making-3d-printed-fabrics-as-soft-as-skin-157609/>) – 2022/04/14.
80. A. Hendricks, S. Nevin, C. Wikoff, M. Dougherty, J. Orlita, and R. Noorani, “The Low-Cost Design and 3D Printing of Structural Knee Orthotics for Athletic Knee Injury Patients,” *World Academy of Science, Engineering and Technology International Journal of Biomedical Engineering*, 12(10), 2018, 445–451.
81. Manuscript, A. (2013). Knee joint forces : prediction , measurement , and significance. 226(2), 95–102.
82. Juntendo University Rehabilitation Training, <https://re-how.net/all/693084/>, 2022/09/14.
83. M. Buckthorpe, A. Tamisari and F. D. Villa, “A Ten Task-Based Progression in Rehabilitation After Acl Reconstruction: From Post-Surgery To Return To Play – a Clinical Commentary,” *International Journal of Sports Physical Therapy*, 15(4), 2020, 611–623. <https://doi.org/10.26603/ijsp20200611>
84. Cellular Solids: Structure, Properties And Applications, Lecture Notes, 2022/04/25, <https://ocw.mit.edu/courses/3-054-cellular-solids-structure-properties-and-applications-spring-2015/pages/lecture-notes/>

85. P. Dachkinov, A. Bhattacharjee B. Bhattacharya and H. Wagatsuma, "A Three-Dimensional Design of the Multi-material Joint System to Realize a Structural Spring-Damper Compliant Mechanism with Versatility in Engineering Fields," THE 2022 International Conference On Artificial Life And Robotics, 2022.
86. P. Dachkinov, S. Kasai, K. Tanaka and H. Wagatsuma, "A computational model of 3d printing orthoses associated with a systematic structural analysis toward reverse engineering oriented production," ICIC-ELB, Vol.13, No.7, July 2022, ISSN 2185-2766.
87. P. Dachkinov, S. Kasai, K. Tanaka and H. Wagatsuma, "Flexible Bar Geometric Designs for Personalized Knee Orthoses Inspired by Compliant Mechanisms," Journal of Robotics, Networking and Artificial Life, in press.
88. Anycubic i3 Mega , <https://www.anycubic.com/products/anycubic-i3-mega>, 2022/05/07.
89. Ninjatek, Ninjaflex,TPU3DPrinting Filament, Technical specifications, <https://ninjatek.com/shop/ninjaflex/#print-guidelines>, 2022/04/22.
90. Ultimaker Cura, 3D Printing slicing software, Infill pattern guide, <https://all3dp.com/2/cura-infill-patterns-all-you-need-to-know/>, 2022/04/22.
91. Ultimaker Cura Infill Settings, <https://support.ultimaker.com/hc/en-us/articles/360012607079-Infill-settings>, 2022/05/08.
92. Autodesk Inventor Professional, <https://www.autodesk.com/products/inventor/overview?term=1-YEAR&tab=subscription>, 2022/05/07.
93. Autodesk Inventor Nastran, <https://www.autodesk.com/products/inventor-nastran/overview?term=1-YEAR&tab=subscription>, 2022/05/06.
94. Ottobok Genu Direxa Stable wraparound, <https://shop.ottobock.us/Orthotics/Bracing-%26-Supports/Knee/Other/Genu-Direxa-Stable-wraparound%2C-black/p/8368~5K>, 22/07/08.
95. Ottobok, Genu Arexa, <https://www.ottobock.com/en-us/product/50K13>, 22/07/08.
96. Miniature Linear Motor Actuonix, <https://s3.amazonaws.com/actuonix/Actuonix+L16+Datasheet.pdf>, 2022/05/09.
97. Linear Actuator Control Board, <https://s3.amazonaws.com/actuonix/Actuonix+LAC+Advanced+Configuration+Datasheet.pdf>, 2022/05/09.

Publications

Symposium:

1. P. Dachkinov, A. Bhattacharjee B. Bhattacharya and H. Wagatsuma, “A Knee Joint Inspired Design of a Compliant Cross-Spring Pivot,” “International Symposium of Applied Engineering and Sciences,” (SAES 2020).
2. P. Dachkinov, A. Bhattacharjee, B. Bhattacharya and H. Wagatsuma, “A Three-Dimensional Design and Analysis of a Multi-material Compliant Joint for Precision Engineering Applications,” “International Symposium on Robotics in Industry, Agriculture and Healthcare” (ISHIAH2022).
3. S. Kasai, P. Dachkinov, K. Tanaka and H. Wagatsuma, “The Effectiveness of Force Measurement System by Using Programmable Actuators for 3D Printed Compliant Mechanisms,” “International Symposium of Applied Engineering and Sciences,” (SAES 2021).

Conference:

1. K. Tsukamoto, P. Dachkinov, D. Batbatar and H. Wagatsuma, “A Simplified Model with Elastic Materials to Reproduce the Jumping Dynamics of Animals and Analyses of the Accumulation-Release Relationship at the Kicking Moment,” NC.
2. S. Kasai, P. Dachkinov, K. Tanaka and H. Wagatsuma, “A Systematic Analysis of the Knee Support Exoskeleton Based on Multibody Dynamics Toward Personalization with 3D printed Spring-Damper Components,” “International Conference on Artificial Life and Robotics”, (ICAROB2022).

Journal:

1. P. Dachkinov, S. Kasai, K. Tanaka and H. Wagatsuma, “A computational model of 3d printing orthoses associated with a systematic structural analysis toward reverse engineering oriented production,” ICIC-ELB, Vol.13, No.7, July 2022, ISSN 2185-2766.
2. P. Dachkinov, S. Kasai, K. Tanaka and Wagatsuma, “Flexible Bar Geometric Designs for Personalized Knee Orthoses Inspired by Compliant Mechanisms,” Journal of Robotics, Networking and Artificial Life, in press.
3. A. Bhattacharjee, P. Dachkinov, H. Wagatsuma and B. Bhattacharya, “3D PRINTED BEAMS WITH VARIABLE INFILL DENSITIES,” International Journal of Engineering Advanced Research (IJEAR), 2022, 2710-7167.
4. P. Dachkinov, A. Bhattacharjee, B. Bhattacharya and H. Wagatsuma, “A Multi-Material Joint System as a Three-Dimensional Spring-Damper Compliant Mechanism Toward Functional Versatility,” “Journal of Advances in Artificial Life Robotics,” JAALR, Volume 3, Issue 2, September 2022, pp. 67–73, online ISSN 2435-8061; ISSN-L 2435-8061.